amjam

amjam

ASIAN MEDICAL JOURNAL & ALTERNATIVE MEDICINE

Asian Medical Journal and Alternative Medicine (AMJAM) aims to publish high quality, peer-review articles. This journal publishes Original article, Review article, Special article, Brief research, Case report, and Letter to the Editor in all health sciences, medical specialties and alternative medicine. Manuscripts submitted to AMJAM should consist of new material that focuses on broad topics in health sciences published in English language. AMJAM published 4 issues annually (January-April, May-August, September-December, and 1 supplemental issue per year). All submitted articles will be evaluated using double-blinded review process by 2-4 reviewers.

Contents

amjam

Contents

Editor's Note

It is my great honor to become a new Editor-in-Chief of AMJAM after the previous Editor-in-Chief, Professor Anucha Apisarnthanarak, M.D. who has contributed significantly to the transformation of AMJAM and the improvement of the journal in regards to scientific value and quality of its published articles. With some changes in and new recruitment of the Editorial Board members, we commit to the continuing dissemination of research results in the fields of Medicine and Alternative Medicine and thrive to become one of the leading journals included in worldwide-accepted scientific citation databases. For this current issue, AMJAM publishes original articles addressing medical properties of various Thai traditional remedies, reviews on adult intraosseous infusion and role of digital health in FGIDs and a rare case report of disseminated nocardiosis, which should be of interest and educational among our readers.

Thana Khawcharoenporn, M.D., M.Sc.
Professor of Medicine
Editor-in-Chief
Asian Medical Journal and Alternative Medicine

Editorial

Diabetes Mellitus in Thai Traditional Medical Theory

Pannawat Chaiyawatthananananthn[*]

Diabetes mellitus (DM) is a chronic metabolic disease which leads to an increase in blood glucose levels. In Thai traditional medicine (TTM), DM is called "Ma-Dhu-Me-Ha" which is combined with two words, "Ma-Dhu-Ra" and "Me-Ha", meaning sweet taste and urination, respectively.[1] Thus, the combination of those two words is sweet urination and is aligned with modern medical theory, in which glucose is found in the urine of DM patients. It is wildly known that DM patients have impairment of pancreatic function and insulin resistance.[2] TTM does not directly discuss the function of the pancreas. TTM theory describes DM via the mechanism of "A-Bhat-Ta-Pitta", a major generator of Pitta in the human body, which means the functions of the liver and pancreas. Consumption of starch, high sugar or high fat foods causes the increased accumulation of nutrients in the blood. The blood becomes "Ma-Dhu-Ros" (sweet) and then increases viscosity.[1] Continuing these events reduces the functions of the liver (Ya-Ka-Nang)[3] which is the source of "Pitta" in the Tridosha system. The system is divided into three sub-systems that are "Pitta" ("Ta-Sho" or fire elements), "Vata" ("Wa-Yo" or wind elements) and "Semha" ("Ar-Po" and "Pa-Tha-Wi" or water and earth elements, respectively) systems.[4,5] TTM theory indicates that DM is the failure of the Semha system which then affects the Pitta and Vata systems.[4] Abnormal liver function causes a decrease the production of Pitta and then it induces the impairment of A-Bhat-Ta-Pitta. It causes the increase of Pa-Tha-Wi

or earth element's function and then decreases the function of the Ar-Po (water) element which presents as an increase in blood viscosity. It causes the Wa-Yo (wind) element to work harder circulating the blood to all parts of the body. The fluctuation of the wind or Wa-Yo element makes the Ta-Sho (fire) element increasingly active. Thus, the fire (Ta-Sho) element moves upward in the body which causes dry mouth and throat. The patients with DM drink a lot of water which has the effect of increasing the water or Ar-Po element. The water (Ar-Po) element moves down the body because it is an element that has weight. This event causes patients to urinate frequently and increases kidney or "Pi-Ha-Kang" functions. Then, DM patients have lower extremity edema which is an effect from the loss of Pi-Ha-Kang functions. Moreover, the abnormality of the wind or Wa-Yo elements flow into all organs in the body i.e. "Hathai-Vata", "Summana-Vata" and "Satthaka-Vata".[1] It can be compared with the nervous system in modern medicine. The abnormality of the nervous system presents with numbness in the hands and feet, which affects sensory loss. A herbal remedy that is widely used for the treatment of DM is "Ma-Dhu-Ra-Me-Ha" recipe and is currently being investigated for its anti-DM effect in animal models[4,6] and clinical trials.[7,8]

In conclusion, DM in TTM theory is triggered by the deficiency of A-Bhat-Ta-Pitta functions, and relates to modern medicine with sweet urination or glucose in the urine, detected in patients with DM.

Department of Applied Thai Traditional Medicine, Faculty of Medicine, Thammasat University, Pathum Thani 12120, Thailand
[*] **Corresponding author:** Pannawat Chaiyawatthananananthn, Ph.D., Department of Applied Thai Traditional Medicine, Faculty of Medicine, Thammasat University, Pathum Thani 12120, Thailand, Email: pannawat@tu.ac.th

References

1. Limprasert K. Applied Thai traditional medicine 2 in elemental theory and diagnosis/analysis of Thai medicine recipes section. Nonthaburi: Sukhothai Thammathirat Open University Printing House. 2016:41-43. (in Thai)

2. Dludla PV, Mabhida SE, Ziqubu K, Nkambule BB, Mazibuko-Mbeje SE, Hanser S, Basson AK, Pheiffer C, Kengne AP. Pancreatic β-cell dysfunction in type 2 diabetes: Implications of inflammation and oxidative stress. *World J Diabetes*.2023;14(3):130-146. doi:10.4239/wjd.v14.i3.130.

3. Limprasert K. Applied Thai traditional medicine 1 in elemental theory and diagnosis section. Nonthaburi: Sukhothai Thammathirat Open University Printing House. 2016:28-30. (in Thai)

4. Peungvicha P, Vallisuta O, Mangmool S, Sirithamwanich T, Sirithamwanich R. Anti-hyperglycemic effect and subchronic toxicity of the combined extract from Sattagavata -Mathurameha - Tubpikarn anti-diabetic herbal formulae. *Thai Journal of Pharmaceutical Sciences*. 2018;42(1):6-13.

5. Thai Traditional Medicine Restoration and Promotion Foundation, Ayurved Thamrong School, Department of Applied Thai Traditional Medicine, Faculty of Medicine Siriraj Hospital, Mahidol University. Traditional Thai medicine textbook (Subsidiary Medicine in conservation edition) Volume 1, paid edition, on the auspicious occasion of the 80th birthday of His Majesty King Bhumibol Adulyadej. Bangkok: Supawanich Printing; 2007. (In Thai)

6. Chayarop K, Peungvicha P, Temsiririrkkul R, Wongkrajang Y, Chuakul W, Rojsanga P. Hypoglycaemic activity of Mathurameha, a Thai traditional herbal formula aqueous extract, and its effect on biochemical profiles of streptozotocin-nicotinamide-induced diabetic rats. *BMC Complementary and Alternative Medicine*. 2017;17(1):343. doi:10.1186/s12906-017-1851-8.

7. Permphol P, Tharavanij T, Itharat A, Srimongkol Y, Chinsoi P, Chanpen O. Efficacy and safety of Mathurameha for type 2 diabetes mellitus treatment. *Thammasat Medical Journal*. 2016;16(4):589-599.

8. Piriyapornpipat S, Panee Wasanat. A Comparison of Efficacy and Safety of Mathurameha and Metformin in New-onset Type 2 Diabetes Patients. *J Thai Trad Alt Med*. 2020;18(3): 478-495.

Original Article

Assessment of *in vitro* Antioxidant Activities and Quantification of Total Phenolic and Flavonoid Contents in Extracts from The Thai Traditional Remedy "Ruean-Khi-Nok" and its Plant Constituents

Atchanika Taingthum[1], Intouch Sakpakdeejaroen[1,2*],
Sumalee Panthong[1,2], Puritat Kanokkangsadal[1,2]

Abstract

Introduction: Psoriasis is an immune-mediated inflammatory skin disease. The pathogenesis of psoriasis has been associated with an increase of oxidative stress. Therefore, natural antioxidant compounds (e.g., phenolics and flavonoids) might be beneficially used as an adjuvant. Ruean-Khi-Nok (RKN) remedy is a Thai traditional preparation used to treat psoriatic skin, consisting of nine plants in an equal proportion.

Objectives: To investigate the antioxidant capability of the RKN remedy and its components using three chemical-based assays, as well as to determine phenolic and flavonoid contents.

Methods: The 95% and 40% ethanolic extracts of RKN remedy and its plant components were investigated for *in vitro* antioxidant activities using DPPH and ABTS radical scavenging assay, as well as FRAP assay. The total phenolic and flavonoid contents in extracts were quantified using the Folin-Ciocalteu's method and the aluminum chloride colorimetric method, respectively.

Results: The results exhibited potential antioxidant activity of the 95% ethanolic extract of RNK remedy in the DPPH, ABTS and FRAP assay. In addition, it also contained high phenolic and flavonoid contents. Among individual plants, *Piper wallichii* extracts displayed outstanding antioxidant capability compared to the others.

Conclusions: The RKN remedy is therefore highly promising antioxidant and might support the traditional use of RKN remedy for treatment of psoriatic skin. However, RKN should be investigated further for psoriasis treatment.

Keywords: Ruean-Khi-Nok remedy, Antioxidant activity, Total phenolic content, Total flavonoid content

[1] Department of Applied Thai Traditional Medicine, Faculty of Medicine, Thammasat University, Pathum Thani, Thailand
[2] Centre of Excellence in Applied Thai Traditional Medicine Research (CEATMR), Thammasat University, Pathum Thani, Thailand
* **Corresponding author:** Intouch Sakpakdeejaroen, Department of Applied Thai Traditional Medicine, Faculty of Medicine, Thammasat University, Pathum Thani, Thailand, Email: intouch@tu.ac.th, Tel. +66 2926 9749

Introduction

Psoriasis is a chronic immune-mediated inflammatory skin disease, affecting about 3% of the world's population.[1] In addition, Psoriatic skin can have negative impact on patients' quality of life.[2] Recently, it has been found that psoriasis pathogenesis may be linked to oxidative stress, an imbalance between oxidants and antioxidants.[3] This condition causes an excess of reactive oxygen species (ROS) and reactive nitrogen species (RNS), leading to cellular damage or dysfunction through various mechanisms, such as the secretion of pro-inflammatory cytokines and hyperproliferation of keratinocytes.[1,4]

In recent years, several studies have emerged involving phenolics and flavonoids, plant-derived natural compounds, as a potential recovery tool for treatment of psoriasis owing to their powerful antioxidant properties.[5-7] Ruean-Khi-Nok (RKN) remedy, a topical preparation in the National Thai Traditional Medicine Formulary (Special Edition), has been used for the treatment of psoriatic skin.[8] It consists of nine plant species in equal proportions: the leaves of *Casearia grewiifolia* Vent. (CG), the leaves of *Crateva religiosa* G. Forst. (CR), the leaves of *Crateva adansonii* DC. (CA), the leaves of *Piper wallichii* (Miq.) Hand. -Mazz. (PW), the leaves of *Datura metel* L. var. *metel* (DM), the leaves of *Persicaria chinensis* (PC) (L.) H. Gross, the aerial part of *Pouzolzia zeylanica* (L.) Benn. (PZ), the aerial part of *Gonostegia pentandra* (Roxb.) Miq. (GP), and the rhizome of *Alpinia galanga* (L.) Willd. (AG). Previous studies suggested that *A. galanga* extract may exert its anti-psoriatic effect by modulating NF-κB signaling biomarkers.[9] In addition, withanolides, the active compounds isolated from *D. metel* leaves also showed promise in treatment of psoriasis by reducing inflammatory cytokines, as well as lowering HIF-1α and VEGF expression in angiogenesis.[10] Furthermore, several studies have reported antioxidant activity of some individual plant components using different assays, including DPPH and ABTS radical scavenging assay.[11-16] Despite this data, there is no scientific research available on antioxidant activity of RKN remedy as well as total phenolic and flavonoid contents. Hence, we aimed to investigate the antioxidant activities of Ruean-Khi-Nok remedy and its plant components using three anti-oxidant methods, DPPH radical scavenging assay, ABTS radical scavenging assay and Ferric reducing antioxidant power (FRAP) assay, as well as total phenolic and total flavonoid contents.

Methods

2.1 Plant materials

The leaves of *C.grewiifolia* Vent. (CG), the leaves of *C. religiosa* G. Forst. (CR), the leaves of *C. adansonii* DC. (CA), the leaves of *P. wallichii* (Miq.) Hand.-Mazz. (PW), the leaves of *D. metel* L. var. *metel* (DM), the leaves of *P. chinensis* (PC) (L.) H. Gross, the aerial part of *P. zeylanica* (L.) Benn. (PZ), the aerial part of *G. pentandra* (Roxb.) Miq. (GP), and the rhizome of *A. galanga* (L.) Willd. (AG) were purchased from a local herbal shop, Bangkok, Thailand. The voucher specimens were identified and deposited at the herbarium of Thai Traditional Medicine Research Institute, Department of Thai Traditional and Alternative Medicine, Bangkok, Thailand, which are TTM 1000658, TTM 1000659, TTM 1000660, TTM 1000663, TTM 0005448, TTM 1000664, TTM 0005449, TTM 1000662 and TTM 0005447, respectively.

2.2 Chemicals and reagents

Butylated hydroxytoluene (BHT) and 1,1-diphenyl-1-picrylhydrazyl (DPPH) were obtained from Fluka (Germany). Aluminum chloride, gallic acid and sodium nitrite were purchased from TCI, Japan. Absolute ethanol, hydrochloric acid (37%) and glacial acetic acid were purchased from RCI Labscan, Thailand. Folin-Ciocalteu's reagent, sodium carbonate, 2,2'-azinobis-(3-ethylbenzothi-azoline-6-sulfonic acid) diammonium salt (ABTS), potassium persulfate, sodium acetate, 2,4,6-Tri (2-pyridyl)-s-triazine (TPTZ), sodium acetate trihydrate, ferric chloride hexahydrate ($FeCl_3 \cdot 6H_2O$), ferrous sulfate heptahydrate ($FeSO_4 \cdot 7H_2O$) and 6-hydroxy-2,5,7,8-tetramethylchromane-2-carboxylic acid (Trolox) and all the other chemicals not specifically mentioned were obtained from Sigma Aldrich, Germany.

2.3 Preparation of Ruean-Khi-Nok (RNK) remedy and its plant component extracts

All plant materials were cleaned, dried and ground into coarse powder. For the preparation of RKN remedy, according to traditional use, each

plant component was used in equal portions.[8] The RKN remedy was then mixed with spirit (about 40% alcohol) before being used. Thus, the extracts of RKN remedy and its plant constituent were obtained by maceration method with 40% and 95% ethanol. To do so, the RKN remedy and its plant components were macerated with 40% and 95% ethanol for 3 days. The extracts were filtrated through Whatman No.1 filter paper and then concentrated under reduced pressure using rotary evaporator. The maceration process was repeated twice (a total of 3 times). Finally, the extracts were dried in a vacuum dryer. All extracts were stored at -20 °C for further experiments.

2.4 *In vitro* antioxidant activity
2.4.1 DPPH radical scavenging assay

The DPPH radical scavenging activity of the ethanolic extracts of the RKN remedy and its components was evaluated according to the modified method described by Yamasaki and colleagues.[17] In brief, the tested samples were firstly prepared with different concentrations (final concentration of 6.25 to 200 µg/mL). DPPH (1.2 mg) was dissolved in absolute ethanol (50 mL) to make up a DPPH reaction solution (6×10^{-5} M). One hundred microliters of the tested samples were added to 96-well plate. Subsequently, DPPH solution (100 µL) was then added to the samples, followed by incubation at room temperature for 30 min (protected from light). The absorbance was measured at a wavelength of 520 nm using a microplate reader. BHT was used as a positive control. The results were expressed as the percent inhibition of absorbance of DPPH and half-maximal effective concentrations (EC_{50}).

2.4.2 ABTS radical scavenging assay

The ABTS radical scavenging activity of the ethanolic extracts of the RKN remedy and its components was determined according to the method described by Re and colleagues[18] with some modifications. Firstly, ABTS solution (7.2 mM) was mixed with potassium persulfate solution (2.45 mM) in an equal portion and allowed them to react overnight (12 -16 hours) at low temperatures (4°C) in the dark. The resulting blue-green colored $ABTS^{\bullet+}$ radical cation solution was diluted with deionized water to obtain the absorbance between 0.680 -0.720 at wavelength of 734 nm before using in the assay. Twenty microliters of the tested samples at different concentrations (final concentration ranging from 1.5625 to 200 µg/mL) were added to 96-well plate. Subsequently, $ABTS^{\bullet+}$ radical cation solution (180 µL) was then added to the samples, followed by incubation at room temperature for 6 min (protected from light). Trolox and BHT were used as positive control. The results were expressed as the percent inhibition of absorbance of ABTS and EC_{50}.

2.4.3 Ferric reducing antioxidant power (FRAP) assay

The antioxidant power of the ethanolic extracts of the RKN remedy and its components was assessed using ferric reducing ability according to the method described by Benzie and Strain.[19] In brief, the FRAP reagent was firstly prepared by mixing 300 mM acetate buffer (pH 3.6) with 10 mM TPTZ solution (in 40 mM HCl), and 20 mM ferric chloride solution at the ratio of 10:1:1 (v/v/v). A standard calibration curve of Trolox and $FeSO_4$ was prepared with different concentration ranging from 6.25 to 300 and 6.25 to 800 µg/mL, respectively. Twenty microliters aliquot of the tested samples solution was added in 96-well plate and mixed with 180 µL of the FRAP reagent (pre-warmed at 37 °C). The mixture was allowed to react at room temperature for 8 min before being measured at a wavelength of 593 nm using a microplate reader. The antioxidant power was calculated by correlating the absorbance of each sample with the standard calibration curve of Trolox and $FeSO_4$. The results were expressed as Trolox equivalent antioxidant capacity (TEAC value; mg TE/g extract) and ferric reducing antioxidant power (FRAP value; mg Fe^{2+}/g extract).

2.5 Total phenolic content

Total phenolic content of the ethanolic extracts of RKN remedy and its components was measured using the Folin-Ciocalteu's method as previously described.[20,21] Briefly, A standard calibration curve of gallic acid was prepared at 6 concentrations (6.25, 12.5, 25, 50, 75 and 100 µg/mL). Twenty microliters aliquot of the tested samples was added in 96-well plate and mixed with Folin-Ciocalteu's reagent (100 µL). Subsequently, sodium carbonate solution (80 µL) was added to the samples, followed by incubation for 30 min at room temperature. The absorbance was determined at a wavelength of 765 nm using a microplate reader. The total phenolic content was calculated by correlating the absorbance of each sample with the standard curve of gallic acid

and expressed as milligrams of gallic acid equivalent per 1 gram of extract (mg GAE/g extract).

2.6 Total flavonoid content

Total flavonoid content of the ethanolic extracts of RKN remedy and its components was determined using the aluminum chloride colorimetric method as previously described.[22] To do so, catechin was firstly prepared as a standard flavonoid solution in absolute ethanol (concentration ranging from 6.25 to 400 µg/mL). Five hundred microliters of the tested samples were mixed with 75 µL of sodium nitrite (5% w/v), 150 µL of aluminum chloride (10% w/v), 500 µL of sodium hydroxide (1M) and 275 µL of distilled water, respectively, in a centrifuge tube. One hundred microliters of the mixture were then transferred into 96 well-plate and incubated at room temperature for 30 minutes. The absorbance was measured at a wavelength of 510 nm using a microplate reader. The total flavonoid content was calculated by correlating the absorbance of each sample with the standard curve of catechin. The results were expressed as milligrams of catechin equivalent per 1 gram of extract (mg CE/g extract).

2.7 Statistical analysis

All experiments were expressed as mean ± standard error of mean (SEM) from at least four separate experiments. Statistically significant differences in radical scavenging activity among plant extracts and positive control were performed using one-way analysis of variance analysis (ANOVA) followed by Dunnett's multiple comparison test. Differences were considered statistically significant for *p-values* lower than 0.05.

Results

3.1 *In vitro* antioxidant activity

3.1.1 DPPH radical scavenging assay

The DPPH radical scavenging activity of the ethanolic extracts of RKN remedy and its plant components are shown in Table 1. No significant differences (p > 0.05) were observed between the activity of RKNE95 extract and BHT (EC$_{50}$: 15.00 ± 0.33 µg/mL for RKNE95 and 15.38 ± 0.22 µg/mL for BHT), while the RKNE40 extract (EC$_{50}$: 183.49 ± 1.28 µg/mL) exhibited very low activity. Among all the plants components extracted with 95% etha-

nol, the PWE95 extract (EC$_{50}$: 3.44 ± 0.10 µg/mL) possessed the highest activity and significantly better than BHT, while the others possessed moderate ability. In contrast, most plants extracted with 40% ethanol exhibited low DPPH radical scavenging activity (EC$_{50}$ >200 µg/mL), except PWE40 (EC$_{50}$: 22.63 ± 0.29 µg/mL) and PCE40 (EC$_{50}$: 38.14 ± 1.15 µg/mL) extracts.

3.1.2 ABTS radical scavenging assay

The ABTS radical scavenging activity of the ethanolic extracts of RKN remedy and its plant components are shown in Table 1. It was evident that RKNE95 extract (EC$_{50}$: 20.32 ± 0.30 µg/mL) had 2-fold higher ABTS scavenging activity than the RKNE40 extract (EC$_{50}$: 43.47 ± 0.94 µg/mL). Among all the ingredients extracts, the PWE95, PWE40 and PCE40 extracts exerted potent ABTS radical scavenging activity (EC$_{50}$: 6.17 ± 0.19, 8.29 ± 0.11 and 8.87 ± 0.20 µg/mL, respectively), but slightly less activity as compared to BHT (EC$_{50}$: 2.53 ± 0.02 µg/mL) and Trolox (EC$_{50}$: 4.16 ± 0.08 µg/mL). Meanwhile, other component plant extracts possessed moderate ABTS radical scavenging activity in accordance with the RKN extracts (EC$_{50}$ ranging from 13.61 to 39.92 µg/mL), except the GPE40, and both extracts of PZ and DM (EC$_{50}$ > 50 µg/mL).

3.1.3 Ferric reducing antioxidant power (FRAP) assay

The FRAP of the ethanolic extracts of RKN remedy and its plant components are shown in Table 2. The results found that the TEAC and FRAP values of the RKNE95 extract (126.48 ± 1.42 mg TE/g extract and 272.14 ± 6.43 mg Fe^{2+}/g extract) were 2.5-fold higher than the RKNE40 extract (51.44 ± 1.96 mg TE/g extract and 112.02 ± 0.93 mg Fe^{2+}/g extract). Among all the component plants extracts, the highest TEAC and FRAP values were found in the PWE95 (419.07 ± 7.24 mg TE/g extract and 902.94 ± 11.44 mg Fe^{2+}/g extract) followed by the PWE40 (268.78 ± 5.72 mg TE/g extract and 582.74 ± 7.98 mg Fe^{2+}/g extract) extracts. In addition, the PCE95, PCE40, CGE40 and CAE40 extracts also exhibited good antioxidant activity compared to PWE40, with values ranging from 224.00 ± 3.20 to 110.92 ± 2.77 mg TE/g extract. However, the others exhibited lower reducing antioxidant power than PWE40.

Table 1 DPPH and ABTS radical scavenging activities of the ethanolic extracts of RKN remedy and its plant components (n = 6)

Sample	Code	EC_{50} (µg/mL)	
		DPPH assay	**ABTS assay**
Ruean-Khi-Nok remedy	RKNE95	15.00 ± 0.33	20.32 ± 0.30[a,b]
	RKNE40	183.49 ± 1.28[a]	43.47 ± 0.94[a,b]
C. grewiifolia Vent.	CGE95	12.39 ± 0.28[a]	23.03 ± 0.21[a,b]
	CGE40	154.13 ± 2.18[a]	13.61 ± 0.54[a,b]
C. religiosa G. Forst.	CRE95	33.02 ± 1.01[a]	35.54 ± 0.49[a,b]
	CRE40	> 200[a]	24.90 ± 0.68[a,b]
C. adansonii DC.	CAE95	26.01 ± 0.88[a]	31.10 ± 0.45[a,b]
	CAE40	176.47 ± 3.26[a]	22.04 ± 0.44[a,b]
P. zeylanica (L.) Benn.	PZE95	69.65 ± 1.38[a]	142.48 ± 2.68[a,b]
	PZE40	> 200[a]	186.49 ± 2.82[a,b]
G. pentandra (Roxb.) Miq.	GPE95	17.29 ± 0.26[a]	39.92 ± 0.29[a,b]
	GPE40	> 200[a]	91.94 ± 1.30[a,b]
A. galanga (L.) Willd.	AGE95	19.87 ± 0.75[a]	21.17 ± 0.86[a,b]
	AGE40	> 200[a]	40.88 ± 1.26[a,b]
P. wallichii (Miq.) Hand.-Mazz.	PWE95	3.44 ± 0.10[a]	6.17 ± 0.19[a,b]
	PWE40	22.63 ± 0.29[a]	8.29 ± 0.11[a,b]
D. metel L. var. *metel*	DME95	37.91 ± 0.94[a]	60.55 ± 1.19[a,b]
	DME40	> 200[a]	80.04 ± 1.00[a,b]
P. chinensis (L.) H. Gross	PCE95	11.08 ± 0.44[a]	17.76 ± 0.18[a,b]
	PCE40	38.14 ± 1.15[a]	8.87 ± 0.20[a,b]
Buthylhydroxytoluene	BHT	15.38 ± 0.22	2.53 ± 0.02
Trolox	Trolox	-	4.16 ± 0.08

Note: Code E95 was 95% ethanolic extract and E40 was 40% ethanolic extract. [a] Significant differences (p < 0.05) were observed compared to BHT and [b] Significant differences (p < 0.05) were observed compared to BHT and Trolox.

Table 2 The ferric reducing antioxidant power (FRAP) assay of the ethanolic extracts of RKN remedy and its plant components

Sample	Code	TEAC value (mg TE/g extract)	FRAP value (mg Fe^{2+}/g extract)
Ruean-Khi-Nok remedy	RKNE95	126.48 ± 1.42	272.14 ± 6.43
	RKNE40	51.44 ± 1.96	112.02 ± 0.93
C. grewiifolia Vent.	CGE95	66.33 ± 1.05	143.91 ± 3.24
	CGE40	207.28 ± 9.91	443.38 ± 8.79
C. religiosa G. Forst.	CRE95	57.51 ± 1.74	125.02 ± 2.30
	CRE40	89.30 ± 3.84	192.52 ± 3.03
C. adansonii DC.	CAE95	81.88 ± 1.02	177.04 ± 3.52
	CAE40	110.92 ± 2.77	238.77 ± 2.82
P. zeylanica (L.) Benn.	PZE95	19.59 ± 0.63	44.28 ± 0.43
	PZE40	9.12 ± 0.68	21.93 ± 0.65
G. pentandra (Roxb.) Miq.	GPE95	54.38 ± 1.09	118.46 ± 3.54
	GPE40	16.73 ± 0.69	38.17 ± 0.57
A. galanga (L.) Willd.	AGE95	52.61 ± 1.68	114.60 ± 2.48
	AGE40	38.56 ± 0.67	84.78 ± 2.85
P. wallichii (Miq.) Hand.-Mazz.	PWE95	419.07 ± 7.24	902.94 ± 11.44
	PWE40	268.78 ± 5.72	582.74 ± 7.98
D. metel L. var. *metel*	DME95	47.24 ± 0.73	103.29 ± 3.47
	DME40	24.59 ± 1.10	54.90 ± 1.48
P. chinensis (L.) H. Gross	PCE95	116.79 ± 2.71	251.26 ± 1.64
	PCE40	224.00 ± 3.20	479.76 ± 6.18

Note: Code E95 was 95% ethanolic extract and E40 was 40% ethanolic extract.

3.2 Total phenolic content

The content of phenolic compounds in the ethanolic extracts of RKN remedy and its plant components are presented in Figure 1. The RKNE95 extract content of phenolics was 100.39 ± 2.29 mg GAE/g extract, while the RKNE40 extract had 68.77 ± 0.98 mg GAE/g extract. The highest total phenolic content was found in both PWE95 and PWE40 (355.69 ± 4.65 mg GAE/g extract for PWE95 and 341.33 ± 2.10 mg GAE/g extract for PWE40).

3.3 Total flavonoid content

The total flavonoid content in the ethanolic extracts of RKN remedy and its plant components are presented in Figure 2. The results showed that the RKNE95 extract contained 3.8-fold higher total content of flavonoids than the RKNE40 extract (133.54 ± 1.62 mg CE/g extract for RKNE95 and 34.82 ± 0.53 mg CE/g extract for RKNE40). Both PWE95 and PWE40 had the highest flavonoid contents of 493.95 ± 2.69 and 451.62 ± 2.00 mg CE/g extract, respectively.
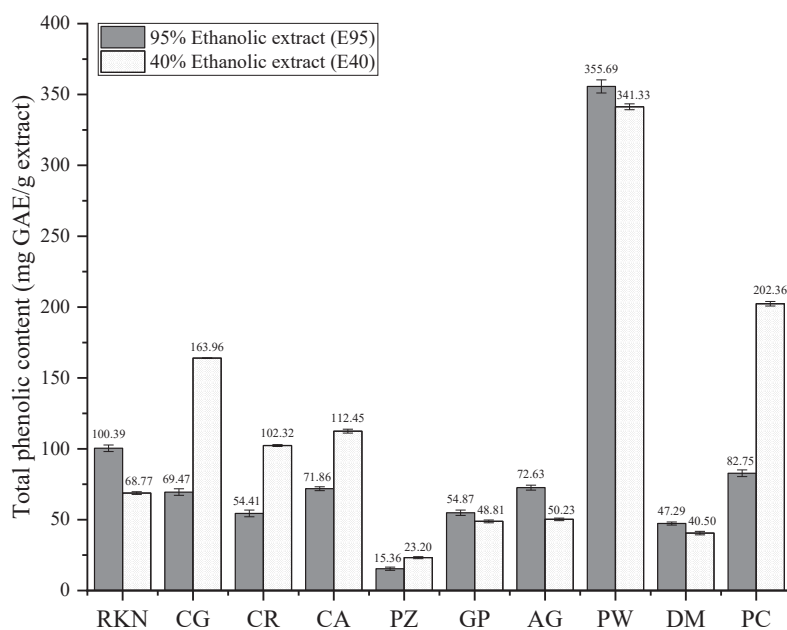
Figure 1 Total phenolic content of the ethanolic extracts of RKN remedy and its plant components (n = 4)
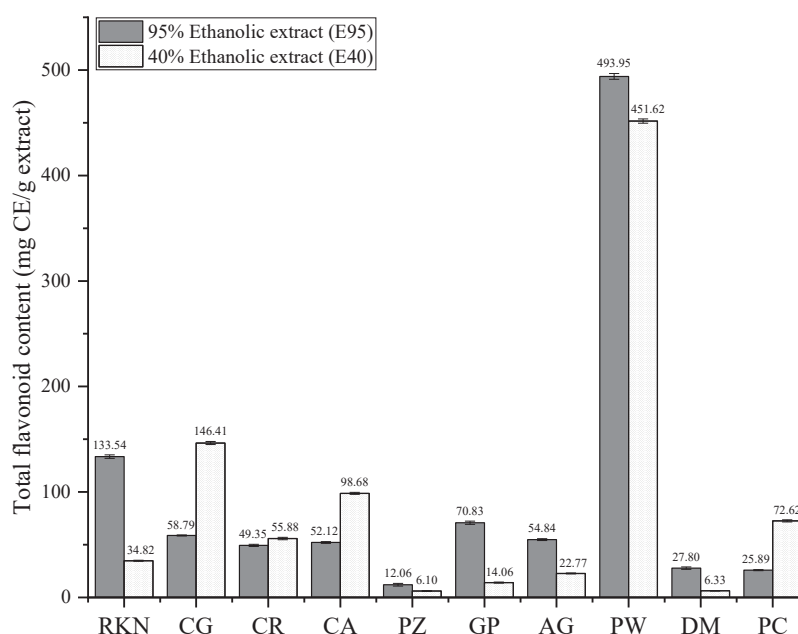
Figure 2 Total flavonoid content of the ethanolic extracts of RKN remedy and its plant components (n = 4)

Discussion

Oxidative stress has been proposed as one of the risk factors involved in the pathogenesis of psoriasis. Therefore, using antioxidant compounds might be a potential adjuvant for treatment of this dermatosis.[3, 23] In this study, we selected several chemical-based antioxidant methods to evaluate the antioxidant activity, as well as to determine total phenolic and flavonoid contents of the RKN remedy and its component plants extracts.

The DPPH radical scavenging assay is one of the most widely used method for screening antioxidant activity of plant extracts due to its simplicity, low cost, and high sensitivity with a rapid reaction.[17] However, the DPPH radical chromogens can only be dissolved in an organic solvent which limits its

application.[24] On the other hand, The ABTS radical scavenging assay is more adaptable for assessing the antioxidant capacity than the DPPH assay because the ABTS cationic radical can be soluble in both organic and aqueous mediums. Therefore, it can be used to screen both lipophilic and hydrophilic tested samples.[25] The FRAP assay is also used to evaluate antioxidant power of a compound based on its capacity to reduce the ferric ion (Fe^{3+}) to the ferrous ion (Fe^{2+}). This method is suitable for screening a wide spectrum of samples, for example biological fluids, organic extracts, foods, and plants.[26]

In this current study, the RNK remedy has been shown to have a promising antioxidant effect in all tested methods, especially for the 95% ethanolic extract, as evidenced by similarly scavenged DPPH and ABTS radicals compared to standard BHT and Trolox. From the FRAP assay, the RKNE95 extract also exhibited a potential antioxidant capacity. Regarding specific plant components, the PW extracts displayed outstanding antioxidant capability. Their activities are similar or even better than the positive control. Additionally, the extracts of PC and CG were shown to be good scavengers against free radicals. The antioxidant activity of several component plants in the RKN remedy have previously been investigated using various experimental models. For example, Tamuly and colleague reported the scavenging activity (DPPH, ABTS and FRAP assay) of the PW (leaves) extracted with methanol and 50% methanol with the EC_{50} value in the range of 48.4 ± 1.83 to 69.7 ± 0.84 µg/mL.[9] Moreover, the methanolic extract of the CG (leaves) was shown to be a potent inhibitor of the ABTS radical with the EC_{50} value of 24.9 µg/mL, consistent with our results.[12]

It is well established that phenolics and flavonoids are classified as free radical scavengers due to their hydroxyl groups bonded to a benzene ring or complex aromatic ring structures.[27] These interesting molecules can interrupt or neutralize the oxidative stress by donating their electrons to free radicals.[28] Our results indicated high content of phenolics and flavonoids in both PWE95 and PWE40 compared to other extracts. In addition, RKNE95 also contained higher phenolics and flavonoids than RKNE40. These findings are in accordance with the results obtained from antioxidant activity assays. Similar outcome was also reported

by several research groups. For instance, the fruit of PW extracted with methanol exhibited the highest phenolic content (75.37 ± 1.75 mg GAE/g) compared to other solvent extracts. This methanolic extract also showed the best DPPH and ABTS radical scavenging activity (EC_{50} values of 46.70 ± 0.85 and 45.23 ± 2.02 µg/mL).[13] By contrast, the methanolic extract of DM which contained low phenolic (46.09 ± 0.4 mg GAE/g extract) and flavonoid content (21.71 ± 0.12 mg rutin equivalent/g extract), resulting in low DPPH and ABTS scavenging activities with the IC_{50} values of 180.97 ± 5.49 and 304.63 ± 25.39 µg/mL), respectively.[15]

In conclusion, this study is the first report to reveal the potential antioxidant ability of the RKN remedy, especially when extracted with 95% ethanol. Among its plant components, the PWE95 displayed the highest antioxidant capacity compared to the others. These results are promising and might support the traditional use of RKN remedy for treatment of psoriatic skin. However, further investigations related to the pathogenesis of psoriasis, as well as preclinical and clinical studies are recommended.

Conflict of interest The author reports no conflicts of interest in this work.

References

1. Pleńkowska J, Gabig-Cimińska M, Mozolewski P. Oxidative Stress as an Important Contributor to the Pathogenesis of Psoriasis. *Int J Mol Sci*. 2020;21(17):6206.
2. Rendon A, Schäkel K. Psoriasis Pathogenesis and Treatment. *Int J Mol Sci*. 2019;20(6):1475.
3. Pual S, Sen S, Nath I, Kumar A, Biswas UK. Psoriasis, An inflammatory condition associated with oxidative stress. *Asian J Med Sci*. 2021;12(4):24-30.
4. Medovic MV, Jakovljevic VL, Zivkovic VI, et al. Psoriasis between Autoimmunity and Oxi-

dative Stress: Changes Induced by Different Therapeutic Approaches. *Oxid Med Cell Longev*. 2022;2022:2249834.

5. Działo M, Mierziak J, Korzun U, Preisner M, Szopa J, Kulma A. The Potential of Plant Phenolics in Prevention and Therapy of Skin Disorders. *Int J Mol Sci*. 2016;17(2):160.

6. Xian D, Guo M, Xu J, Yang Y, Zhao Y, Zhong J. Current evidence to support the therapeutic potential of flavonoids in oxidative stress-related dermatoses. *Redox Rep*. 2021;26(1):134-146.

7. Čižmárová B, Hubková B, Tomečková V, Birková A. Flavonoids as Promising Natural Compounds in the Prevention and Treatment of Selected Skin Diseases. *Int J Mol Sci*. 2023;24(7):6324.

8. Department of Thai Traditional and Alternative Medicine. Nationality Thai Traditional Medicine Formulary Special Edition to Commemorate the Auspicious Occasion of the Coronation of H.M. King Rama X, B.E.2562. Samcharoen Panich (Bangkok) Co., Ltd. 2020:97-98.

9. Cheng Y, Liu Y, Tan J, Sun Y, Guan W, Jiang P, et al. Integrated serum metabolomics and network pharmacology approach to reveal the potential mechanisms of withanolides from the leaves of Datura metel L. on psoriasis. *J Pharm Biomed Anal*. 2020;186:113277.

10. Saelee C, Thongrakard V, Tencomnao T. Effects of Thai medicinal herb extracts with anti-psoriatic activity on the expression of NF-κB signaling biomarkers in HaCaT keratinocytes. *Molecules*. 2011;16(5):3908-3932.

11. Mosaddik MA, Banbury L, Forster P, et al. Screening of some Australian Flacourtiaceae species for in vitro antioxidant, cytotoxic and antimicrobial activity. *Phytomedicine*. 2004;11(5):461-466.

12. Tamuly C, Hazarika M, Bora J, Bordoloi M, Boruah MP, Gajurel PR. In vitro study on antioxidant activity and phenolic content of three Piper species from North East India. *J Food Sci Technol*. 2015;52:117-128.

13. Tamuly C, Hazarika M, Bora J, Gajurel PR. Antioxidant Activities and Phenolic Content of *Piper wallichii* (Miq.) Hand.-Mazz. *Int J Food Prop*. 2014;17:309-320.

14. Klinthong S, Khammanit R, Phornchirasilp S, Temsiririrkkul R, Siriwatanametanon N. In vivo anti-inflammatory and in vitro antioxidant activities of a Thai traditional formula, Rid-si-duang-ma-ha-kan, for hemorrhoid treatment. *Mahidol Univ J Pharm Sci*. 2015;42(3):144-152.

15. Bhardwaj K, Kumar S, Ojha S. Antioxidant activity and FT-IR analysis of Datura innoxia and Datura metel leaf and seed methanolic extracts. *Afr J Tradit Complement Altern Med*. 2016;13(5):7-16.

16. Roland MN, Moussa C, Cristina M, Laurian V, Brânduşa T, Georges O. Antioxidant Capacity and Phenolic Composition of Crateva adansonii DC. (Capparaceae). *Int J Sci Res*. 2018;7(8): 493-497.

17. Yamasaki K, Hashimoto A, Kokusenya Y, Miyamoto T, Sato T. Electrochemical method for estimating the antioxidative effects of methanol extracts of crude drugs. *Chem Pharm Bull (Tokyo)*. 1994;42(8):1663-1665.

18. Re R, Pellegrini N, Proteggente A, Pannala A, Yang M, Rice-Evans C. Antioxidant activity applying an improved ABTS radical cation decolorization assay. *Free Radic Biol Med*. 1999;26(9):1231-1237.

19. Benzie IF, Strain JJ. The ferric reducing ability of plasma (FRAP) as a measure of "antioxidant power" : the FRAP assay. *Anal Biochem*. 1996;239(1):70-76.

20. Folin O, Ciocalteu V. On Tyrosine and tryptophane determinations in proteins. *J Biol Chem*. 1927;73:627-650.

21. Agbor A, Vinson A, Donnelly E. Folin-Ciocalteu reagent for polyphenolic assay. *Int J Food Sci Nutr Diet*. 2014;8:147-156.

22. Zhu H, Wang Y, Liu Y, Xia Y, Tang T. Analysis of flavonoids in Portulaca oleracea L. by UV-Vis spectrophotometry with comparative study on different extraction technologies. *Food Anal Methods*. 2010;3:90-97.

23. Umbert I, Márquez-Kisinousky L, Farrera C, Valls J, Valledor A, Fernández-Fernández L. New Treatment for psoriasis: therapeutic efficiency in patients and antiinflammatory effect in vitro. *Juniper Online J Dermatol Cosmet*. 2020;3(1):6-11.

24. Kedare SB, Singh RP. Genesis and development of DPPH method of antioxidant assay. *J Food Sci Technol*. 2011;48(4):412-422.

25. López-Alarcón C, Denicola A. Evaluating the antioxidant capacity of natural products: a review on chemical and cellular-based assays. *Anal Chim Acta*. 2013;763:1-10.

26. Bibi Sadeer N, Montesano D, Albrizio S, Zengin G, Mahomoodally MF. The Versatility of Antioxidant Assays in Food Science and Safety-Chemistry, Applications, Strengths, and Limitations. *Antioxidants (Basel)*. 2020;9(8):709.

27. Bié J, Sepodes B, Fernandes PCB, Ribeiro MHL. Polyphenols in Health and Disease: Gut Microbiota, Bioaccessibility, and Bioavailability. *Compounds*. 2023;3(1):40-72.

28. Shahidi F, Ambigaipalan P. Phenolics and polyphenolics in foods, beverages and spices: Antioxidant activity and health effects - A review. *J Funct Foods*. 2015;18:820-897.

Original Article

Exploring Antioxidant and Anti-diabetic Activities, and Chemical Contents of Extracts from Thai Traditional Medicine (Pra-Sa-Ka-Phrao Remedies) and Its Plant Ingredients

Theeraphong Ninlaor[1], Arunporn Itharat[2,3*], Srisopa Ruangnoo[2,3], Chadchom Choockong[3], Suchada Naknarin[3], Neal M. Davies[4]

Abstract

Introduction: Pra-Sa-Ka-Phrao complete (PSKPC) remedy is a Thai traditional medicine published in the Thailand National List of Essential Medicines (NLEM). In this research, we have developed a modified version of the remedy, named as Pra-Sa-Ka-Phrao incomplete (PSKPIC), following the FDA Thailand's guidelines for using it as a food supplement. Notably, there is a lack of studies concerning biological activities and chemical constituents of both remedies.

Objectives: This study aimed to investigate and compare the antioxidant and anti-diabetic activities, and chemical contents derived from both remedies and its plant ingredient extracts.

Methods: Extraction was performed by maceration in 95% ethanol and decoction. The antioxidant activity was investigated using a DPPH, ABTS, FRAP, and TBARS assays, while the anti-diabetic (α-amylase, α-glucosidase inhibitory activities) were also evaluated, along with the determination of total phenolic (TPC) and total flavonoid (TFC) contents.

Results: The ethanolic extract of *Zingiber officinale* (ZOE) and water extract of *Ocimum sanctum* (OSW) exhibited the highest antioxidant activity, TPC, and TFC contents. The antioxidant results revealed that the PSKPIC water extract (PSKPICW) showed greater potency than PSKPC water extract in all assays. Additionally, the PSKPICW demonstrated higher TPC and TFC levels compared to the PSKPC remedy. *Glycyrrhiza glabra* (GGE) presented the strongest α-glucosidase inhibitory activity. However, all remedy extracts did not significantly affect anti-diabetic activity.

Conclusions: These results show the efficacy of the PSKPICW remedy, used as food ingredients or food supplements extract, and selected active extracts, such as ZOE and OSW, which supports their use in antioxidant products.

Keywords: Pra-Sa-Ka-Phrao remedy, Antioxidant activity, Anti-diabetic activity, Chemical content, Thai traditional medicine

[1] Student of Doctor of Philosophy Program in Applied Thai Traditional Medicine, Faculty of Medicine, Thammasat University, Pathum Thani, Thailand

[2] Department of Applied Thai Traditional Medicine, Faculty of Medicine, Thammasat University, Pathum Thani, Thailand

[3] Center of Excellence in Applied Thai Traditional Medicine Research (CEATMR), Faculty of Medicine, Thammasat University, Pathum Thani, Thailand

[4] Faculty of Pharmacy and Pharmaceutical Sciences, University of Alberta, Edmonton, Canada

* **Corresponding author:** Arunporn Itharat, Ph.D., Department of Applied Thai Traditional Medicine and Center of Excellence in Applied Thai Traditional Medicine Research (CEATMR), Faculty of Medicine, Thammasat University, Pathum Thani, Thailand Email: iarunporn@yahoo.com, iarunporn@gmail.com; Tel. +66 2926 9749

Introduction

Oxidative stress is a primary driver of cell and tissue damage that underpins the development of non-communicable diseases (NCDs) by life-style-associated activation.[1] NCDs have been well documented and studied, and some standard vital features have been identified; these include the intracellular presence of oxidative stress due to abnormal production of reactive oxidative species (ROS), inadequate antioxidant defense, and dysregulation of the autophagy pathway, which is responsible for the maintenance of cellular proteostasis and hyperglycemia.[2,3] Moreover, lipid peroxidation is one of the markers for oxidative stress; it also plays a crucial role in necrotic and apoptotic processes.[4]

Pra-Sa-Ka-Phrao (PSKP) remedy is a Thai traditional medicine published in Thailand National List of Essential Medicines (NLEM). It has long been used to treat flatulence and colic pain. It has a spicy taste and contains eight medicinal plants, including *Ocimum sanctum* L., *Citrus hystrix* DC., *Glycyrrhiza glabra* L., *Ferula assafoetida* L., *Piper nigrum* L., *Zingiber officinale* Roscoe, *Piper retrofractum* Vahl and *Allium sativum* L.

Half of the remedy's composition consists of *Ocimum sanctum* and the other half features other plants, with proportions shown in Table 1. In this study, the original remedy was named Pra-Sa-Ka-Phrao complete (PSKPC). Since the Food and Drug Administration of Thailand (FDA) implements certain regulation concerning the use of plants as food supplements, and the latest list issued by the FDA has excluded *Citrus hystrix*, *Ferula assafoetida*, and *Piper retrofractum*.[5,6] Consequently, we prepared the remedy without these three plants and named it Pra-Sa-Ka-Phrao incomplete remedy (PSKPIC) with proportions as shown in Table 1.

In previous studies, all plant ingredients of Pra-Sa-Ka-Phrao remedy showed antioxidant and antidiabetic activities. Notably, *Ocimum sanctum* possessed antidiabetic and anti-oxidant activities.[7] *Citrus hystrix* displayed antioxidant activity,[8] and *Glycyrrhiza glabra* showed activity against hyperglycemia, hyperlipidemia, and associated oxidative stress.[9] Furthermore, *Zingiber officinale* contained antioxidants,[10,11] and *Piper retrofractum* also demonstrated antioxidant activity.[12]

PSKP remedy has the potential for being developed as dietary supplement for the treatment of diabetes mellitus and NCDs patients. However, studies have yet to be conducted on the biological activities and chemical contents of the Pra-Sa-Ka-Phrao remedy. Therefore, this study aimed to investigate and compare antioxidant and antidiabetic activities and chemical contents of complete and incomplete PSKP remedies and its plant ingredient extracts.

Methods
Plant materials and extraction method

The plant ingredients were purchased from different sources in 2019. The identification of plants was carried out by the Herbarium of Southern Center of Thai Medicinal Plants at the Faculty of Pharmaceutical Science, Prince of Songkla University, Songkhla province, Thailand (Table 1). All dried plant materials were cleaned and grinded into coarse powder. The crude powders were extracted by maceration in 95% ethanol at room temperature (RT) for 3 days, then filtered and the process repeated twice. The combined filtrates were evaporated by rotary evaporator at 45 °C. Furthermore, a decoction in distilled water at boiling point for 15 minutes was conducted three times (3×1 L, for each time), filtered and freeze-dried using a lyophilizer. All crude extracts were kept in a freezer (-20 °C) until used.

Table 1 Plant ingredients of Pra-Sa-Ka-Phrao remedies.

Scientific name	Family	Code	Voucher specimen number	Part used	PSKPC* (%w/w)	PSKPIC* (%w/w)
Ocimum sanctum L.	LABIATAE	OS	SKP 095 15 19 01	Leaf	50.00	75.00
Citrus hystrix DC.	RUTACEAE	CH	SKP 166 03 08 01	Peel	22.22	-
Glycyrrhiza glabra L.	LEGUMINOSAE	GG	SKP 072 07 07 01	Root	8.90	13.33
Ferula assafoetida L.	UMBELLIFERAE	FA	SKP 199 06 01 01	Resin	8.90	-
Piper nigrum L.	PIPERACEAE	PN	SKP 146 16 14 01	Fruit	2.22	3.33
Zingiber officinale Roscoe	ZINGIBERACEAE	ZO	SKP 206 26 15 01	Rhizome	2.22	3.33
Piper retrofractum Vahl	PIPERACEAE	PR	SKP 146 16 03 01	Fruit-spike	2.22	-
Allium sativum L.	LILIACEAE	AS	SKP 006 01 19 01	Bulb	2.22	3.33
Sodium chloride	-	-	-	-	1.10	1.68

* PSKPC means Pra-Sa-Ka-Phrao remedy (complete) and PSKPIC means Pra-Sa-Ka-Phrao remedy (incomplete).

Preparation
***In vitro* assay for antioxidant activities**
DPPH radical scavenging assay

The scavenging effect on the DPPH radical was conducted according to Yamasaki et al., 1994.[13] The ethanolic extracts were dissolved in absolute ethanol, and the water extracts were dissolved in sterile water at different concentrations (1, 10, 50, 100 µg/mL). A 100 µL of sample solution was added into 96-well microplates, and 100 µL of DPPH solution was placed into each well. Solution control was absolute ethanol and distilled water, each 100 µL with DPPH 100 µL, and incubated for 30 minutes in the dark at RT. Finally, the absorbance was measured at 520 nm using a microplate reader. The Prism program calculated the EC_{50} values. The positive control was butylated hydroxytoluene (BHT).

$$\% \text{ Inhibition} = \frac{OD_{control} - OD_{sample}}{OD_{control}} \times 100$$

Where $OD_{control}$ was the optical density of solvent without sample solution, OD_{sample} was the optical density of sample solution and the EC_{50} value was calculated by the prism software.

ABTS radical scavenging assay

ABTS radical scavenging was determined according to the modified method of Re et al., 1999.[14] The ABTS⁺ working solution was added to a microcentrifuge tube (1,000 µL), followed by 10 µL of Standard (final concentration of Trolox 0.1-20 µM, sample 100 µg/mL) or Blank (ultra-pure

water). After mixing and incubation in the dark at RT for 6 min, the absorbance of the solution was measured at 734 nm.

The percentage of inhibition was calculated as the follow formular:

$$\% \text{ Inhibition} = \frac{OD_{control} - (OD_{sample} - OD_{negative})}{OD_{control}} \times 100$$

Where $OD_{control}$ was the optical density of solvent without sample solution, OD_{sample} was the optical density of sample solution, $OD_{negative}$ was the optical density of sample solution without ABTS⁺ solution and the IC_{50} value was calculated by the prism software.

FRAP radical scavenging assay

The FRAP radical scavenging assay was determined by a modified method of Benzie and Szeto, 1999.[15] 20 µL of Standard (The final concentration of Trolox 5-300 µg/mL, ferrous sulphate ($FeSO_4$) 5-800 µg/mL, and sample (100 µg/mL) or Blank (distilled water) were added to 96-well microplates, followed by 180 µL of FRAP reagent (incubated at 37°C for 4 min before use). After incubating at RT for 8 min, the absorbance of the solution was measured at 593 nm, using FRAP working solution as Blank. The reading of relative absorbance should be within the range of 0-2.0; otherwise, the sample should be diluted. The antioxidant potential was determined from a standard curve plotted using Trolox or $FeSO_4 \cdot 7H_2O$ linear regression equation to calculate the FRAP values of the sample.

Assay of thiobarbituric acid reactive substances (TBARS)

TBARS assay was determined by a modified method of Ruberto and Baratta, 2000.[16] 50 µL of sample solution was added into the sample centrifuge tube, and 50 µL of sample solvent (DI/Abs.EtOH) was added into the full reaction mixture (FRM) tube. Then, 25 µL of PBS was added into each tube. After that, 1,250 µL of 2% intralipid was added into each tube (without blank (BLK) sample, PBS 1,250 µL was added). 25 µL of DI was added into BLK FRM and BLK sample, and 25 µL of $FeSO_4 \cdot 7H_2O$ was added into FRM and each sample was incubated at 37 °C for 20 minutes in a water bath. 1,000 µL of 0.6 w/v TBA in 20% w/v TCA was added into each tube and heated in a water bath at 95 °C for 30 min, then the reaction was stopped in a cooled ice bath for around 10 min. 2,500 µL of butanol was added, mixed and centrifuged at 5,000 g 25 °C for 20 minutes. The butanol fraction's upper layer was removed and 200 µL pipetted into the 96-well plate, then optical absorbance was determined at 532 nm. BHT was used as a positive control, and butanol as a Blank.

The percentage of inhibition was calculated using the following equation:

$$\% \text{ Inhibition} = \frac{(\text{FRM} - (\text{ST} - \text{SA}))}{\text{FRM}} \times 100$$

Where FRM was the optical density of full reaction mixture, ST was the optical density of sample test mixture, SA was the optical density of sample alone and the IC_{50} value was calculated by the prism software.

In vitro assay for anti-diabetic activities
In vitro alpha-amylase inhibitory assay

According to some modifications of Yuan, et al. (2018),[17] 100 µL sample solution (10 mg/mL), ethanolic extracts were dissolved in dimethyl sulf-oxide (DMSO), and water extracts were dissolved in ultra-pure water. Then, it was mixed with 100 µL of a substrate (starch solution 1% w/w) in 20 mM phosphate buffer pH 6.9 containing 6.7 mM sodium chloride and pre-incubate at 37 °C for 10 min in a water bath. 100 µL of alpha-amylase enzyme (1 mg/mL) in buffer pH 6.9 was added and the Blank was added to buffer pH 6.9 and incubated in a water bath at 37 °C for 10 min. The reaction was stopped by adding 200 µL of dinitro salicylic acid (DNSA) reagent and heating 95 °C for 5 minutes in a heated box. Then, it was placed on an ice bath for 5 minutes. 50 µL of solution mixture was removed and placed into a 96-well plate and diluted with 200 µL ultra-pure water, then optical absorbance was determined at 540 nm. Acarbose was used as a positive control.

In vitro alpha-glucosidase inhibitory assay

A slight modification of the method of Wongnawa, et al. (2014) was conducted for inhibitory activity on alpha-glucosidase.[18] 20 µL of sample extract (50 mg/mL), 80 µL of phosphate buffer (pH 6.8), and 50 µL of the substrate 5 mM p-nitro-phenyl alpha-D-glucopyranoside (p-NPG) in phosphate buffer, a blank phosphate buffer pH 6.8, was added and pre-incubated at 37 °C for 15 min. After pre-incubation, 50 µL of alpha-glucosidase (0.15 unit/mL) was added; blank phosphate buffer pH 6.8 was added and then incubated at 37 °C for 15 min. The reaction was stopped by adding 100 µL of 1 M Na_2CO_3. The release of p-nitrophenol was measured at 405 nm. Acarbose was used as a positive control.

The percentage inhibition of both alpha-amylase and alpha-glucosidase were calculated as the follow formular:

$$\% \text{ Inhibition} = \frac{(\text{OD}_{control} - \text{OD}_{sample})}{\text{OD}_{control}} \times 100$$

Where $\text{OD}_{control}$ was the optical density of solvent without sample solution, OD_{sample} was the optical density of sample solution and the IC_{50} value was calculated by the prism software.

Chemical contents
Determination of total phenolic content

The total phenolic content was determined according to modified Folin-Ciocalteu's method.[19] 20 µL of the sample solution was pipetted into a 96-well microplate and then, 100 µL of Folin-Ciocalteu's reagent was added into the well, and 80 µL of a sodium carbonate solution was added in the last step. After that, the 96-well plate was kept at RT for 30 minutes. The absorbance was measured at 765 nm. The total phenolic content was expressed as gallic acid equivalent (GAE) in milligrams per gram of dry material.

Determination of total flavonoid content

 The following method, with slight modification of Zhu, et al. (2009), was conducted to determine total flavonoids in extracts.[20] Sample (1 mg/mL) of 500 µL was mixed with 75 µL of sodium nitrite (5% w/v) and 150 µL of AlCl$_3$ (10% w/v) and incubated at RT for 5 min. Then 500 µL of 1 M NaOH solution was added and 275 µL of distilled water placed in a centrifuge tube, incubated for 30 minutes at RT and transferred 200 µL to a 96-well microplate. Finally, the absorbance was measured at 510 nm. Absolute ethanol and distilled water were used as a Blank for the ethanolic and water extracts. The total flavonoid content was expressed as milligram quercetin equivalents (QE)/g dry extract.

Data and Statistical Analysis

 All determinations were expressed as the means ± SEM (standard error of mean) of three independent samples in triplicate. The value of EC$_{50}$ and IC$_{50}$ was calculated using GraphPad Prism 8. Linear regression to correlate the total phenolics and total flavonoids was carried out using Microsoft Excel 2019. The differences among the mean values from at least two independent experiments were analyzed with the GraphPad Prism 8, one-way ANOVA. Significant differences were considered statistically significant at the level of p-value < 0.05.

Results
In vitro assay for antioxidant activities
DPPH radical scavenging assay

 The results are depicted in Table 2. The PSKPICW remedy showed high antioxidant activity with an EC$_{50}$ value of 18.06 ± 0.36 µg/mL, while the EC$_{50}$ value of the PSKPCW remedy was 32.69 ± 1.59 µg/mL. OSW demonstrated DPPH scavenging activity with an EC$_{50}$ value of 8.93 ± 0.50 µg/mL better than positive control, BHT (EC$_{50}$ = 16.22 ± 1.03 µg/mL). In addition, 95% ethanolic extracts of PSKPICE and PSKPCE remedies showed EC$_{50}$ of 52.88 ± 1.86 and 65.65 ± 1.52 µg/mL, respectively. The ZOE also showed higher antioxidant activity than BHT (EC$_{50}$ of ZOE = 9.56 ± 0.15 µg/mL).

ABTS radical cation scavenging assay

 The PSKPICW remedy had the highest scavenging activity at 43.44 ± 2.32 µg/mL when compared with standard Trolox (IC$_{50}$ = 14.68 ± 0.82 µg/mL). In contrast, the PSKPCW remedy showed an IC$_{50}$ value of 73.73 ± 1.38 µg/mL. The OSW showed scavenging activity with IC$_{50}$ values of 32.86 ± 2.72 µg/mL. While the PSKPCE and PSKPICE remedies showed IC$_{50}$ values of 62.83 ± 0.66 and 88.75 ± 1.65 µg/mL, respectively. The ZOE (IC$_{50}$ = 8.98 ± 0.20 µg/mL) showed stronger scavenging activity than Trolox (Table 2).

Ferric reducing / antioxidant power (FRAP) assay

 The ethanolic extracts showed FRAP values ranging from 4.06 ± 1.80 to 839.68 ± 10.17 mg Fe^{2+} equivalent/g extract. The PSKPCE and PSKPICE remedies showed high antioxidant activity with FRAP values of 183.17± 1.26 and 145.65 ± 6.55 mg Fe^{2+} equivalent/g extract, respectively. The ZOE showed the highest antioxidant activity (FRAP values = 839.68 ± 10.17 mg Fe^{2+} equivalent/g extract). For the aqueous extracts, FRAP values ranged from 7.84 ± 2.19 to 383.47 ± 13.22 mg Fe^{2+} equivalent/g extract; the PSKPCW and PSKPICW remedies showed antioxidant activity with FRAP values of 172.59 ± 5.72 and 261.54 ± 5.66 mg Fe^{2+} equivalent/g extract, respectively. The OSW showed the highest antioxidant activity of 383.47 ± 13.22 mg Fe^{2+} equivalent/g extract (Table 2).

 The trolox equivalent antioxidant capacity (TEAC), the ethanolic extracts showed FRAP values ranging from 0.35 ± 0.02 to 342.17 ± 6.30 mg Trolox equivalent/g extract, and water extracts showed TEAC values ranging from 2.26 ± 0.67 to 147.63 ± 4.85 mg trolox equivalent/g extract (Table 2).

Determination of lipid peroxidation on thiobarbituric acid reactive substances (TBARS) assay

 The results are presented in Table 2. The PSKPCE and PSKPICE remedies showed IC$_{50}$ of 1.02 ± 0.02 and 4.99 ± 0.69 µg/mL, respectively, followed by the OSE showed higher lipid peroxidation inhibitory activity than BHT as a positive control (IC$_{50}$ = 2.33 ± 0.31 µg/mL) while IC$_{50}$ value of BHT as 3.36 ± 0.09 µg/mL. The PSKPCW remedy showed high antioxidant activity with an IC$_{50}$ value of 1.18 ± 0.15 µg/mL, while the IC$_{50}$ value of the PSKPICW remedy was 8.23 ± 0.52 µg/mL. The OSW, with IC$_{50}$ values of 1.04 ± 0.01 µg/mL, showed higher antioxidant activity than BHT.

Determination of *In vitro* assay for anti-diabetic activities
***In vitro* alpha-amylase and alpha-glucosidase inhibitory assay**
    The results of the alpha-amylase and alpha-glucosidase inhibitory activity inhibitory activity are showed in Table 3. The finding revealed that all sample solutions at a concentration of 1,000 µg/mL demonstrated no significant effect on alpha-amylase activity ($IC_{50} > 1,000$ µg/mL) when compared to the positive control, acarbose ($IC_{50} = 39.19 \pm 0.38$ µg/mL), for both the ethanolic and water extracts. Regarding alpha-glucosidase inhibition, GGE and ASE exhibited stronger activity with IC_{50} values of 39.37 ± 1.55 µg/mL and 109.46 ± 4.84 µg/mL, respectively, better than the positive control, acarbose ($IC_{50} = 215.75 \pm 1.40$ µg/mL). CHE and CHW showed moderate activity with IC_{50} values of 599.39 ± 13.26 and $2,579.93 \pm 48.71$ µg/mL, respectively.

Determination of chemical contents
Determination of total phenolic content by using Folin-Ciocalteau's reagent
    The ethanolic extracts range from 37.03 ± 2.87 to 178.20 ± 1.86 mg GAE/g extract, the PSKPCE and PSKPICE remedies showed a total phenolic content of 59.37 ± 0.37 and 57.02 ± 0.35 mg GAE/g extract, and the ZOE showed the highest total phenolic contents of 178.20 ± 1.86 mg GAE/g extract. The water extracts range from 3.33 ± 1.16 to 115.64 ± 2.60 mg GAE/g extract, the PSKPCW and PSKPICW remedies showed a total phenolic content of 55.79 ± 1.23 and 83.19 ± 1.67 mg GAE/g extract, respectively, and OSW showed the highest total phenolic contents of 115.64 ± 2.60 mg GAE/g extract (Table 2).

Determination of total flavonoid content by using aluminum chloride ($AlCl_3$) colorimetric method
    The ethanolic extracts range from 96.13 ± 3.83 to 816.90 ± 4.35 mg QE/g extract, PSKPCE and PSKPICE remedies showed a total flavonoid content of 202.58 ± 1.22 and 192.79 ± 2.06 mg QE/g extract, respectively. The ZOE showed the highest total flavonoid contents of 816.90 ± 4.35 mg QE/g extract. The water extracts range from 85.14 ± 4.83 to 470.58 ± 3.60 mg QE/g extract, PSKPCW and PSKPICW remedies showed a total flavonoid content of 225.40 ± 1.72 and 334.77 ± 4.93 mg QE/g extract, respectively. The OSW showed the highest total flavonoid contents of 470.58 ± 3.60 mg QE/g extract (Table 2).

Table 2 Antioxidant activities (DPPH, ABTS, FRAP and TBARS assay) and chemical contents (total phenolic and flavonoid contents) of PSKP remedies and its plant ingredient extracts (mean ± SEM, n = 3).

Botanical name (Thai name)	CODE	DPPH EC_{50} (μg/mL)	ABTS IC_{50} (μg/mL)	FRAP mg Fe^{2+} eq./g1	FRAP mg Trolox eq./g2	TBARS IC_{50} (μg/mL)	TPC mg GAE/g3	TFC mg QE/g4
Ocimum sanctum (Ka-Phrao-Daeng)	OSE	31.21 ± 2.38*	98.47 ± 0.90*	165.43 ± 4.63	62.37 ± 1.95	2.33 ± 0.31	53.60 ± 1.15	215.97 ± 3.23
	OSW	8.93 ± 0.50	32.86 ± 2.72*	383.47 ± 13.22	147.63 ± 4.85	1.04 ± 0.01	115.64 ± 2.60	470.58 ± 3.60
Citrus hystrix (Ma-Krut)	CHE	>100*	85.56 ± 0.62*	126.15 ± 6.84	47.27 ± 0.70	14.29 ± 1.69*	48.98 ± 0.50	242.77 ± 2.02
	CHW	>100*	>100*	83.05 ± 4.52	30.10 ± 0.62	15.35 ± 1.99*	42.06 ± 0.58	121.69 ± 3.74
Glycyrrhiza glabra (Cha-Em-Thet)	GGE	58.75 ± 3.00*	43.10 ± 2.00*	154.18 ± 7.28	57.10 ± 4.36	7.07 ± 1.11	61.62 ± 2.40	234.48 ± 4.96
	GGW	>100*	>100*	13.11 ± 2.07	3.18 ± 0.26	33.27 ± 2.33*	14.46 ± 1.16	103.78 ± 4.75
Ferula assafoetida (Ma-Ha-Hing)	FAE	>100*	>100*	4.06 ± 1.80	0.35 ± 0.02	2.51 ± 0.24	42.08 ± 1.41	96.13 ± 3.83
	FAW	>100*	>100*	7.84 ± 2.19	2.26 ± 0.67	1.10 ± 0.04	3.33 ± 1.16	105.77 ± 0.66
Piper nigrum (Phrik-Thai-Lon)	PNE	94.96 ± 1.97*	>100*	185.69 ± 5.92	71.48 ± 4.27	>100*	68.49 ± 0.78	167.93 ± 1.96
	PNW	>100*	>100*	15.08 ± 2.80	3.76 ± 0.13	>100*	11.25 ± 0.94	100.29 ± 4.52
Zingiber officinale (Khing)	ZOE	9.56 ± 0.15	8.98 ± 0.20	839.68 ± 10.17	342.17 ± 6.30	5.17 ± 0.50	178.20 ± 1.86	816.90 ± 4.35
	ZOW	66.63 ± 1.00*	91.41 ± 0.16*	88.61 ± 5.29	32.28 ± 0.15	11.68 ± 1.71*	33.32 ± 0.63	143.04 ± 4.41
Piper retrofractum (Di-Pli)	PRE	>100*	>100*	87.12 ± 9.81	38.87 ± 4.83	>100*	37.03 ± 2.87	225.12 ± 2.55
	PRW	89.39 ± 1.97*	>100*	62.90 ± 4.54	22.04 ± 1.09	>100*	30.76 ± 0.68	114.14 ± 4.83
Allium sativum (Kra-Thiam)	ASE	>100*	>100*	60.33 ± 0.78	21.23 ± 1.33	15.28 ± 2.42*	41.97 ± 3.00	105.74 ± 3.24
	ASW	>100*	>100*	21.93 ± 3.56	6.62 ± 0.21	4.80 ± 1.43	13.84 ± 1.17	85.14 ± 4.83
Pra-Sa-Ka-Phrao remedy (Complete)	PSKPCE	65.65 ± 1.52*#	62.83 ± 0.66*#	183.17 ± 1.26	70.60 ± 4.19	1.02 ± 0.02	59.37 ± 0.37	202.58 ± 1.22
	PSKPCW	32.69 ± 1.59*#	73.73 ± 1.38*#	172.59 ± 5.72#	65.98 ± 2.49#	1.18 ± 0.15	55.79 ± 1.23#	225.40 ± 1.72#
Pra-Sa-Ka-Phrao remedy (Incomplete)	PSKPICE	52.88 ± 1.86*#	88.75 ± 1.65*#	145.65 ± 6.55	56.85 ± 4.77	4.99 ± 0.69	57.02 ± 0.35	192.79 ± 2.06
	PSKPICW	18.06 ± 0.36#	43.44 ± 2.32*#	261.54 ± 5.66#	104.32 ± 1.62#	8.23 ± 0.52	83.19 ± 1.67#	334.77 ± 4.93#
Positive control	BHT	16.22 ± 1.03	NT	NT	NT	3.36 ± 0.09	NT	NT
	Trolox	NT	14.68 ± 0.82	NT	NT	NT	NT	NT

Note; 1 mean (y = 0.004x+0.01299, R2 = 0.9997), 2 mean (y = 0.0094x+0.01588, R2 = 0.9998), 3 mean (y = 0.0045x+0.0146, R2 = 0.9992), 4 mean (y = 0.0009x-0.0189, R2 = 0.9997). (NT) means not tested. E means ethanolic extract and W means water extract. BHT and Trolox as positive controls (* Significant difference: $p < 0.05$ vs BHT and Trolox; #: $p < 0.05$ vs complete and incomplete remedies). Data were analyzed by using one-way ANOVA.

Table 3 IC$_{50}$ of alpha-amylase and alpha-glucosidase inhibitory activities of PSKP remedies and its plant ingredient extracts (n = 3).

Botanical name (Thai name)	CODE	IC$_{50}$ (µg/mL; mean ± SEM)	
		Alpha-amylase inhibitory activity	Alpha-glucosidase inhibitory activity
Ocimum sanctum	OSE	>1,000*	>1,000*
(Ka-Phrao-Daeng)	OSW	>1,000*	>500*
Citrus hystrix	CHE	>1,000*	599.39 ± 13.26*
(Ma-Krut)	CHW	>1,000*	2,579.93 ± 48.71*
Glycyrrhiza glabra	GGE	>1,000*	39.37 ± 1.55*
(Cha-Em-Thet)	GGW	>1,000*	>3,000*
Ferula assafoetida	FAE	>1,000*	>3,000*
(Ma-Ha-Hing)	FAW	>1,000*	>3,000*
Piper nigrum	PNE	>1,000*	>1,500*
(Phrik-Thai-Lon)	PNW	>1,000*	>3,000*
Zingiber officinale	ZOE	>1,000*	>1,500*
(Khing)	ZOW	>1,000*	>3,000*
Piper retrofractum	PRE	>1,000*	>1,500*
(Di-Pli)	PRW	>1,000*	>3,000*
Allium sativum	ASE	>1,000*	109.46 ± 4.84*
(Kra-Thiam)	ASW	>1,000*	>3,000*
Pra-Sa-Ka-Phrao remedy	PSKPCE	>1,000*	>1,000*
(Complete)	PSKPCW	>1,000*	>1,000*
Pra-Sa-Ka-Phrao remedy	PSKPICE	>1,000*	>1,000*
(Incomplete)	PSKPICW	>1,000*	>1,000*
Acarbose		39.19 ± 0.38	215.75 ± 1.40

Note;   E means Ethanolic extract and W means Water extract. Acarbose as positive control (* Significant difference: $p < 0.05$ vs Acarbose; #: $p < 0.05$ vs complete and incomplete remedies). Data were analyzed by using one-way ANOVA.

Discussion

PSKP remedy, a Thai traditional medicine included in the NLEM of Thailand for anti-flatulent and carminative properties in children. This study found that PSKP remedy exhibited the highest activity on anti-oxidant activity, however, it showed no effectiveness against alpha-amylase and alpha-glucosidase. Interestingly, both PSKP remedies and its plant ingredients demonstrated a potent effect in inhibiting lipid peroxidation through the inhibition of TBARS formation, except for PN and PR. The PSKPC extracts also showed a superior inhibitory effect compared to PSKPIC extracts, suggesting that the plant ingredients in the complete remedy, particularly CH and FA, also played an essential role in this activity. The inhibitory effect on TBARS relate to lipid peroxidation and malondialdehyde (MDA). TBARS are formed as a by-product of lipid peroxidation and MDA is one of several end products formed by the decomposition of lipid peroxidation products, serving as a marker of oxidative stress.[21] Therefore, inhibition of TBARS formation may result from the reduction of lipid peroxidation, which could lead to a decrease in MDA level. This finding represents the first research, indicating that PSKP and its plant ingredients exhibited significant potential as lipid peroxidation inhibitors. Further studies should be investigated to explore the under-

lying mechanisms and conduct *in vivo* studies for a more comprehensive understanding.

Regarding the radical scavenging activities, both PSKP extracts exhibited moderate scavenging activities against both DPPH and ABTS$^{\bullet+}$ radicals, except for PSKPICW, which showed strong scavenging activity on DPPH radical. OSW and ZOE also exhibited potent scavenging activities. The aqueous extract of OS exhibited higher activity than the ethanol extract, and the aqueous extract of PSKP also showed similar results. This indicated that DPPH and ABTS$^{\bullet+}$ scavenging activities of PSKP extracts relate to the OS. Our radical scavenging results of OS related to previous studies, which showed potent DPPH and ABTS$^{\bullet+}$ scavenging activities with EC_{50} not more than 20 µg/mL.[22] For ZO rhizome, a previous study of Ali et al., 2018 showed potent DPPH scavenging activity with IC_{50} value of 8.29 ± 1.73 µg/mL,[23] as well as ABTS•+, ZO presented a strong activity with an IC_{50} value of 0.81 µg/mL.[24]

Additionally, we found that the FRAP and TEAC values showed a similar trend to the scavenging activity. PSKPICW showed the highest FRAP and TEAC, while OSW and ZOE demonstrated higher values than other plant extracts. Our results were consistent with previous *in vitro* studies conducted in 95% ethanol extract of red holy basil (OS) presented higher antioxidant activity than white holy basil for both TEAC and FRAP values.[25] In addition, the FRAP assay of the rhizomes of ZO displayed a potent antioxidant capacity expressed as trolox equivalents.[26]

Both PSKP remedies lack inhibitory activity on alpha-amylase and alpha-glucosidase, as well as their plants ingredients, except CH, GG and AS. The ethanolic extract of GG and AS demonstrated stronger alpha-glucosidase inhibitory activity than the positive control, acarbose, whereas CHE showed moderate activity. Previous research has demonstrated that both GG methanolic and aqueous extracts inhibited enzyme alpha-amylase and alpha-glucosidase activities.[27,28] Interestingly, AS displayed significant results in rat everted intestinal sac experiments, showing the increasing of glucose uptake and reduction in all observed parameters. In addition, treatment with aged garlic extract positively reversed the diabetic changes in the targeted parameters to levels significantly lower than those measured in the control diabetic group.[29,30]

With regard to TPC and TFC, most of the PSKP extracts showed comparable TPC, except for the aqueous PSKPIC extract, which presented the highest TPC. Moreover, the aqueous extracts of PSKPC and PSKPIC showed higher flavonoid contents compared to the ethanolic extracts. Among the plant ingredients, ZOE demonstrated the highest TPC and TFC, followed by OSW. Interestingly, ZOE showed potent activity against DPPH, ABTS and TBARS, whereas, OSW showed better inhibitory effect on TBARS but lesser effect on DPPH and ABTS. These results suggested that the compounds in OSW specifically affected inhibitory activity on TBARS, while ZOE excelled in ABTS. However, ZOE still retained potent activity on TBARS with IC_{50} less than 10 µg/mL. When considering PSKP, the extracts showed potent activity on TBARS, highlighting the significance of OS in the remedies. In addition, although the ethanolic extract of CH, GG and PR showed comparable TPC and TFC to both the aqueous and ethanol extracts of PSKPC, they showed lesser effects on TBARS. These results indicated that the phenolic and flavonoid compounds in these plants did not specifically inhibit the lipid peroxidation.

In conclusion, this study investigated the biological activities of the PSKP remedy for the first time. We also modified the remedy according to the FDA plant list for use as a food supplement, assessing a comparison to the original formula. Our findings indicated that both original (complete; PSKPC) and modified (incomplete; PSKPIC) remedies exhibited potent inhibitory effect on TBARS formation, but the original remedy showed superior activity compared to the modified one. Therefore, the effect of PSKP remedy on insight into the mechanism of lipid peroxidation should be investigated. Detailed phytochemistry analysis should be conducted to identify compounds serving as markers,as well as to develop products for oxidative stress reduction.

Compliance with Ethics Requirements. Not applicable.

Author Contributions. Conceptualization, A.I., S.R. and T.N.; methodology, A.I. and S.R.; formal analysis, N.M.D., A.I. and T.N.; investigation, T.N., S.N. and C.C.; data curation, T.N. and A.I.; writing—original draft preparation, A.I., N.M.D., T.N. and S.R.; writing—review and editing, N.M.D. and A.I.; funding acquisition, A.I. All authors have read and agreed to the published version of the manuscript.

References

1. Seyedsadjadi N, Grant R. The Potential Benefit of Monitoring Oxidative Stress and Inflammation in the Prevention of Non-Communicable Diseases (NCDs). *Antioxidants*. 2020;10(1):15.
2. Peña-Oyarzun D, Bravo-Sagua R, Diaz-Vega A, et al. Autophagy and oxidative stress in non-communicable diseases: A matter of the inflammatory state? *Free Radic Biol Med*. 2018;124:61-78.
3. Burgos-Morón, Abad-Jiménez, Marañón, et al. Relationship Between Oxidative Stress, ER Stress, and Inflammation in Type 2 Diabetes: The Battle Continues. *J Clin Med*. 2019;8(9):1385.
4. Angelova PR, Esteras N, Abramov AY. Mitochondria and lipid peroxidation in the mechanism of neurodegeneration: Finding ways for prevention. *Med Res Rev.* 2020;41(2):770-784.
5. The Thai Food and Drug Administration. *A list of the plants allowed for food supplement 2017*. Bangkok: The Thai Food and Drug Administration; 2017 Aug 7:1-53. https://food.fda.moph.go.th/media.php?id=509562086569943040&name=PlantName. Published 2017. Accessed February 18, 2019.
6. The Thai Food and Drug Administration. *A list of the plants allowed for food supplement (No.2)*. Bangkok: The Thai Food and Drug Administration; 2018 Aug 22:1-10. https://food.fda.moph.go.th/media.php?id=509583079023714304&name=PlantName_2. Published 2018. Accessed February 18, 2019.
7. Suanarunsawat T, Anantasomboon G, Piewbang C. Anti-diabetic and anti-oxidative activity of fixed oil extracted from *Ocimum sanctum* L. leaves in diabetic rats. *Exp Ther Med*. 2016;11(3):832-840.
8. Warsito W, Noorhamdani N, Sukardi S, Suratmo S. Assessment of antioxidant activity of citronellal extract and fractions of essential oils of *Citrus hystrix* DC. *Trop J Pharm Res*. 2018;17(6):1119.
9. Sen S, Roy M, Chakraborti AS. Ameliorative effects of glycyrrhizin on streptozotocin-induced diabetes in rats. *J Pharm Pharmacol*. 2011;63(2):287-296.
10. Yousfi F, Abrigach F, Petrovic JD, Sokovic M, Ramdani M. Phytochemical screening and evaluation of the antioxidant and antibacterial potential of *Zingiber officinale* extracts. *S Afr J Bot*. 2021;142:433-440.
11. Ghafoor K, Al Juhaimi F, Özcan MM, Uslu N, Babiker EE, Mohamed Ahmed IA. Total phenolics, total carotenoids, individual phenolics and antioxidant activity of ginger (*Zingiber officinale*) rhizome as affected by drying methods. *LWT*. 2020;126:109354.
12. Jadid N, Hidayati D, Hartanti SR, Arraniry BA, Rachman RY, Wikanta W. Antioxidant activities of different solvent extracts of *Piper retrofractum* Vahl. using DPPH assay. *AIP Conf Proc*. 2017;1854(1):020019.
13. Yamasaki K, Hashimoto A, Kokusenya Y, Miyamoto T, Sato T. Electrochemical Method for Estimating the Antioxidative Effects of Methanol Extracts of Crude Drugs. *Chem Pharm Bull*. 1994;42(8):1663-1665.
14. Re R, Pellegrini N, Proteggente A, Pannala A, Yang M, Rice-Evans C. Antioxidant activity applying an improved ABTS radical cation decolorization assay. *Free Radic Biol Med*. 1999;26(9-10):1231-1237.

15. Benzie IFF, Szeto YT. Total Antioxidant Capacity of Teas by the Ferric Reducing/Antioxidant Power Assay. *J Agric Food Chem*. 1999;47(2):633-636.

16. Ruberto G, Baratta MT. Antioxidant activity of selected essential oil components in two lipid model systems. *Food Chem*. 2000;69(2):167-174.

17. Yuan G, Li W, Pan Y, Wang C, Chen H. Shrimp shell wastes: Optimization of peptide hydrolysis and peptide inhibition of α-amylase. *Food Biosci*. 2018;25:52-60.

18. Wongnawa M, Tohkayomatee R, Bumrungwong N, Wongnawa S. Alpha-glucosidase inhibitory effect and inorganic constituents of *Phyllanthus amarus* Schum. & Thonn. ash. *Songklanakarin J Sci Technol*. 2014;36(5):541-546.

19. Miliauskas G, Venskutonis PR, van Beek TA. Screening of radical scavenging activity of some medicinal and aromatic plant extracts. *Food Chem*. 2004;85(2):231-237.

20. Zhu H, Wang Y, Liu Y, Xia Y, Tang T. Analysis of Flavonoids in *Portulaca oleracea* L. by UV-Vis Spectrophotometry with Comparative Study on Different Extraction Technologies. *Food Anal Methods*. 2009;3(2):90-97.

21. Catalán V, Frühbeck G, Gómez-Ambrosi J. Inflammatory and oxidative stress markers in skeletal muscle of obese subjects. *Obesity*. 2018:163-189.

22. Chaudhary A, Sharma S, Mittal A, Gupta S, Dua A. Phytochemical and antioxidant profiling of *Ocimum sanctum*. *J Food Sci Technol*. 2020;57(10):3852-3863.

23. Ali AMA, El-Nour MEM, Yagi SM. Total phenolic and flavonoid contents and antioxidant activity of ginger (*Zingiber officinale* Rosc.) rhizome, callus and callus treated with some elicitors. *J Genet Eng Biotechnol*. 2018;16(2):677-682.

24. Loizzo MR, Formoso P, Leporini M, Sicari V, Falco T, Tundis R. Influence of Organic and Conventional Agricultural Practices on Chemical Profile, In Vitro Antioxidant and Anti-Obesity Properties of *Zingiber officinale* Roscoe. *The 1st International e-Conference on Antioxidants in Health and Disease*. 2020;2(1):3.

25. Wangcharoen W, Morasuk W. Antioxidant capacity and phenolic content of holy basil. *Songklanakarin J Sci Technol*. 2007;29(5):1407-1415.

26. Diaz-Flores J, Ybañez-Julca RO, Asunción-Alvarez D, Quispe-Díaz IM, Asmat-Marrufo P. Capacidad antioxidante in vitro del liofilizado de la pulpa y cáscara del rizoma de *Zingiber officinale* Roscoe (jengibre). *Rev Peru Med Integr*. 2019;4(4):121-126.

27. Gholam HA, Falah H, Sharififar F, Mirtaj AS. The inhibitory effect of some Iranian plants extracts on the alpha glucosidase. *Iran J Basic Med Sci*. 2008;11(1):1-9.

28. Molan AL, Saleh Mahdy A. Total Phenolics, Antioxidant Activity and Anti-Diabetic Capacities of Selected Iraqi Medicinal Plants. *Am J Life Sci Res*. 2016;4(2):47-59.

29. Belemkar S, Dhameliya K, Pata MK. Comparative study of garlic species (*Allium sativum* and *Allium porrum*) on glucose uptake in diabetic rats. *J Taibah Univ Med Sci*. 2013;8(2):80-85.

30. Thomson M, Al-Qattan KK, JS D, Ali M. Anti-diabetic and anti-oxidant potential of aged garlic extract (AGE) in streptozotocin-induced diabetic rats. *BMC Complement Altern Med*. 2015;16(1):17.

Original Article

Field Expansion for Homonymous Hemianopia by Mobile Application with Virtual Reality Glasses

Suntaree Thitiwichienlert[1*], Nattha Paenkhumyat[1]
Kosol Kampitak[1], Wimolwan Tangpagasit[1]

Abstract

Introduction: Homonymous hemianopia interferes with the daily living activities of patients.

Objectives: To present a mobile application using the camera function in combination with three-dimensional virtual reality (VR) glasses to expand the visual field by transferring images toward the residual field.

Methods: The authors included patients with homonymous hemianopia who could provide consent and communicate during examinations. The authors prospectively tested patients using an iOS-mobile application with a mobile camera and VR headsets to compare the binocular visual field before and after the test.

Results: Six patients were included in the study. The mean age was 50 (43-57 years). We found that the patients had a range in field expansion from 0 to 39.9 degrees (average of 21.28 degrees). Five patients were satisfied with the expanded visual field in adaptive confrontation testing.

Conclusions: This study has shown some effectiveness, we demonstrated a positive result of field expansion and patient satisfaction.

Keywords: Homonymous hemianopia, Mobile application, Virtual reality glasses, Visual field, Field expansion

[1] Department of Ophthalmology, Faculty of Medicine, Thammasat University, Khlong Luang, Pathum Thani 12130, Thailand
[*] **Corresponding author:** Suntaree Thitiwichienlert M.D, Department of Ophthalmology, Faculty of Medicine, Thammasat University, Khlong Luang, Pathum Thani 12130, Thailand Email: punoipunoi@hotmail.com, Tel. +669 8059 9191

Introduction

Homonymous hemianopia is a visual field defect in which a patient loses the use of the right or left side of both eyes. It is a common visual field defect that is caused by retrochiasmal brain lesions. This hemifield loss has a substantial impact on activities of daily living such as driving and reading, especially the speed of reading. Patients with right homonymous hemianopia have difficulty shifting their eyes from left to right to read letters in words, while patients with left homonymous hemianopia have difficulty finding the beginning of the next line on the left side when starting a new line.

In 2000, Peli, et al. described binocular sector prism glasses, which use the principle of Fresnel prisms to expand the visual field by about 15-20 degrees by placing a base-out prism 30-40 prism diopter (PD) to shift the image into the residual hemifield of each eye.[1] However, no studies have been carried out with these glasses or other methods for expanding the visual field in homonymous hemianopia in Thailand. This study aims to present a mobile application using the camera function on a phone, in combination with three-dimensional virtual reality (VR) glasses, to expand the visual field by transferring images toward the residual field.

Methods

The study was approved by the Medical Ethics Committee of Thammasat University (MTU-EC-OP-1-006/64), Pathum Thani, Thailand, and was conducted in accordance with the tenets of the Declaration of Helsinki. The computerized visual field (CTVF) was measured with the Swedish Interactive Threshold Algorithm (SITA) standard 30-2 program of the Humphrey Field Analyzer (Carl Zeiss Meditec, Dublin, CA). Homonymous hemianopia is considered a localized defect present in the same hemifield (i.e., right or left) of each eye. Congruous homonymous hemianopia was diagnosed if the pattern of visual field defects was nearly identical in each eye. Incongruous homonymous hemianopia was diagnosed if the pattern of visual field defects was less identical in each eye. All patients had at least 6 months of follow-up until the visual field was thought to be stable. We tested the patients in an eye examination room and the lighting in the test room was at comfortable levels for indoor settings. All patients performed neuroimaging and had stable visual field defects defined by performing at least two tests per clinical visit at least 6 months apart before enrolling in the study. Inclusion criteria were 1) patients who were diagnosed with homonymous hemianopia based on examinations by neuro-ophthalmologist and neuroimaging, 2) the age range was between 18 and 70 years old, and 3) the patients had sufficient cognitive awareness to comply with examination procedures. The outcome of the study was to measure how many degrees of field expansion and assess whether the patient is satisfied after the test. To assess patient satisfaction, a Thai-language questionnaire was administered, referring to the 14 measurement items of the previous study that determined user satisfaction with mobile VR Headsets.[2] The authors excluded patients with retinal or optic nerve diseases (prechiasmal and chiasmal lesions) causing visual field defects and those who had problems in language communication or cognitive impairment which could interfere with the use of the application. We collected data including age, gender, etiology, eye examination findings, visual field testing, neuroimaging, problems encountered with field defects in daily activities, and expectations of visual field restoration. All patients were informed about and consented to the research methodology.

First, the authors conducted self-tests using an iOS-mobile application with a mobile camera and VR headset (BOBOVR Z6, Xiaozhai technologies). The VR headset can adjust focus to correct the refractive error in the range from +2.00 to -4.00 diopter. The lens used was an aspherical lens with a diameter of 52 mm and a field of view of 120 degrees (Figure 1). The standard confrontation visual field is done at 0.5 meters; however, Kodsi et al. demonstrated a four-meter confrontation test which is useful as a screening test for evaluating paracentral vision. They calculate the approximate area of the blind spot at 0.5 meters and at 4 meters.[3] We tested at an intermediate distance (1.5 meters) due to the limitation of the VR headset lens, which we used to expand a field of view and thus making it unable to focus at closer (0.5 meters) or farther distances (4 meters). Based on this previous study, we will calculate the area using the same principle below: vertical height of the optic nerve head = 1.75 mm; horizontal width of the optic nerve head = 1.50 mm;

and nodal point of the eye from the retina = 17 mm. At 1.5 meters we calculate the vertical height of the blind spot to be 15.4 cm and the horizontal width to be 13.2 cm (Figure 1).
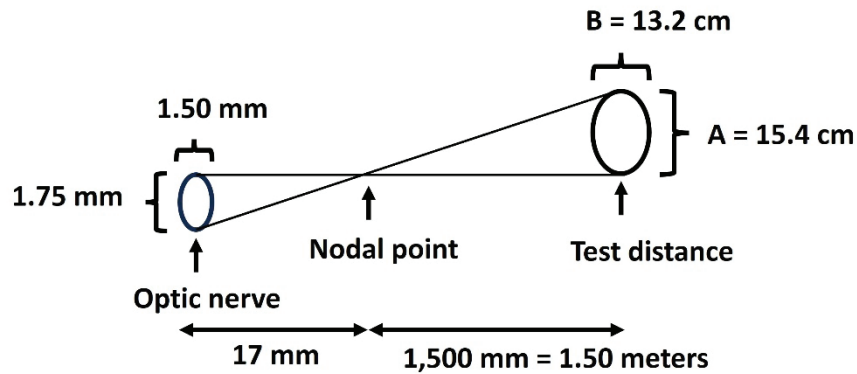
Figure 1 The geometry concept of calculation of the approximate area of the optic nerve head at 1.5 meters compares with a nodal point. (adapted from reference number 3.)

$$1.75 \text{ mm}/17 \text{ mm} = A/1,500 \text{ mm}$$
$$A = 15.4 \text{ cm}$$
$$1.50 \text{ mm}/17 \text{ mm} = B/1,500 \text{ mm}$$
$$B = 13.2 \text{ cm}$$

We use the examiner's outstretched hand as a simple measuring device to compare to the examiner's hand (length 15.52 cm ~ 15.4 cm) at arms' length (0.5 meters) and make rough estimates of the binocular field of view in degrees (Figure 2). With the examiner's arms stretched out straight in front of the patient, the width of the examiner's fist measures about 10°. If the examiner moves both arms upward, hand over hand, from the horizon to a point straight above the patient it should take about 9 hands to cover that 90° distance. Therefore, the examiner will use this method of moving the hand in and out of the patient's peripheral vision to the central vision to find the binocular confrontation visual field defect first, and then convert the distance from arm's length to the test distance (1.5 meters) into degrees.
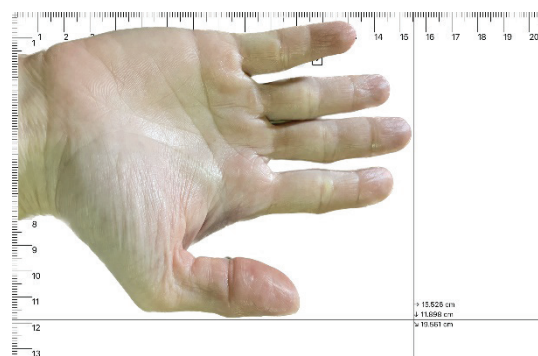
Figure 2 Estimation of the binocular field of view in degrees by comparing the examiner's hand (length 15.52 cm ~ 15.4 cm) at arms' length (0.5 meters).

The steps of testing are described below;

1. Perform a binocular confrontation visual field at 1.5 meters without equipment and record the results.

2. Open the application name "VRexpandedfield" (our application is currently a demo version: it cannot be downloaded from the apple store or google play store) on the mobile phone and select the parameters setting such as right-sided or left-sided.

3. Instruct the patient to put on the VR glasses, adjust the strap of the glasses, and then have the patient start looking at the surroundings in the room to get used to the glasses first.

4. Perform a binocular confrontation visual field at 1.5 meters with equipment and record the results.

5. Instruct the patient to take a short walk, if possible, in a safely enclosed eye examination room.

6. Ask the patient to describe the quality of the subjective image and answer the satisfaction questionnaire.

7. We compared the binocular confronta-tion visual field at 1.5 meters before and during the use the application. We simulated the binocular confrontation scale for a 120-degree visual field for a total of 9 visualized quadrants (13.3 degrees per quadrant) and recorded the number of expanded fields in the binocular visual field (Figure 4, 5, Table 2).

An ophthalmology resident is a single interpreter who performs binocular confrontation and provides interpretation for all patients. This study is a prospective case series in which the interpreter (single-blinded) does not know which informa-tion or neuroimaging results are being given to the patient.
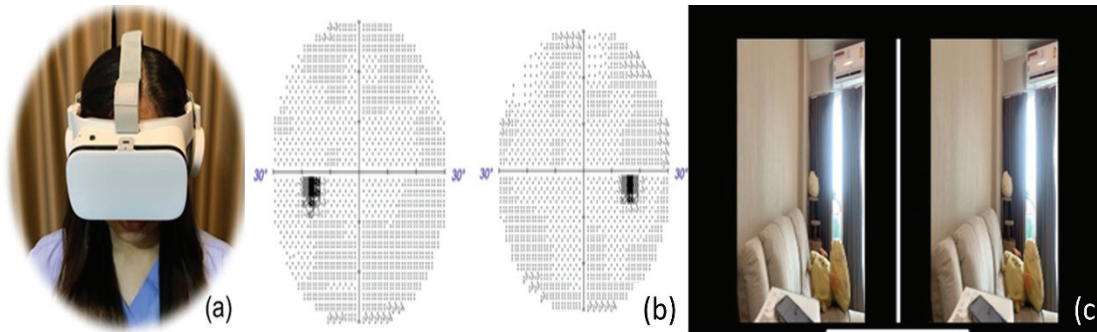
Figure 3 (a) A self-test, (b) CTVF 30-2 of a normal visual field, and (c) a normal VR view
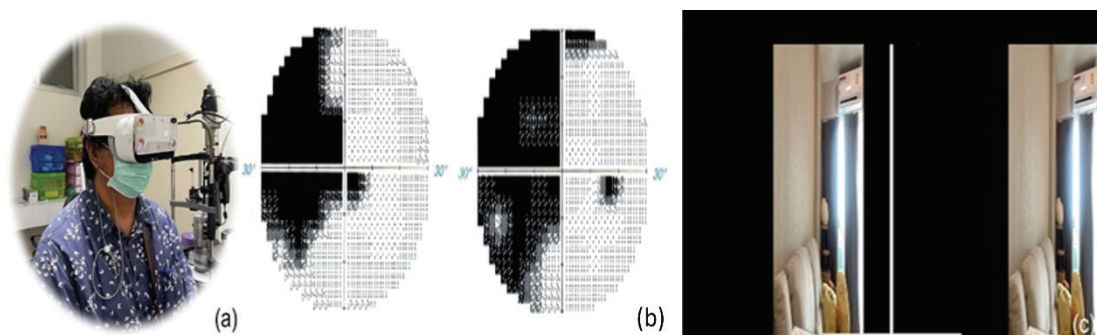
Figure 4 (a) A patient test, (b) CTVF 30-2 of left homonymous hemianopia, and (c) a VR view in left homonymous hemianopia
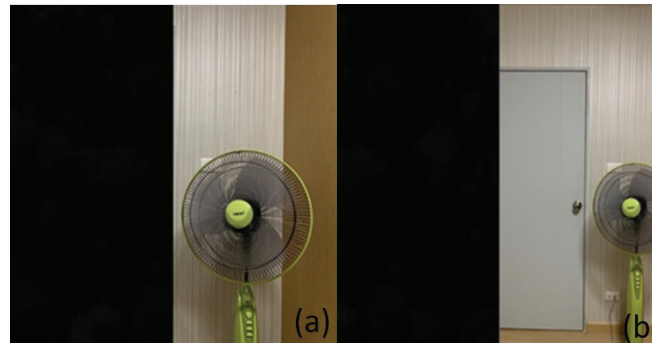
Figure 5 (a) VR view in left homonymous hemianopia, and (b) VR view of field expansion in left homonymous hemianopia

Results

Initially, eleven patients were enrolled in the present study, but five patients did not test the application because of non-visual related problems such as bedridden status and poor communication skills. Thus, six patients were included in the study. The mean age was 50 years with a range of 43 to 57 years. Three were male and three were female. Etiologies of homonymous hemianopia were ischemic stroke in 5 patients (83.3%) and a brain tumor in one patient (16.7%). In the test, the patients had to wear VR glasses on the head, so they were unable to wear glasses, meaning we had to record the central acuity as uncorrected visual acuity (UCVA). Patients had UCVA between 20/20 and 20/50 in both eyes. All patients received neuro-imaging such as computed tomography (CT) or magnetic resonance imaging (MRI) of the brain. Neuroimaging results were compatible with CTVF measured with the SITA standard 30-2 program of the Humphrey Field Analyzer. From asking the patients about the problems they encountered from the abnormal visual field, it was found that everyone felt the abnormal visual field was a problem in their daily lives. Two of them had experienced a car accident and three understood that they had to acclimate to having an abnormal visual field. In terms of expectations, most patients expressed a desire to have a device or glasses to help improve their visual fields (Table 1).
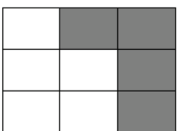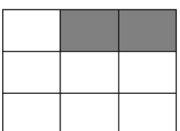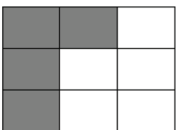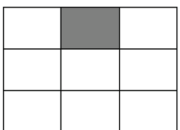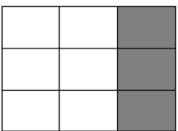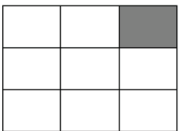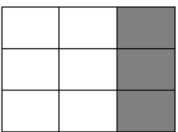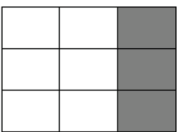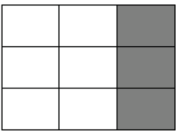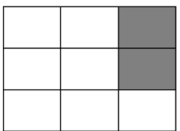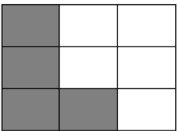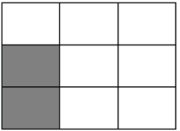
Table 1 Demographics and characteristics of patients using the application

No	Age (years)	Gender	Etiologies	UCVA	CTVF30-2	Neuroimaging (CT/MRI brain)	Problems in daily activities	Expectations of VF restoration
1	43	Female	Stroke	OD 20/30 OS 20/20	Complete right homonymous hemianopia	Severe atrophy of the left optic tract	I have difficulty reading inconsistent texts.	I want to restore my visual field defect to a normal field.
2	44	Male	Stroke	OD 20/20 OS 20/20	Incomplete left homonymous hemianopia	Hypodensity lesion at the right occipital lobe	I have difficulty seeing and finding things, even if the things are near me.	I am familiar with abnormal VF defects, but if I have glasses or a device that can see near normal people, it would be good.
3	51	Male	Stroke	OD 20/30 OS 20/20	Incomplete right homonymous hemianopia	Hypodensity lesion at the left occipital lobe	I have difficulty seeing things. I had an accident because I couldn't see the obstacles.	I want my normal visual field. I also want an instrument that can protect me from accidents caused by abnormal field defects.
4	53	Male	Sphenoid wing meningioma	OD 20/40 OS 20/50	Incomplete right homonymous hemianopia	Left medial sphenoid wing meningioma	I have difficulty seeing things and people.	I want the normal visual field I had in the past.
5	55	Female	Stroke	OD 20/50 OS 20/30	Incomplete right homonymous hemianopia	Encephalomalacia with old hemorrhage at the left inferior temporal-occipital lobes	I had an accident with a defect in the visual field, but I have adapted myself.	I want to restore my visual field defect.
6	57	Female	Stroke	OD 20/20 OS 20/20	Incomplete left homonymous hemianopia	Subacute infarction involving the cortical gray and white matter of the right occipital lobe with cortical laminar necrosis	I have difficulty seeing things. I am used to living with an abnormal visual field.	I hope that there will be an instrument that increases the field of view, and we can use it in our daily life.

A normal person has a total visual field of approximately 180 degrees, with each eye seeing a peripheral field of approximately 150 degrees, with an overlap binocular visual field of roughly 120 degrees. The human field of view is not square. Since the present study was tested through VR, however, the visualized image seen is divided into 9 small quadrants. In interpreting the test results, we calculated the binocular visual field expansion and found that the patients had a mean change in the increased field of view of 1.6 quadrants (ranging from zero to 3 quadrants) (Table 2). Five patients were satisfied with the expanded visual field in adaptive confrontation testing.

Table 2 Comparison of the binocular confrontation visual field before and during testing (the gray color shows a quadrant of the field that cannot be seen on either side)

No.	Binocular confrontation VF before testing	Binocular confrontation VF during testing	Binocular visual field expansion
1			Two quadrants = 26.6 degrees
2			Three quadrants = 39.9 degrees
3			Two quadrants = 26.6 degrees
4			Zero quadrant = 0 degrees
5			One quadrant = 13.3 degrees
6			Two quadrants = 26.6 degrees

Discussion

The principle of helping patients with homonymous hemianopia is to shift the visual field from the invisible side to the remaining side, with or without increased magnification. [4,5] A previous study used a base-out binocular sector prism placed in a specific quadrant area of the visual field by locating it on that part of the spectacle lens. [1] These prism glasses have the advantage of convenience and can correct their refractive error but are not available in Thailand. In 2008, Lane AR et al. evaluated visual restoration training (VRT), optical aids, and compensatory training, which aimed to restore the residualvisual field in homonymous hemianopia. They found that randomized placebo-controlled studies were lacking, making it difficult to establish which ones were clinically useful. [6] In 2018, Jung JH et al. relied on the basic principles of full-

field prisms to shift a portion of the blind side to the residual seeing side by applied meniscus and flat full-field 7 PD and 12 PD yoked prisms and compared kinetic visual field by Goldmann perimetry in patients with homonymous hemianopia and acquired monocular vision. They found that full-field prisms that filled the entire spectacle eye width did not effectively expand the visual field because patients had to turn their faces away from the blind side for foveal fixation on the object of interest, thereby negating the image shift to the blind side.[7]

In the present study, the patients wore VR glasses, so it was not possible to test each eye separately. Moreover, the patients could not wear VR glasses while testing the CTVF due to the limitation of the size of the device used. We could not interpret in detail how many degrees the visual field of each eye was expanded by the device or how much change there was compared to automated CTVF. In fact, the visual field should have been able to compare more clearly if we tested with the Goldmann kinetic visual field. However, our hospital does not have Goldmann perimetry, so a simulation of the degrees that the patient sees must be used to compare how much the patient sees. We found that patients had a range in field expansion from 0 to 39.9 degrees (average of 21.28 degrees; 13.3 degrees per quadrant). The patient who had the widest binocular visual field expansion said he was already familiar with homonymous hemianopia. This probably explains why he saw the most because the test had to adjust the visualized image through VR glasses as well. Five patients were satisfied with the expanded visual field in adaptive confrontation testing, but one patient was unable to adapt to the binocular visual field expansion. Consequently, we did not record any increase in the binocular visual field.

Normal reading requires a sufficient visual field wherein patients can simply sweep their eyes from left to right or vice versa.[8] Previous studies have found that reading in a horizontal direction requires at least 5 degrees to the right of fixation and 1-2 degrees to the left, while reading in a vertical direction tends to be slower than horizontal reading, in part because most patients are unfamiliar with rolling their eyes vertically in a saccadic way.[9,10] Previous studies have shown that patients with homonymous hemianopia have difficulty reading because they require at least 5 degrees of visual space to read, and the scotoma in homonymous hemianopia covers the central visual field.[11] Driving requires that the field of vision be at least 120 degrees horizontally and at least 20 degrees vertically according to the Department of Land Transport regulations applicable to visually impaired patients. In clinical application to activities for daily living, the average binocular visual field expansion from our study might be insufficient for driving but could be sufficient to aid in horizontal reading. Unfortunately, there are limitations of the lens used, making it impossible to apply VR glasses near work distances.

The limitations of this application were as follows: (1) VR glasses could not sufficiently correct patients' refractive error and presbyopia, so patients could not tolerate the long durations of use for this application and experienced eye discomfort; (2) Motion sickness was triggered by the motion of the VR glasses, which is a common occurrence among people who use VR headsets. It has been reported that people usually find themselves feeling overwhelmingly nauseous, even after a short session, while testing this technology for the first time; (3) Patients must adapt to the expanded visual field; (4) Small sample sizes make it difficult to determine if etiology of visual field defect may affect the results because only one patient with sphenoid wing meningioma failed to show field expansion using VR glasses. Recruitment for the study was difficult because of the low incidence of homonymous hemianopia. The authors suggested that further studies are needed to address the limitation of using VR glasses to improve the patient's quality of life and should be done with a larger sample size.

In conclusion, this mobile application did not enable a significant improvement in activities for daily living and also had limitations in clinical practice. However, this study has shown some effectiveness, we demonstrated a positive result of field expansion and patient satisfaction, even though we did not study the relationship between the achievement of field expansion and satisfaction. The authors believe that future technological developments will lead to new instruments for expanding the visual field and/or training patients with homonymous hemianopia.

References

1. Peli E. Field expansion for homonymous hemianopia by optically induced peripheral exotropia. *Optom Vis Sci*. 2000;77(9):453-64.
2. Jinhae C, Kahyun L, Junho C. Determinants of user satisfaction with mobile VR headsets: the human factors approach by the user reviews analysis and product lab testing. *International Journal of Contents*. 2019;15(1):1-9.
3. Kodsi SR, Younge BR. The four-meter confrontation visual field test. *J Clin Neuroophthalmol*. 1993;13(1):40-3.
4. Pambakian AL, Kennard C. Can visual function be restored in patients with homonymous hemianopia? *Br J Ophthalmol*. 1997;81(4):324-8.
5. Bowers AR, Keeney K, Peli E. Community-based trial of a peripheral prism visual field expansion device for hemianopia. *Arch Ophthalmol*. 2008;126(5):657-64.
6. Lane AR, Smith DT, Schenk T. Clinical treatment options for patients with homonymous visual field defects. *Clin Ophthalmol*. 2008;2(1):93-102.
7. Jung JH, Peli E. No Useful Field Expansion with Full-field Prisms. *Optom Vis Sci*. 2018;95(9):805-813.
8. Legge GE, Ahn SJ, Klitz TS, Luebker A. Psychophysics of reading--XVI. The visual span in normal and low vision. *Vision Res*. 1997;37(14):1999-2010.
9. Jordan TR, Almabruk AA, Gadalla EA, McGowan VA, White SJ, Abedipour L, Paterson KB. Reading direction and the central perceptual span: evidence from Arabic and English. *Psychon Bull Rev*. 2014;21(2):505-11.
10. Kuester-Gruber S, Kabisch P, Cordey A, Karnath HO, Trauzettel-Klosinski S. Training of vertical versus horizontal reading in patients with hemianopia - a randomized and controlled study. *Graefes Arch Clin Exp Ophthalmol*. 2021;259(3):745-757.
11. Trauzettel-Klosinski S, Brendler K. Eye movements in reading with hemianopic field defects: the significance of clinical parameters. *Graefes Arch Clin Exp Ophthalmol*. 1998;236(2):91-102.

Original Article

Prediction of COVID-19 with Statistical Data on Chest Radiography using Artificial Intelligence

Titipong Kaewlek*, Waritsara Sakaekhum, Warisa Promton,
Areeya Tharama, Thunyarat Chusin, Sumalee Yabsantia, Nuntawat Udee

Abstract

Introduction: COVID-19 is rapidly spreading around the world and has a high mortality rate. Artificial intelligence (AI) technology is a method that can be used to diagnose the presence of COVID-19 via chest radiographic apparatus. AI can be found to provide accurate results and increased diagnostic efficiency.

Objectives: To evaluate the efficacy of artificial intelligence for COVID-19 diagnosis using statistical data from radiographic chest images.

Methods: The research population sample consisted of 10,000 normal heathy individuals and 10,000 COVID-19 chest radiographs of patients were used for training (70.0%), validating (20.0%), and testing (10.0%). The images were segmented into the left and right lung regions by using the U-net architecture and then statistical data was calculated, including integrated density, mean, standard deviation, skewness, and kurtosis. Three artificial intelligence methods (support vector machine, K-mean clustering, and restricted Boltzmann machine) were compared the models' predictions. The performance of three methods were analyzed for accuracy, sensitivity, specificity, precision, and F1-score.

Results: The accuracy of the support vector machine, K-mean clustering, and restricted Boltzmann machine were 70.5%, 62.5%, and 63.2%, respectively. The trend of the sensitivity, specificity, precision, and F1-score were similar in terms of accuracy, sensitivity, specificity, precision, and F1-score of the support vector machine, which were 64.2%, 73.5%, 68.2%, and 68.5%, respectively.

Conclusions: The most successful technique for diagnosing COVID-19 from chest radiographs was the support vector machine. It outperformed the restricted Boltzmann machine, which was followed by K-mean clustering.

Keywords: Prediction, Artificial intelligence (AI), Chest radiography, COVID-19, Statistical data

Department of Radiological Technology, Faculty of Allied Health Sciences, Naresuan University, Phitsanulok 65000, Thailand
* **Corresponding Author:** Titipong Kaewlek, Department of Radiological Technology, Faculty of Allied Health Sciences, Naresuan University, Email: titipongk@nu.ac.th

Introduction

The infectious Coronavirus disease 2019 known as COVID-19 has proven to be difficult to initially identify. COVID-19 has rapidly spread worldwide, resulting in hardship and economic turmoil. The virus triggers severe acute respiratory syndrome disorders that can lead to death. In April 2022, the World Health Organization (WHO) reported 6 million deaths due to the virus in addition to more than 500 million confirmed infected cases. In April 2022, the highest numbers of new weekly cases were reported from the Republic of Korea (972,082 new cases), France (827,350 new cases), Germany (769,466 new cases), Italy (421,707 new cases), and Japan (342,665 new cases). In the South-East Asia Region, since mid-January 2022 Thailand had reported both the highest number of new cases and new deaths (146,474 new cases and 799 new deaths).[1]

A highly specific and sensitive method for diagnosis of the COVID-19 virus detects the presence of specific genetic material, real time-polymerase chain reaction (RT-PCR). The World Health Organization (WHO) recommends that COVID-19 self-testing procedures using Severe Acute Respiratory Syndrome Coronavirus 2 Antigen Rapid Diagnostic Tests (SARS-CoV-2 Ag-RDTs) can reliably and accurately be used to self-test for the COVID-19 virus.[2] In hospitals, computed tomography imagery and chest radiography can be utilized to confirm and detect the effects of COVID-19 in the lung region. An automatic detection program using artificial intelligence (AI) can be used to aid physicians to screen for COVID-19 lesions.

Deep learning and machine learning are commonly used forms of artificial intelligence used with medical imaging for the diagnosis of lesions. AI can automatically detect and identify COVID-19 on the image, but the AI model must learn from a large dataset.[3,4] The deep learning model can automatically extract features of the image and learn the differences in the structure of the image. Several works have used the deep convolutional neural network (DCNN) model to detect COVID-19 on computed tomography and chest radiography.[5-10] The Visual Geometry Group 16-layer model (VGG-16) and the Residual Network with 50 layers (ResNet-50) model can predict COVID-19 with more than 96.0% accuracy.[11] Machine learning is

an alternative method to learn information from image data. Medical images consist of many small pixels that fill the number of pixel values. Machine learning can analyze and classify image data from pixel values. Many studies have used machine learning models to detect COVID-19, such as K-nearest neighbor, support vector machine, decision tree, and K-means clustering.[12-13] The objective of this research is to evaluate the efficacy of artificial intelligence to detect COVID-19 using statistical data from chest radiography.

Methods

The study approved by the ethics committee of Naresuan University, Thailand (IRB No. P10110/64). The chest radiography dataset is available on www.kaggle.com, which includes 10,000 normal and 10,000 COVID-19 chest radiography images, all image were labeled as normal and COVID-19.[14] The image files are in the portable network graphics (PNG) format. All images were divided into three groups, with 70.0% in the training group, 20.0% in the validation group, and 10.0% in the test group. The images were uploaded to google drive and converted to 256 x 256 matrix size before processing by Google Colaboratory.[15]

Figure 1 shows how the chest radiography was segmented using the artificial intelligence called U-shaped Network (U-net) architecture[16] to separate the lung regions. The area of the lung segmented in the initial image was separated to calculate statistical data. Pixel values of the lung segmented regions were calculated using statistical data, including integrated density, mean, standard deviation, skewness, and kurtosis. The integrated density shows the summation of the pixel value of the segmented lung region. The mean is the average pixel value of the lung region. The standard deviation is the variation of the pixel value. Skewness refers to the distortion or asymmetry of the probability of distribution of the pixel value. Kurtosis is the measure of the sharpness of the peak of a pixel value distribution.

The statistical data of normal and COVID-19 images were divided into five characteristic groups. First is a group of five types of statistical data (integrated density, mean, standard deviation, skewness, and kurtosis). Second, four of the statistical data were alternated. Third, three of

the statistical data were alternated. Fourth, two of the statistical data were alternated. Fifth, each of the statistical data without an alternative are presented in Table 1.

The statistical data alternative was chosen to reduce the number of types from five data in category (Cate) 1 to a single type in Cate 5. This involved swapping and changing the type of statistical data.

To evaluate the mean difference in five statistical data sets between normal and COVID-19 chest radiography, the Mann-Whitney U test was conducted with a significance level set at 0.05 (*P-value* = 0.05).

Statistical data was evaluated by three artificial intelligence methods (support vector machine, K-mean clustering, and restricted Boltzmann machine). The total statistical data, 14,000 training and 4,000 validation items, was processed using three method parameters, as shown in Table 2.

After training and validation examination, 2,000 items of test statistical data were tested by the same parameters.

Performance evaluation of three artificial intelligence methods

To assess the classification of COVID-19 using statistical data from chest radiography, the two-confusion matrix of this study describes the performance of a classifier in four terms:

True Positives (TP): AI detects COVID-19 on a COVID-19 image.

True Negatives (TN): AI cannot detect COVID-19 on a non-COVID-19 image.

False Positives (FP): AI detects COVID-19 on a non-COVID-19 image.

False Negatives (FN): AI cannot detect COVID-19 on a COVID-19 image.

Each normal and COVID-19 image was labeled by the database on each website[14] to indicate the true result regarding whether the images were normal or COVID-19.

The equation of performance evaluation, accuracy, sensitivity (recall), specificity, precision, and F1-score can be evaluated by Equations (1) - (5).

$$\text{Accuracy} = \frac{TP+TN}{TP+TN+FP+FN} \quad (1)$$

$$\text{Precision} = \frac{TP}{TP+FP} \quad (2)$$

$$\text{Sensitivity (recall)} = \frac{TP}{TP+FN} \quad (3)$$

$$\text{Specificity} = \frac{TN}{TN+FP} \quad (4)$$

$$\text{F1 score} = 2 \times \frac{\text{precision} \times \text{recall}}{\text{prescision} + \text{recall}} \quad (5)$$

Results

Table 3 presents the results of the statistical data of normal and COVID-19 chest radiography. The mean of the statistical data (integrated density, mean, standard deviation, skewness, and kurtosis) of normal and COVID-19 chest radiography images are compared, with the results indicating they are significantly different (*P-value* < 0.05).

Figure 2 (a) shows the best values of accuracy, precision, sensitivity, specificity, and F1-score for each group test of the support vector machine methods. The highest accuracy ratio (0.705) was attained with the Cate 1 group (integrated density, mean, standard deviation, skewness, and kurtosis). Next, the Cate 2 group (mean, standard deviation, skewness, and kurtosis) achieved an accuracy ratio of 0.704, followed by the Cate 3 group (integrated density, standard deviation, and kurtosis) with an accuracy ratio of 0.687. The Cate 4 group (skewness and kurtosis) obtained an accuracy ratio of 0.677, and finally, the Cate 5 group (kurtosis) achieved the lowest accuracy ratio at 0.665.

The performance of sensitivity, specificity, and F1-score of the support vector machine methods is similar to the accuracy tendency, except for the precision of the Cate 2 group (mean, standard deviation, skewness, and kurtosis: 0.646), which was expected to be higher than that of the Cate 1 group (integrated density, mean, standard deviation, skewness, and kurtosis: 0.642).

In addition, Figure 2 (b) shows the best value of accuracy, precision, sensitivity, specificity, and F1-score of each group test of the K-mean clustering methods. The result of the Cate 4 group (skewness, and kurtosis) was able to classify COVID-19 with the highest accuracy ratio (0.632), second was the Cate 3 group (standard deviation, skewness, and kurtosis: 0.628), third was Cate 5 group (kurtosis: 0.625), fourth was the Cate 1 group (0.615), and finally, the Cate 2 group (integrated density, mean, skewness, and kurtosis) achieved the lowest accuracy ratio at 0.560.

The Cate 3 group achieved the highest precision performance. The sensitivity of the Cate 4 group was highest. The specificity and F1-score of the Cate 1 group was the highest.

Moreover, the best values of accuracy, precision, sensitivity, specificity, and F1-score of each group test of the restricted Boltzmann machine methods are shown in Figure 3. The result of Cate 5 group (kurtosis) can classify COVID-19 with the highest accuracy ratio (0.644), second was the Cate 2 group (mean, standard deviation, skewness, and kurtosis: 0.632), third was the Cate 3 group (mean, skewness, and kurtosis: 0.631), fourth was the Cate 4 group (skewness, and kurtosis: 0.630), and fifth is a Cate 1 group (0.552).

Cate 5 group (kurtosis) had the highest tendency of precision, sensitivity, specificity, and F1-score.

Figure 4 presents the best performance comparison of three artificial intelligence methods. Accuracy, sensitivity, specificity, and F1-score of the support vector machine (SVM) were highest, followed by the restricted Boltzmann machine (RBM), and finally K-mean clustering. With the exception of precision, the restricted Boltzmann machine (RBM) performed the best.
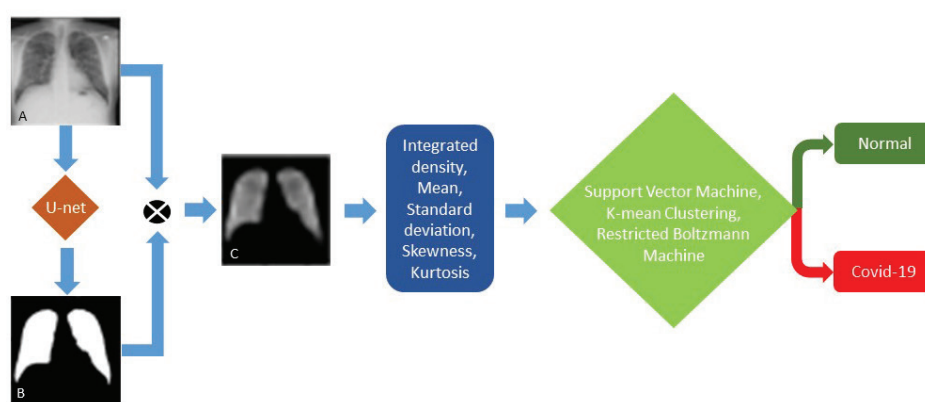
Figure 1 The workflow of this research shows the chest radiography was segmented by U-net architecture and statistical data was calculated from the image, and three methods (support vector machine, K-mean clustering, and restricted Boltzmann machine) were used to detect COVID-19.
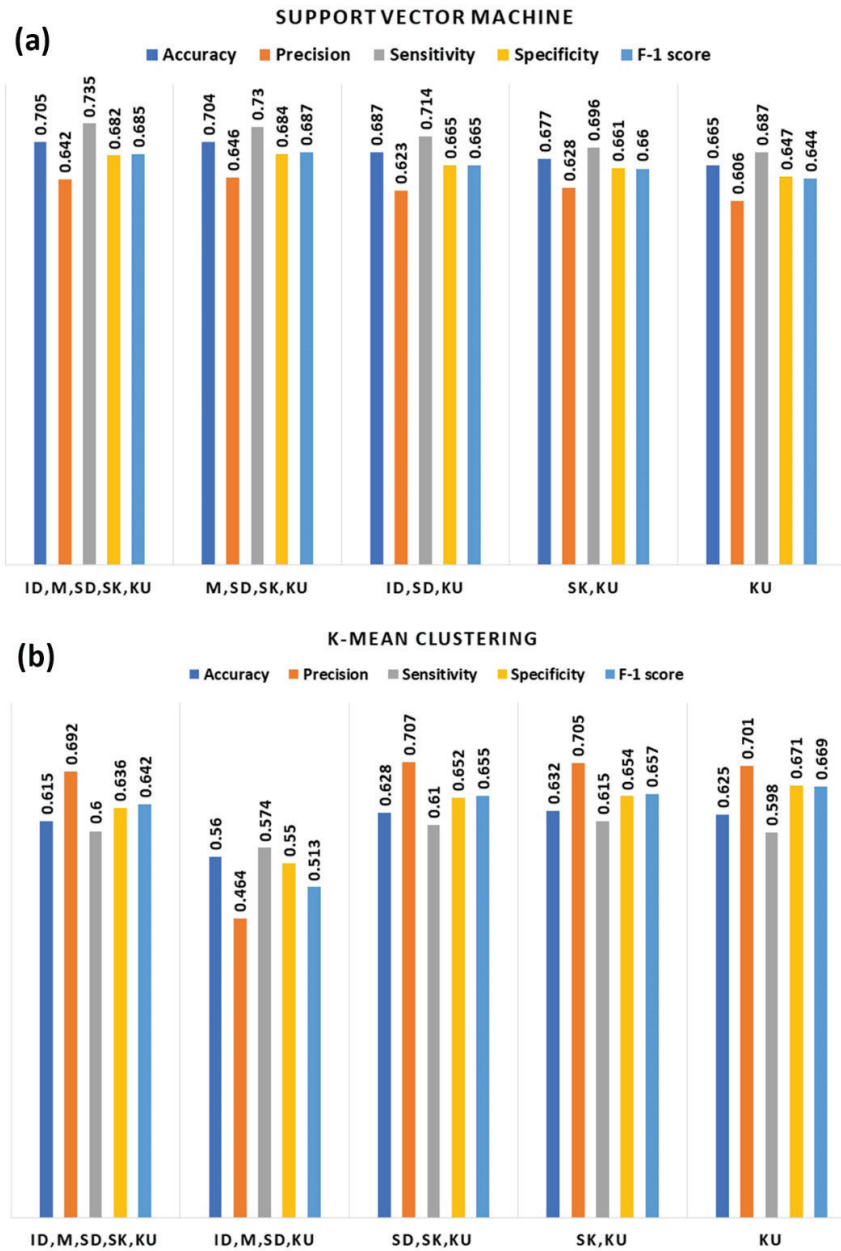
Figure 2 Accuracy, precision, sensitivity, specificity, and F1- score of (a) support vector machine and (b) of K-mean clustering. (ID is integrated density, M is mean, SD is standard deviation, SK is skewness, and KU is kurtosis).

RESTRICTED BOLTZMANN MACHINE
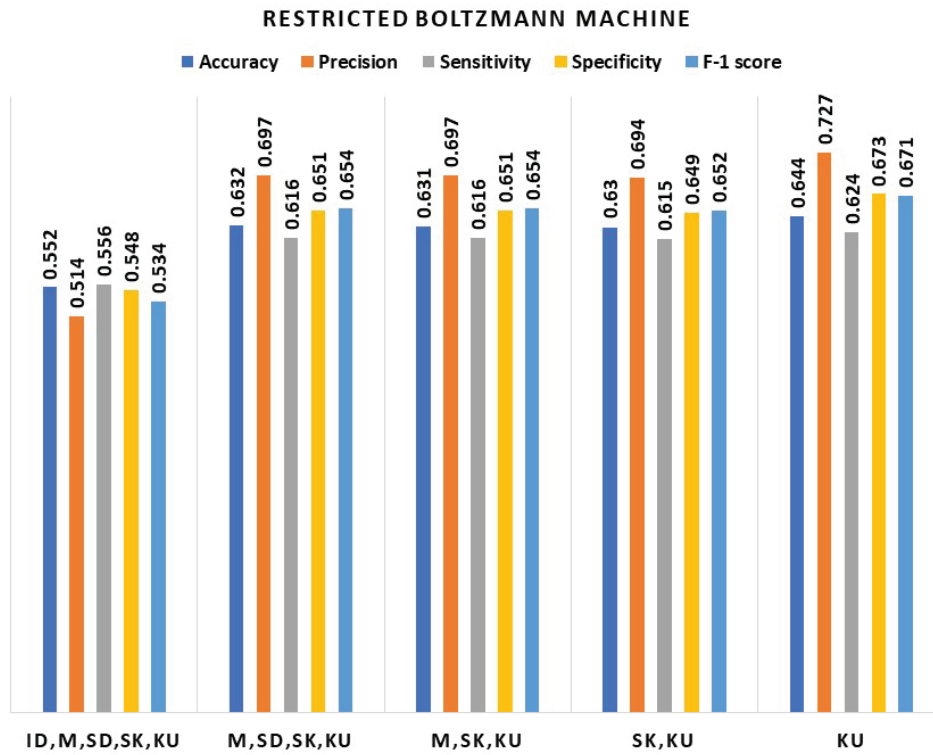
Figure 3 Accuracy, precision, sensitivity, specificity, and F1- score of restricted Boltzmann machine on the group of statistical data (ID is integrated density, M is mean, SD is standard deviation, SK is skewness, and KU is kurtosis).

Figure 4 The best performance comparison of three artificial intelligence methods: support vector machine (SVM); K-mean clustering; and restricted Boltzmann machine (RBM).

Table 1 The five characteristic groups of the statistical data for analysis

A group of five statistical data (Cate 1)	Four statistical data were alternated (Cate 2)	Three statistical data were alternated (Cate 3)	Two statistical data were alternated (Cate 4)	Statistical data (Cate 5)
Integrated density, Mean, Standard deviation, Skewness, and Kurtosis.	1. Integrated density, Mean, Standard deviation, Skewness 2. Integrated density, Mean, Standard deviation, Kurtosis 3. Mean, Standard deviation, Skewness, Kurtosis.	1. Integrated density, Mean, Standard deviation 2. Integrated density, Mean, Skewness 3. Integrated density, Mean, Kurtosis 4. Integrated density, Standard deviation, Skewness 5. Integrated density, Standard deviation, Kurtosis 6. Integrated density, Skewness, Kurtosis 7. Mean, Standard deviation, Skewness 8. Mean, Standard deviation, Kurtosis 9. Mean, Skewness, Kurtosis 10. Standard deviation, Skewness, Kurtosis	1. Integrated density, Mean 2. Integrated density, Standard deviation 3. Integrated density, Skewness 4. Integrated density, Kurtosis 5. Mean, Standard deviation 6. Mean, Skewness 7. Mean, Kurtosis 8. Standard deviation, Skewness 9. Standard deviation, Kurtosis 10. Skewness, Kurtosis	1. Integrated density 2. Mean 3. Standard deviation 4. Skewness 5. Kurtosis

Table 2 The parameter of three methods (support vector machine, K-mean clustering, and restricted Boltzmann machine)

Support vector machine (SVM)	K-mean clustering	Restricted Boltzmann machine
regularisation parameter (C) = 0.1, **kernel = *rbf*,** degree of the polynomial kernel function = 3, **gamma = *scale*,** the shrinking heuristic = *True*, probability estimates = *False*, tolerance for stopping criterion = *1e-3*, size of the kernel cache = 200, **class weight = *None*,** **verbose = *False*,** **maximum iteration = -1,** **decision function shape = ovr;** **break ties = *False*,** **random state = *None*.**	number of clusters = 2, number of times the k-means algorithm = 10, maximum number of iterations = 300, relative tolerance = *1e-4*, **verbose = 0,** **random state = *None*,** **copy_x = *True*,** **the algorithm = *Auto*.**	**number of components = 2,** learning rate = 0.1, **batch size = 10,** number of iterations = 50, verbosity level = *True*, **random state = 0,** **logistic regression parameters; solver = *newton-cg*,** tolerance for stopping criteria (**tol**) = **1,** inverse of regularisation strength = 60.

Table 3 Example statistical data of 10,000 normal and 10,000 COVID-19 chest radiography images

	Statistical data of normal chest radiography						Statistical data of COVID-19 chest radiography				
No	Integrated density	Mean	Standard deviation	Skewness	Kurtosis	No	Integrated density	Mean	Standard deviation	Skewness	Kurtosis
0	1379434	21.050	30.027	1.053	1.109	0	1923475	29.350	27.153	1.079	1.478
1	664312	10.140	26.703	1.057	0.679	1	701134	10.698	27.526	0.477	-0.124
2	1028326	15.690	32.736	1.01	0.958	2	826680	12.614	33.059	0.918	0.622
3	1142249	17.430	37.128	0.726	-0.127	3	2299892	35.094	40.997	0.334	-0.874
.	.	.	.	.	.	.	.	.	.	.	.
.	.	.	.	.	.	.	.	.	.	.	.
.	.	.	.	.	.	.	.	.	.	.	.
9,999	1028977	15.700	41.125	0.9222	0.262	9,999	2036144	31.069	20.52	-0.114	-0.749
Mean	1678901	25.620	30.254	0.667	0.265	Mean	1623907	24.779	31.686	0.547	-0.026

The mean difference of all couple of statistical data between normal and COVID-19 were significantly different ($P = 0.000$)

Discussion

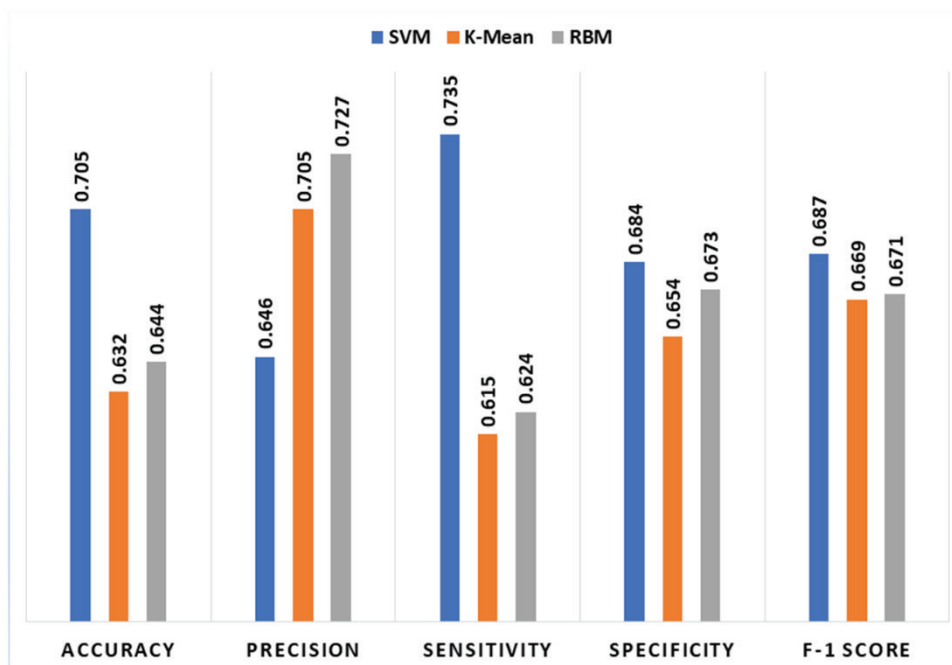This research compared the performance of three artificial intelligence methods: support vector machine (SVM); K-mean clustering; and restricted Boltzmann machine (RBM). Statistical data was calculated to evaluate the three artificial intelligence methods. Statistical data (integrated density, mean, standard deviation, skewness, and kurtosis) of chest radiography was utilized to identify structure characteristics on the images. Five statistical data sets were extracted from the chest radiography, were trained and tested by three above artificial intelligence methods.

The statistical analysis comparing the mean differences between all pairs of statistical data in normal and COVID-19 images indicates that the means were significantly different.

The overall performance result for the support vector machine was the best, with an accuracy of 0.705 for Cate 1, sensitivity of 0.735 for Cate 1, specificity of 0.684 for Cate 2, F1-score of 0.687 for Cate 2, and precision of 0.646 for Cate 2.

For Cate 5, the accuracy of the restricted Boltzmann machine was 0.644, sensitivity was 0.624, specificity was 0.673, F1-score was 0.671, and precision was 0.727.

The accuracy of K-mean clustering was 0.632 for Cate 4, sensitivity was 0.615 for Cate 4, specificity was 0.671 for Cate 5, F1-score was 0.669 for Cate 5, and the precision was 0.707 for Cate 3.

The support vector machine indicates that the multi-parameters of statistical data for Cate 1 (integrated density, mean, standard deviation, skewness, and kurtosis) and Cate 2 (mean, standard deviation, skewness, and kurtosis) are suitable for classifying COVID-19 chest radiography. For the restricted Boltzmann machine, Cate 5 (kurtosis) achieved the highest score, while for K-mean clustering, Cate 4 (skewness and kurtosis) and Cate 5 (kurtosis) obtained the highest scores for classifying chest images.

The multi-parameters were not suitable for two artificial intelligences (restricted Boltzmann machine and K-mean clustering). Overfitting was the reason for the misclassification of COVID-19 images, possibly due to the differing size of integrated density data compared to other data, which may be the main cause of overfitting. To address this issue, normalizing the data will be the solution in future work. The lower performance of the restricted Boltzmann machine and K-mean clustering highlights the effectiveness of using one or two parameters of statistical data.

The statistical data of this work were extracted using the first-order features technique.[17] Other features extraction techniques[17], such as gray level co-occurrence matrix (GLCM), gray level size zone matrix (GLRZM), or neighboring gray tone matrix (GLDM), may be alternative choices for extracting data from chest radiography.

Compared with the present study, Khan identified COVID-19 on chest radiography using K-mean clustering and support vector machine, with the support vector machine achieving an accuracy of 94.1%.[14] Nour et al. studied COVID-19 classification by K-nearest neighbor, support vector machine, and decision tree.[18] The support vector machine was found to be the best method to detect COVID-19 with an accuracy of 98.9%, sensitivity of 89.4%, specificity of 99.8%, and F1-score of 96.7%. In the present study, Figure 4 also illustrates that the support vector machine achieved the best performance. The limitation of this study is that the data closely resemble values in normal and COVID-19 images. Therefore, it is advisable to consider using different statistical data or employing artificial intelligence methods such as deep learning to enhance performance.

Conclusions

This study compared the COVID-19 prediction capabilities of three artificial intelligence methods. The support vector machine demonstrated the highest potential for detecting COVID-19 with chest radiography, achieving accuracy (70.5%), precision (64.2%), sensitivity (73.5%), specificity (68.2%), and F1-score (68.5%). In future work, researchers will analyze statistical data of chest radiography using other artificial intelligence methods.

Compliance with Ethics Requirements This study approved by the ethics committee of Naresuan University, Thailand (IRB No. P10111/64).

Conflict of interest : None

References

1. World Health Organization. Weekly epidemiological update on COVID-19-20 April 2022. Geneva: WHO. https://www.who.int/publications/m/item/weekly-epidemiological-update-on-COVID-19---20-april-2022. Published 2022. Accessed April 28, 2022.

2. World Health Organization. Use of SARS-CoV-2 antigen-detection rapid diagnostic tests for COVID-19 self-testing (2022). Geneva: WHO. https://www.who.int/publications/i/item/WHO-2019-nCoV-Ag-RDTs-Self_testing-2022.1 Published 2022. Accessed April 28, 2022.

3. Hassantabar S, Ahmadi M, Sharifi A. Diagnosis and detection of infected tissue of covid-19 patients based on lung x-ray image using convolutional neural network approaches. *Chaos Solit Fractals*. 2020;140:110170.

4. Sethy PK, Behera SK. Detection of coronavirus disease (covid-19) based on deep features. *Prepr*. 2020:2020030300.

5. Lakhani P, Sundaram B. Deep Learning at Chest Radiography: Automated Classification of Pulmonary Tuberculosis by Using Convolutional Neural Networks. *Radiology*. 2017;284(2):574-582.

6. Ni Q, Sun Z Y, Qi L, Chen W, Yang Y, Wang L, et al. A deep learning approach to characterize 2019 coronavirus disease (COVID-19) pneumonia in chest CT images. *Eur Radiol*. 2020;30:6517-6527.

7. Kumar R, Arora R, Bansal V, Sahayasheela V J, Buckchash H, Imran J, et al. Accurate prediction of COVID-19 using chest x-ray images through deep feature learning model with SMOTE and machine learning classifiers. *medRxiv*. 2020;20063461.

8. Liu B, Gao X, He M, Lv F, Yin G. Online COVID-19 diagnosis with chest CT images: Lesion-attention deep neural networks. *medRxiv.* 2020;20097907.

9. Ibrahim D M, Elshennawy N M, Sarhan A M. Deep-chest: multi-classification deep learning model for diagnosing COVID-19, pneumonia, and lung cancer chest diseases. *Comput Biol Med*. 2021;132:1-13.

10. Yang D, Martinez C, Visuña L, Khandhar H, Bhatt C, Carretero J. Detection and analysis of COVID-19 in medical images using deep learning techniques. *Sci Rep*. 2021;11:1-13.

11. Das AK, Kalam S, Kumar C, Sinha D. TLCoV-An automated Covid-19 screening model using transfer learning from chest x-ray images. *Chaos Solit Fractals*. 2021;144:110713.

12. Joshi RC, Yadav S, Pathak VK, Malhotra HS, Khokhar HVS, Parihar A, et al. A deep learning-based COVID-19 automatic diagnostic framework using chest X-ray images. *Biocybern Biomed Eng*. 2021;41(1):239-254.

13. Khan MA. An automated and fast system to identify COVID-19 from X-ray radiograph of the chest using image processing and machine learning. *Int j Imaging Syst Technol*. 2021;31(2):499-508.

14. COVID-19 Radiography Database. Kaggle Inc. https://www.kaggle.com/datasets/tawsifurrahman/covid19-radiography-database. Published 2022. Accessed April 28, 2022.

15. Google colaboratory. Google Research. colab.research.google.com Published 2022. Accessed April 28, 2022.

16. Pandey N. Lung segmentation from Chest X-Ray dataset. Kaggle Inc. https://www.kaggle.com/code/nikhilpandey360/lung-segmentation-from-chest-x-ray-dataset/notebook. Published 2022. Accessed April 28, 2022.

17. Pyradiomics. Radiomics features, https://www.pyradiomics.readthedocs.io. Published 2016. Accessed December 12, 2023.

18. Nour M, Cömert Z, Polat K. A novel medical diagnosis model for COVID-19 infection detection based on deep features and Bayesian optimization. *Applied Soft Computing*. 2020;97:106580.

Original Article

Quality Control of Raw Plant Materials and Stability Testing under Accelerated Storage Conditions of Kheaw-Hom Remedy Extract

Kanmanee Sukkasem[1], Arunporn Itharat[2,3*], Pakakrong Thongdeeying[2,3], Weerachai Pipatrattanaseree[4], Sunita Makchuchit[2,3], Chonthicha Kongkwamcharoen[2,3], Neal M. Davies[5]

Abstract

Introduction: Kheaw-Hom remedy (KH), a Thai traditional antipyretic medicine, is included in the National List of Essential Medicine. Currently, there is no scientific report on its standard requirements for quality control and stability testing.

Objectives: To determine the quality control and stability testing of KH on anti-inflammatory activity and its bioactive marker

Methods: Quality control methods (loss on drying, total ash, acid-insoluble ash, extractive values, and heavy metals) of KH and raw plant materials were performed according to Thai Herbal Pharmacopoeia (THP). The stability testing of the ethanolic extract of KH (KHE) was stored under 40 ± 2 ºC and $75 \pm 5\%$ relative humidity for 180 days. Anti-inflammatory activity on LPS-induced nitric oxide (NO) production in RAW264.7 macrophage cells were evaluated. Ethyl p-methoxycinnamate (EPMC), a bioactive marker, was analyzed using high performance liquid chromatography (HPLC).

Results: KH showed loss on drying, total ash, acid-insoluble ash, ethanol soluble extractive and water-soluble extractive values of $8.66 \pm 0.47\%$, $6.17 \pm 0.06\%$, $1.14 \pm 0.07\%$, $10.62 \pm 0.12\%$, and $13.78 \pm 0.54\%$, respectively. Eighteen plant materials met the requirements of THP. The anti-inflammatory activity on nitric oxide inhibition and EPMC content of KHE on day 180 exhibited no significant difference when compared with day 0.

Conclusions: This study is the first report on quality control and stability testing of KH. All KH and its plant components conformed to the standard requirements of THP. KHE could be stored at room temperature for two years.

Keywords: Quality control, Stability testing, Accelerated storage conditions, Kheaw-Hom

[1] Student of Doctor of Philosophy Program in Applied Thai Traditional Medicine, Faculty of Medicine, Thammasat University, Pathum Thani, Thailand
[2] Department of Applied Thai Traditional Medicine, Faculty of Medicine, Thammasat University, Pathum Thani, Thailand
[3] Center of Excellence in Applied Thai Traditional Medicine Research (CEATMR), Faculty of Medicine, Thammasat University, Pathum Thani, Thailand
[4] Regional Medical Science Center 12 Songkhla, Department of Medical Sciences, Songkhla, Thailand
[5] Faculty of Pharmacy and Pharmaceutical Sciences, University of Alberta, Edmonton, Canada
* **Corresponding author:** Arunporn Itharat, Ph.D., Department of Applied Thai Traditional Medicine and Center of Excellence in Applied Thai Traditional Medicine Research (CEATMR), Faculty of Medicine, Thammasat University, Pathum Thani, Thailand Email: iarunporn@yahoo.com Tel: +66 2926 9749, +668 6964 5964

Introduction

Kheaw-Hom remedy (KH) is a Thai traditional antipyretic medicine, which has been officially published in the National List of Essential Medicine (NLEM).[1] Folk doctors and Thai traditional practitioners in hospitals have long used this remedy to treat fever with rash in children with illnesses, such as measles, chickenpox, and aphthous ulcers.[2-4] The remedy has a cool and bitter taste which serves dual purposes, as it can be ingested and also applied externally to reduce body temperature during fever.[5]

KH is composed of eighteen medicinal plants, i.e., *Pogostemon cablin* (Blanco) Benth. (Phim-Sen), *Limnophila rugosa* (Roth) Merr. (Phak-Kra-Chom), *Cordyline fruticosa* (L.) A.Chev. (Red leaf, Mak-Phu), *Cordyline fruticosa* (L.) A.Chev. (Green leaf, Mak-Mia), *Eupatorium fortunei* Turcz. (San-Phra-Hom), *Vetiveria zizanioides* (L.) Nash ex Small (Faek-Hom), *Kaempferia galanga* L. (Proh-Hom), *Myristica fragrans* Houtt. (Chan-Thet), *Dracaena cochinchinensis* (Lour.) S.C.Chen (Chan-Daeng), *Angiopteris evecta* (G.Forst.) Hoffm. (Wan-Kip-Rat), *Globba variabilis* Ridl. (Wan-Ron-Thong), *Tacca chantrieri* André (Nae-Ra-Phu-Sri), *Sophora exigua* Craib (Phit-Sa-Nat), *Cyathea gigantea* (Wall. ex Hook.) Holttum (Ma-Had-Sa-Dam), *Mimusops elengi* L. (Phi-Kun), *Mesua ferrea* L. (Bun-Nak), *Mammea siamensis* T. Anderson (Sa-Ra-Phi) and *Nelumbo nucifera* Gaertn. (Bua-Luang).[1] Each medicinal plant composition is added at an equivalent ratio. Previous studies on KH have demonstrated its various beneficial properties, including anti-inflammatory activity, antioxidant activity, antimicrobial activity, and antimalarial activity.[6-9] Currently, there is no established monograph on the quality control of KH in Thai Herbal Preparation Pharmacopoeia (THPP) and there is a lack of scientific reports on stability testing.[10] Recently, the standardized monographs are only available for 5 out of the 18 raw plant materials listed in this remedy in the Thai Herbal Pharmacopoeia (THP) i.e., *K. galanga*, *D. cochinchinensis*, *M. elengi*, *M. ferrea*, *N. nucifera*.[11]

Quality control and stability testing are very important since it impacts the efficacy and shelf life of a medicine product.[12,13] Therefore, the objectives of this study were to evaluate the quality control of raw plant materials and stability testing of the ethanolic extract of KH (KHE) under accelerated storage conditions: in terms of the inhibitory effect on lipopolysaccharide (LPS)-induced nitric oxide (NO) production in RAW 264.7 macrophage cells and the quantitation of the bioactive marker. These results are essential for establishing precise specifications to ensure the consistent quality and shelf life of KH.

Methods

Chemicals and Reagents

Acetonitrile, chloroform, dimethyl sulfoxide (DMSO), hydrochloric acid (HCl), methanol, were purchased from RCI Labscan (Bangkok, Thailand). Commercial grade 95% ethanol was purchased from C.M.J. Anchor Co., Thailand. Fetal bovine serum (FBS), penicillin-streptomycin, trypan blue, 0.5% trypsin-EDTA, Roswell Park Memorial Institute (RPMI) 1640 medium, penicillin-streptomycin were purchased from Gibco BRL Life Technologies (NY, USA). Phosphate buffer saline (PBS) was purchased from Amreso 27 (OH, USA). Lipopolysaccharide (LPS, Serotype: *Escherichia coli* O55:B5), 3-(4,5-dimethyl-2-thiazolyl)-2,5 diphenyl-2H-tetrazolium bromide (MTT), *N*-(1-naphthy) ethylenediamine dihydrochloride, sulfanilamide, and phosphoric acid were purchased from Sigma-Aldrich (MO, USA).

Plant materials

KH consists of eighteen medicinal plants. Each plant was purchased from Charoensuk Osot Pharmacy, Nakhon Pathom, Thailand. The identification of plant materials was confirmed by comparison with authentic voucher specimens deposited at the Herbarium of Southern Center of Thai Medicinal Plants, Faculty of Pharmaceutical Science, Prince of Songkla University, Songkhla Province, Thailand. The plant material details are shown in Table 1.

Table 1 List of plant materials of Kheaw-Hom remedy

Scientific name	Family name	Voucher specimen number	Thai name	Part used	Source	Proportion (%w/w)
Angiopteris evecta (G.Forst.) Hoffm.	Marattiaceae	SKP 110-1 01 05 01	Wan-Kip-Rat	Rhizome	Sukhothai	5.56
Cordyline fruticosa (L.) A.Chev.	Asparagaceae	SKP 005 03 06 01	Mak-Phu	Green leaf	Phetchaburi	5.56
Cordyline fruticosa (L.) A.Chev.	Asparagaceae	SKP 005 03 06 01	Mak-Mia	Red Leaf	Phetchaburi	5.56
Cyathea gigantea (Wall. ex Hook.) Holttum	Cyatheaceae	SKP 059 03 07 01	Ma-Had-Sa-Dam	Rhizome	Suratthani	5.56
Dracaena cochinchinensis (Lour.) S.C.Chen	Asparagaceae	SKP 065 04 12 01	Chan-Daeng	Wood	Nakhon Ratchasima	5.56
Eupatorium fortunei Turcz.	Compositae	SKP 051 05 19 01	San-Phra-Hom	Leaf	Ratchaburi	5.56
Globba variabilis Ridl.	Zingiberaceae	SKP 206 07 13 01	Wan-Ron-Thong	Rhizome	Nakhon Pathom	5.56
Kaempferia galanga L.	Zingiberaceae	SKP 206 11 07 01	Proh-Hom	Rhizome	Ratchaburi	5.56
Limnophila rugosa (Roth) Merr.	Plantaginaceae	SKP 177 12 18 01	Phak-Kra-Chom	Leaf	Nakhon Pathom	5.56
Mammea siamensis T. Anderson	Calophyllaceae	SKP 083 13 19 01	Sa-Ra-Phi	Flower	Ang Thong	5.56
Mesua ferrea L.	Calophyllaceae	SKP 083 13 06 01	Bun-Nak	Flower	Phetchabun	5.56
Mimusops elengi L.	Sapotaceae	SKP 171 13 05 01	Phi-Kun	Flower	Nakhon Pathom	5.56
Myristica fragrans Houtt.	Myristicaceae	SKP 121 13 06 01	Chan-Thet	Wood	Australia	5.56
Nelumbo nucifera Gaertn.	Nelumbonaceae	SKP 125 14 14 01	Bua-Luang	Stamen	Nakhon Sawan	5.56
Pogostemon cablin (Blanco) Benth.	Lamiaceae	SKP 095 16 03 01	Phim-Sen	Leaf	Phetchaburi	5.56
Sophora exigua Craib.	Leguminosae	SKP 072 19 05 01	Phit-Sa-Nat	Rhizome	Sukhothai	5.56
Tacca chantrieri André.	Taccaceae	SKP 189 20 03 01	Nae-Ra-Phu-Sri	Rhizome	Nakhon Ratchasima	5.56
Vetiveria zizanioides (L.) Nash ex Small	Poaceae	SKP 081 22 26 01	Faek-Hom	Root	Nakhon Ratchasima	5.56

Quality control of raw plant materials

Quality control methods include loss on drying, extractive values, total ash, acid-insoluble ash, and heavy metals. These methods were performed following the THP guideline and the quality control methods for herbal materials by World Health Organization (WHO).[8,14]

Loss on drying[14]

Loss on drying or moisture content was analyzed using an electric moisture analyzer (Scaltec instrument, Germany). The sample powder (2 g) was placed on moisture analyzer at 105 °C. The weight of dried sample was displayed. The loss on drying value was calculated using the following equation:

$$\% \text{ Loss on drying} = \frac{\text{Weight of sample before dry (g) - Weight of sample after dry (g)}}{\text{Weight of sample before dry (g)}} \times 100$$

Total ash[11]

The sample powder (2 g) was weighed in a crucible and burned in a muffle furnace (Nabertherm, Germany) at 450 °C for 9 hours. After cooling down in a desiccator, the crucible was burned in a muffle furnace at 450 °C for 5 hours and put in a desiccator until cool down. This process was repeated until the weight was constant. The percentage of total ash was calculated using the following equation:

$$\% \text{ Total ash} = \frac{\text{Stable weight after burning (g)}}{\text{Weight of beginning sample (g)}} \times 100$$

Acid-insoluble ash[11]

The total ash was boiled in 25 ml of 10% HCl for 5 minutes. The insoluble matter was collected on a Whatman ashless filter paper No. 42 and washed with deionized water until the filtrate is neutral. The filter paper was put in the crucible and burned in a muffle furnace at 500 °C for 9 hours. The crucible was cooled in a desiccator and weighed. The procedure was repeated until the weight was constant. The percentage of acid-insoluble ash was calculated using the following equation:

$$\% \text{ Acid-insoluble ash} = \frac{\text{Stable weight after burning (g)}}{\text{Weight of beginning sample (g)}} \times 100$$

Extractive values[11]

Extractive values include ethanol-soluble extractive value and water-soluble extractive value. The sample powder (5 g) was macerated with 100 ml of 95% ethanol in an Erlenmeyer flask for 24 hours, shaking frequently during the first 6 hours and then allowing it to stand for 18 hours. The extract was filtered rapidly. The filtrate (20 mL) was transferred to an evaporating dish and evaporated to dryness at 105 °C until the weight was constant. The water-soluble extractive value method is similar to the above method but uses 0.25% chloroform in water instead of ethanol. The percentage of ethanol and water-soluble extractive values were calculated using the following equation:

$$\% \text{ Ethanol or water-soluble extractive} = \frac{\text{Weight of the extract (g)}}{\text{Weight of dried powder (g)}} \times 100$$

Heavy metals[11]

The sample was prepared using the wet digestion method following THP. The contents of arsenic (As), cadmium (Cd), and lead (Pb) were determined using Graphite Furnace Atomic Absorption Spectrophotometry (GFAAS) (Hitachi®, Model Z-8200 Series) with the modified methods.[15,16] The concentration of As, Cd, and Pb was diluted in the ranges of 5-80 ppb, 0.25-4.00 ppb, and 10-80 ppb, respectively with correlation coefficients (R^2) greater than 0.995.

Stability testing under accelerated storage conditions[13]

Stability testing was performed according to the International Conference on Harmonization (ICH) Q1A (R2) guideline.[13] KHE was contained in amber glass bottles with lids and stored in a stability chamber (Termaks, Norway) under accelerated storage conditions of 40 ± 2 ºC and 75 ± 5% relative humidity (RH) for 180 days. KHE inhibitory effect on LPS-induced NO production in RAW264.7 macrophage cells and bioactive marker stability was determined using high performance liquid chromatography (HPLC) on days 0, 15, 30, 60, 90, 120, 150, and 180, respectively.

Determination of NO production in LPS-induced RAW 264.7 cells[17]

Cell culture

RAW 264.7 (ATCC® TIB-71™), murine macrophage cells, were purchased from American Type Culture Collection (ATCC). The cells were cultured in RPMI 1640 medium containing 10% FBS, 10,000 units/ml of penicillin, and 10,000 µg/mL of streptomycin at 37 °C, 5% CO_2 and 95% relative humidity (RH). All experiments were approved by Institute Biosafety Committee of Thammasat University (Number 067/2018) and performed under biosafety level 2.

Determination of NO production using Griess reagent

RAW 264.7 cells ($1x10^5$ cells/well) were seeded into a sterile 96-well plate and incubated at 37 °C, 5% CO_2, and 95% RH for 24 hours. The old medium was replaced with fresh medium, some without LPS (100 µL/well) and some containing 10 ng/ml LPS (100 µL/well), together with the test samples at various concentrations (100 µL/well). Medium containing 0.2% DMSO without any sample served as a negative control. Prednisolone was used as a positive control. After incubation for 24 hours, 100 µL of supernatant was transferred to another sterile 96-well plate, followed by 100 µL of Griess reagent. The NO production was determined by measuring the accumulation of nitrite which interacted with the Griess reagent. The optical density (OD) was measured using a microplate reader at 570 nm. The percentage of inhibition was calculated using the following equation and IC_{50} values were calculated using a Prism program.

$$\% \text{ Inhibition} = \frac{(OD_{control} - OD_{sample})}{OD_{control}} \times 100$$

Where, $OD_{control}$ = mean of $OD_{control\,(+LPS)}$ - mean of $OD_{control\,(-LPS)}$
OD_{sample} = mean of $OD_{sample\,(+LPS)}$ - mean of $OD_{sample\,(-LPS)}$

Determination of cytotoxicity using MTT assay

Viable cells were determined using the MTT assay as described by Makchuchit.[17] The method used was the same as above. MTT solution (10 µL, 5 mg/ml in PBS) was added into the well, which was without LPS, and incubated at 37 °C in 5% CO_2 for 2 hours. The supernatant was removed and 100 µL of isopropanol contained 0.04 M HCl was added to dissolve the formazan production produced in the cells. The OD was measured using the microplate reader at 570 nm. The percentage of toxicity was calculated using the equation given below and performed in triplicate. If the percentage of toxicity was greater than 30%, the test samples were considered to be toxic.

$$\% \text{ Toxicity} = \frac{(OD_{control} - OD_{sample})}{OD_{control}} \times 100$$

Where; mean of $OD_{control}$ = mean of $OD_{control\,(-LPS)}$
mean of OD_{sample} = mean of $OD_{sample\,(-LPS)}$

Determination of bioactive marker using HPLC

Ethyl *p*-methoxycinnamate (EPMC), a bioactive marker of KHE, was determined using HPLC system, with diode array detector and automatic injector. A reversed-phase column, Agilent® Eclipse XDB-C18 (size 4.6 x 250 mm, 5µm) with guard column was used as a stationary phase. The mobile phase was composed of water : acetonitrile starting from 95:5 v/v to 90:10 v/v in total run time 60 minutes. The pump flow rate was set at 1 ml/min. Diode array detector was set at 320 nm. KHE (10 mg) was dissolved in 1 ml of methanol and filtered through a 0.45 µm nylon filter. EPMC was determined within the concentrations of 1-400 µg/mL. A volume of 10 µL was injected into the HPLC column and EPMC was separated under the above chromatographic condition. The peak area of EPMC was calculated against the standard curve using the linear least-squares regression equation.

Statistical analysis

All experiments were performed in triplicate. The quality control results are expressed as the mean ± standard deviation (SD). The stability testing results are expressed as mean ± standard error of mean (SEM). IC_{50} values were calculated by Prism program. The difference between each group was analyzed using one-way of variance (ANOVA). *P*-value less than 0.05 was considered significant.

Results

Quality control of raw plant materials

The results of quality control are shown in Table 2. The percentage loss on drying of KH was 8.66 ± 0.47%. Among all the samples tested, *A. evecta* demonstrated the highest percentage of loss on drying (9.93 ± 0.27%), while *D. cochinchinensis* showed the lowest percentage (5.98 ± 0.33%).

The percentage of total ash of KH was 6.17 ± 0.06%. *V. zizanioides* showed the highest percentage of total ash (10.94 ± 0.57%), whereas *A. evecta* showed the lowest percentage (3.15 ± 0.11%). The percentage of acid-insoluble ash of KH was 1.14 ± 0.07%. Among all the samples tested, *V. zizanioides* demonstrated the highest percentage of acid-insoluble ash (2.23 ± 0.05%), whereas *D. cochinchinensis* showed the lowest percentage (0.32 ± 0.03%).

The percentage of ethanol and water-soluble extractive values of KH were 10.62 ± 0.12 and 13.78 ± 0.54%, respectively. *D. cochinchinensis* showed the highest percentage of ethanol-soluble extractive value (25.25 ± 1.04%), whereas *N. nucifera* demonstrated the lowest (1.22 ± 0.02%). The highest water-soluble extractive value was found in *V. zizanioides* (56.49 ± 0.13%), whereas *M. fragrans* showed the lowest (1.69 ± 0.06%).

The results revealed that KH met the requirements of THP. The heavy metals of KH and its plant ingredients are shown in Table 3. Arsenic (As), cadmium (Cd), and lead (Pb) contents of KH were 0.01 ± 0.00 ppm, 0.01 ± 0.00 ppm, and 0.02 ± 0.00 ppm, respectively. The amounts of heavy metals of eighteen plant materials in this study met the standard criteria.

Table 2 The results of quality control of KH and eighteen plant materials

| Sample | % Loss on drying | | % Total ash | | %Acid insoluble ash | | % Extractive values | | | |
| | | | | | | | Ethanol-soluble | | Water-soluble | |
	Mean ± SD	Limit	Mean ± SD	Limit	Mean ± SD	Limit	Mean ± SD	Limit	Mean ± SD	Limit
Angiopteris evecta	9.93 ± 0.27	≤10	3.15 ± 0.11	≤10	0.46 ± 0.01	≤2	2.08 ± 0.08	-	14.43 ± 0.33	-
Cordyline fruticosa (Green leaf)	7.11 ± 0.70	≤10	7.68 ± 0.22	≤10	0.59 ± 0.04	≤2	5.24 ± 0.28	-	17.96 ± 0.76	-
Cordyline fruticosa (Red leaf)	7.17 ± 0.66	≤10	7.99 ± 0.46	≤10	0.53 ± 0.12	≤2	5.71 ± 1.12	-	17.42 ± 0.58	-
Cyathea gigantea	7.63 ± 0.12	≤10	3.37 ± 0.33	≤10	0.57 ± 0.23	≤2	2.89 ± 0.31	-	6.72 ± 0.35	-
Dracaena cochinchinensis	5.98 ± 0.33	≤8*	0.95 ± 0.32	≤1*	0.32 ± 0.03	≤2	25.25 ± 1.04	≥12*	3.04 ± 0.23	≥1*
Eupatorium fortunei	6.39 ± 0.18	≤10	5.63 ± 0.52	≤10	0.67 ± 0.08	≤2	3.36 ± 0.17	-	18.48 ± 0.85	-
Globba variabilis	8.85 ± 0.64	≤10	7.42 ± 0.16	≤10	1.10 ± 0.02	≤2	4.84 ± 1.08	-	11.34 ± 0.94	-
Kaempferia galanga	6.67 ± 0.23	≤11*	5.52 ± 0.14	≤8*	1.32 ± 0.04	≤2*	3.45 ± 1.21	≥2.5*	14.61 ± 0.55	≥14*
Limnophila rugosa	6.39 ± 0.18	≤10	9.82 ± 0.71	≤10	0.83 ± 0.21	≤2	7.62 ± 0.70	-	15.55 ± 1.12	-
Mammea siamensis	7.74 ± 0.17	≤10	7.98 ± 0.32	≤10	0.43 ± 0.02	≤2	2.84 ± 0.17	-	25.39 ± 1.27	-
Mesua ferrea	8.57 ± 0.59	≤11*	4.91 ± 0.21	≤5*	1.49 ± 0.34	≤1.5*	5.66 ± 0.10	≥4.5*	8.24 ± 0.49	≥2.5*
Mimusops elengi	8.59 ± 0.36	≤16*	5.97 ± 0.19	≤7*	1.29 ± 0.30	≤3*	8.23 ± 1.31	≥8*	10.30 ± 0.27	-
Myristica fragrans	6.10 ± 0.22	≤10	8.58 ± 0.26	≤10	1.78 ± 0.02	≤2	1.39 ± 0.09	-	1.69 ± 0.06	-
Nelumbo nucifera	8.69 ± 0.34	≤12*	5.01 ± 0.63	≤6*	0.69 ± 0.31	≤1*	1.22 ± 0.02	-	10.62 ± 0.49	≥10.5*
Pogostemon cablin	9.55 ± 0.39	≤10	9.52 ± 0.11	≤10	1.18 ± 0.14	≤2	3.37 ± 0.29	-	13.13 ± 0.37	-
Sophora exigua	6.35 ± 0.32	≤10	4.60 ± 0.06	≤10	1.07 ± 0.08	≤2	13.52 ± 0.58	-	15.78 ± 0.65	-
Tacca chantrieri	7.31 ± 0.98	≤10	4.89 ± 0.07	≤10	0.82 ± 0.08	≤2	5.61 ± 0.84	-	17.55 ± 0.23	-
Vetiveria zizanioides	8.84 ± 0.74	≤10	10.94 ± 0.57	≤10	2.23 ± 0.05	≤2	2.36 ± 0.21	-	56.49 ± 0.13	-
Kheaw-Hom remedy	**8.66 ± 0.47**	-	**6.17 ± 0.06**	-	**1.14 ± 0.07**	-	**10.62 ± 0.12**	-	**13.78 ± 0.54**	-

Note: * indicated the standard value of THP 2022
- indicated not reported

Table 3 The results of heavy metals of KH and eighteen plant materials

Sample	Heavy metal (ppm)		
	As	Cd	Pb
Angiopteris evecta	0.14 ± 0.01	0.03 ± 0.00	ND
Cordyline fruticosa (Green leaf)	0.18 ± 0.07	0.03 ± 0.02	ND
Cordyline fruticosa (Red leaf)	0.10 ± 0.04	0.01 ± 0.00	ND
Cyathea gigantea	0.16 ± 0.04	0.02 ± 0.01	ND
Dracaena cochinchinensis	0.13 ± 0.03	0.04 ± 0.05	ND
Eupatorium fortunei	0.13 ± 0.05	0.20 ± 0.01	ND
Globba variabilis	0.11 ± 0.06	0.05 ± 0.06	ND
Kaempferia galanga	0.03 ± 0.00	0.16 ± 0.00	ND
Limnophila rugosa	0.09 ± 0.02	0.03 ± 0.02	ND
Mammea siamensis	0.19 ± 0.06	0.04 ± 0.06	ND
Mesua ferrea	0.17 ± 0.04	0.00 ± 0.00	ND
Mimusops elengi	0.17 ± 0.00	0.11 ± 0.01	ND
Myristica fragrans	0.09 ± 0.02	0.00 ± 0.00	ND
Nelumbo nucifera	0.13 ± 0.05	0.02 ± 0.02	ND
Pogostemon cablin	0.15 ± 0.06	0.00 ± 0.00	ND
Sophora exigua	0.11 ± 0.03	0.11 ± 0.06	ND
Tacca chantrieri	0.12 ± 0.10	0.12 ± 0.03	ND
Vetiveria zizanioides	0.19 ± 0.03	0.03 ± 0.01	ND
Kheaw-Hom	0.01 ± 0.00	0.01 ± 0.00	0.02 ± 0.00
Limit*	**≤ 4**	**≤ 0.3**	**≤ 10**

Note: * indicated the standard value of THP 2022
       ND = not detected

Stability testing under accelerated conditions

The stability testing results of KHE under accelerated conditions at day 0, 15, 30, 60, 90, 120, 150, and 180 on inhibitory effects of NO production and EPMC content are shown in Table 4. The inhibitory effect on NO production and EPMC content of KHE from day 15 until day 180 did not show a significant difference when compared with day 0 ($p > 0.05$). The chromatograms on the stability of EPMC content are shown in Figure 1.

Table 4 Stability of KHE on inhibitory effects of NO production and EPMC content during 180-day storage under accelerated conditions at 40 ± 2 °C and $75 \pm 5\%$ RH

Samples	IC_{50} of NO production (µg/mL)	EPMC content (mg/g of extract)	% Remaining of EPMC
Day 0	34.79 ± 0.90	16.53 ± 0.15	100.00
Day 15	36.63 ± 2.85	16.50 ± 2.93	99.77
Day 30	37.33 ± 3.55	15.97 ± 1.91	96.60
Day 60	32.86 ± 3.19	16.22 ± 1.65	98.13
Day 90	33.44 ± 2.68	15.94 ± 2.73	96.41
Day 120	36.97 ± 2.51	16.30 ± 0.81	98.61
Day 150	38.91 ± 2.01	16.91 ± 0.08	102.26
Day 180	39.09 ± 1.37	15.02 ± 2.21	90.87

The data were analyzed using one-way ANOVA followed by Dunnett's Multiple Comparison Test.
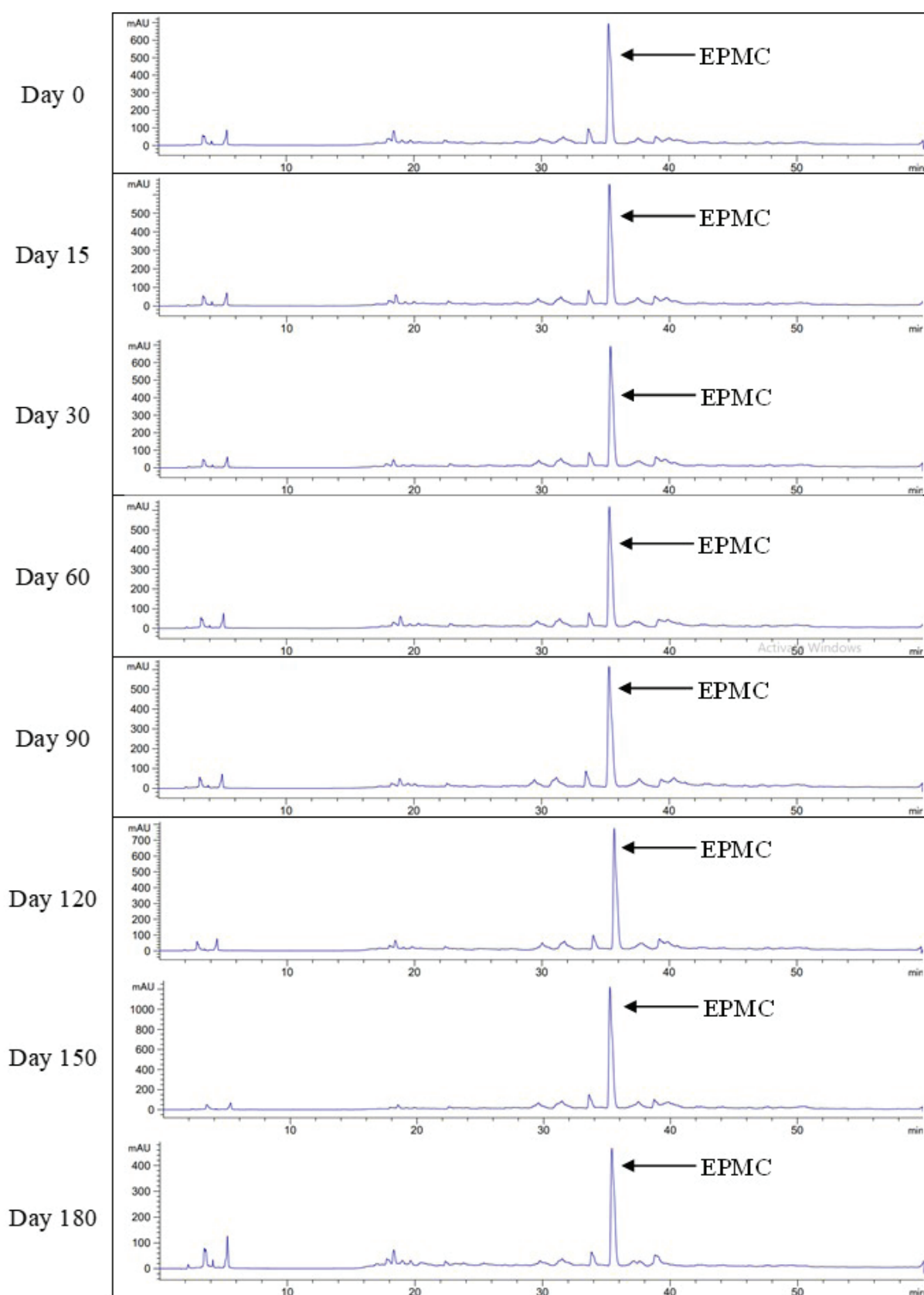[*]Significantly differences ($p < 0.05$) compared with day 0

Figure 1 HPLC chromatogram on the stability of EPMC content in KHE during 180-day storage under accelerated conditions at 40 ± 2 °C and 75 ± 5% RH

Discussion

KH, a Thai traditional antipyretic remedy for children, has been included in the NLEM. However, according to the THPP, there are four monographs of antipyretic remedies, namely Chan-Tha-Li-La, Ha-Rak, Pra-Sa-Chan-Daeng, and Pra-Sa-Pro-Yai remedy.[10] Unfortunately, there is currently a lack of available data on the quality control of KH within the THPP. In this study, the quality control and stability of KH were evaluated following the standard guidelines to support the establishment of a quality specification for ensuring and controlling the quality of KH.

The quality controls of KH and its eighteen plant materials were conducted in accordance with the THP and WHO guidelines including loss on drying, extractive values, total ash, acid-insoluble ash, and heavy metals.[11,14] Loss on drying is one of the most important for quality control because an excess of water in plant materials will encourage microbial growth, the presence of fungi or insects, and the deterioration of active compounds following hydrolysis. Total ash includes both physiological ash, which is from the plant tissue itself, and non-physiological ash, which is from extraneous matter (sand and soil) adhering to the plant surface. Acid-insoluble ash is the amount of silica, especially sand and siliceous earth, that is a residue derived after boiling the total ash with diluted acid and burning the remaining insoluble matter. Extractive values are used to determine the quantity of active constituents extracted with solvents of plant materials because no suitable chemical or biological assay exists.[14]

The standard requirements on quality control are only available for 5 out of 18 of the raw plant materials listed of this remedy in THP i.e., *K. galanga*, *D. cochinchinensis*, *M. elengi*, *M. ferrea*, and *N. nucifera*.[11] Although there is no specific requirement for KH in THPP, the general requirements of loss on drying, total ash, and acid-insoluble ash for the herbal plants should be less than 10%, 10%, and 2%, respectively.[18] The results revealed that KH and all plant materials met the standard criteria except *V. zizanioides*. The total ash and acid-insoluble ash values of *V. zizanioides* were higher than the general standard values. These results were similar to the previous study which reported that the total ash and acid-insoluble ash of *V. zizanioides* roots were 10.63 ± 3.68% and 9.10 ± 3.41%, respectively.[19] A possible explanation for the high values of total ash and acid-insoluble ash is contamination from sand or small amounts of gravel in the root part of the plant.

The amounts of heavy metals which are As, Cd, and Pb depends on the location, the soil quality, or the water quality during cultivation. THP suggested that the maximum amounts of the heavy metals, based on the acceptable daily intake values, are as follows: As 4 ppm, Cd 0.3 ppm and Pb 10 ppm.[11] The results revealed that the amounts of heavy metals of KH and all plant materials in this study met the standard criteria of THP.

Stability testing was performed following the ICH guideline to provide evidence related to shelf life and recommended storage conditions of the drug.[13] Previous studies reported that KHE and EPMC exhibited high anti-inflammatory activities by inhibition of NO and prostaglandin E_2 (PGE_2) production. Similarly, KHE also exhibited high EPMC content. These results correlated with its bioactivity.[20] Therefore, EPMC was used as bioactive marker of KHE. The results indicated that KHE was stable under accelerated storage conditions until day 180 without losing the NO production inhibitory activity and EPMC content. Thus, KHE could be stored at room temperature for at least 2 years. However, a long-term storage stability study of KHE should be conducted to confirm the results from accelerated storage conditions testing.

This study is the first report on the quality control and stability testing of KH. The information on quality control and stability of KH can serve as a valuable dataset for the establishment of a reference standard for KH remedy and become a reference standard for future scientific studies and manufacturing to ensure the quality and shelf life of KH.

Compliance with Ethics Requirements

The experiments were approved by the Institute Biosafety Committee of Thammasat University (Number 014/2561) and performed under biosafety level 2.

Conflict of interest

The authors declare that they have no conflict of interests.

Author Contributions

Kanmanee Sukkasem, a Ph.D. degree student, carried out all experiments, performed the data analyses, and drafted the manuscript. **Arunporn Itharat**, the supervisor of Kanmanee Sukkasem, contributed to submitting all research grants, designed the study, evaluated the results, and approved this manuscript. **Pakakrong Thong-deeying**, **Weerachai Pipatrattanaseree, Sunita Makchuchit** provided technical guidance for the experiments. **Chonthicha Kongkwamcharoen** contributed to the implementation of the experiment. **Neal M. Davies** edited the manuscript.

References

1. Notification of the National Drug System Development Committee Re: National List of Essential Medicines. Ministry of Public Health. http://dmsic.moph.go.th/index/download/852. Published 2021. Accessed June 12, 2023.
2. Sanguansermsri D, Lamlertthon S, Pongcharoen S, Preechanukool K, Chumpol S, Promkhatkaew D. Anti-varicella zoster virus of Ya-keaw remedies. Thailand Science Research and Innovation. http://elibrary.trf.or.th/project_content.asp?PJID=MRG4680174. Published June 30, 2005. Accessed June 12, 2023.
3. Chaihad P, Pholor N, Khamseetha P, Kongmuang S, Pongpirul K, Phadungkit M. Efficacy and safety of Ya-Khiao-Hom powder for the treatment of aphthous ulcer. *J Thai Trad Alt Med*. 2021; 19(2):344-353.
4. Khamsetha P, Chaihad P, Kongmuang S, et al. Oral and topical application of Kheaw Hom powder on oral ulcer: efficacy and patient preference (KHOU). *Gut*. 2019;68(1):A77-A77.
5. Kongkeaw P, Seba N. Comparative study of tepid sponging using Ya Khiao-Hom and traditional method for reducing body temperatures on pediatric patients with pneumonia and high fever: A Retrospective Case-Cohort Study. *J Thai Trad Alt Med*. 2023;21(1):18-24.
6. Sukkasem K. *Biological activities of Thai traditional remedy called Kheaw-Hom and its plant ingredients*. [Master's thesis]. Faculty of Medicine: Thammasat University; 2015.
7. Ouncharoen K, Itharat A, Chaiyawatthanananthn P. In vitro free radical scavenging and cell-based antioxidant activities of Kheaw-Hom remedy extracts and its plant ingredients. *J Med Assoc Thai.* 2017;100(6):241-249.
8. Sukkasem K, Panthong S, Itharat A. Antimicrobial activities of Thai traditional remedy "Kheaw-Hom" and its plant ingredients for skin infection treatment in chickenpox. *J Med Assoc Thai*. 2016;99(4):116-123.
9. Chaniad P, Techarang T, Phuwajaroanpong A, et al. Exploring potential antimalarial candidate from medicinal plants of Kheaw Hom remedy. *Trop Med Infect Dis*. 2022;7(11):368.
10. Thai Herbal Preparation Pharmacopoeia. Department of Thai Traditional and Alternative Medicine, Ministry of Public Health. https://thpp.dtam.moph.go.th/. Published 2022. Accessed June 12, 2023.
11. Thai Herbal Pharmacopoeia. Department of Medical Science, Ministry of Public Health. https://bdn.go.th/thp/home. Published 2021. Accessed June 12, 2023.
12. Department of Thai Traditional and Alternative Medicine, Ministry of Public Health. *Quality control of Thai Herbal Preparation. 2nd ed.* Bangkok: Chulalongkorn University Press; 2021.
13. European Medicine Agency. *ICH topic Q1A (R2) stability testing of new drug substances and products, Note for guidance on stability testing: stability testing of new drug substances and products (CPMP/ICH/2736/99)*. London, England: EMEA; 2006.
14. World Health Organization. *Quality control methods for herbal materials*. Geneva: World Health Organization Press; 2011.
15. Jansom C, Jansom V. Development and validation of analytical methods for arsenic and mercury determination by atomic absorption spectrophotometry. *Tham Med J*. 2019;19(1):25-35.
16. Duangteraprecha S, Jamtaweekul J, Sukphan P, Inthongkaew P. Method development and validation for determination of arsenic, lead and cadmium in herbal medicines by graphite

furnace atomic absorption spectrophotometry. *Bull Dept Med Sci*. 2015;1:20-33.

17. Makchuchit S, Rattarom R, Itharat A. The anti-allergic and anti-inflammatory effects of Benjakul extract (a Thai traditional medicine), its constituent plants and its some pure constituents using in vitro experiments. *Biomed Pharmacother*. 2017;89:1018-1026.

18. Chokevivat V. Quality of crude drug. *J Thai Trad Alt Med*. 2004;2:84-91.

19. Issaravanich S, Palanuvej C, Tunsaringkarn T, et al. Pharmacognostic specification of Vetiveria zizanioides roots in Thailand. *J Health Res*. 2008;22(1):9-14.

20. Sukkasem K, Itharat A, Thisayakorn K, et al. Exploring in vitro and in vivo anti-inflammatory activities of the Thai traditional remedy Kheaw-Hom and its bioactive compound, ethyl *p*-methoxycinnamate, and ethnopharmacological analysis. *J Ethnopharmacol*. 2024; 319:117131.

Review Article

An Update in Adult Intraosseous Infusion

Wirot Sombatthavoankun*

Abstract

The Intraosseous (IO) needle was developed in 1920s to access the vascular system via the bone marrow cavity. Around the 2010s, there was widespread interest in IO after the American Heart Association (AHA) recommended that intraosseous access is an optional route when intravenous (IV) access cannot be obtained quickly. IO had a higher success rate (99.6%), was faster to perform (15-24 seconds), had a nearly equal flow rate (1-5L/hr), and had almost equal drug bioavailability to IV. The complication of IO becoming dislodged was 10-16%, needle dislocation was 0.8%, needle bending was 0.4% and parafusion (defined as fluid leakage at the insertion site causing tissue edema surrounding the leakage point) was 0.4%. Most retrospective trials and meta-analysis studies found that hospital discharge, return of spontaneous circulation (ROSC), and favorable neurological outcome was higher with IV than with the IO group. In conclusion, IO is still beneficial for immediate vascular access and should be placed after and/or simultaneously to IV insertion.

Objectives: to update content of adult intraosseous infusion in critical situations.

Keywords: intraosseous infusion, intraosseous access, IO, intravenous access, IV

Bangkhla Hospital, Chachoengsao 24110, Thailand
* **Corresponding author:** Wirot Sombatthavoankun, M.D., Bangkhla Hospital, Chachoengsao 24110, Thailand Email: wxwsody@hotmail.com
Tel. +66 3854 1009-10

Introduction

The Intraosseous (IO) needle was developed in the 1920s[1] to access the vascular system via the bone marrow cavity but was decreasingly used when an intravenous needle was developed in the 1950s.[2] In the 1980s, intraosseous devices were reintroduced in combat or emergency conditions.

The Food and Drug Administration (FDA) approved the use of a manual-driven First Access for Shock and Trauma (FAST1™) device in 1997, an automatic spring-loaded impact-driven Bone Injection Gun (BIG™) in 2000 which was developed to NIO™ later, and Semi-automatic battery driven EZ-IO™ in 2004.[2] Around the 2010s, there was wide interest in IO after the American Heart Association (AHA) recommended that intraosseous access is an optional route when intravenous (IV) access cannot be obtained quickly. In 2020, AHA recommended that epinephrine should be given as soon as possible in non-shockable cardiac arrest and that IO is the best possible option to achieve this.

Success rate

Overall, IO success rate was 99.6%[3] with a first attempt success rate of 85.9-94.8%,[3,4] while first attempt success rate of IV is 50-81.6%.[4,5] In addition, first-attempt success rate was 95% for proximal humerus,[6] 95% for distal femur,[6] 84-92% for proximal tibial[2,6] and 72% for sternum using FAST1™.[7,8] And there was no significant difference between EZ-IO™ and NIO™ device.[2]

Indications

- Failure of venous insertion in 2 attempts and/or taking more than 90 seconds.[9-11]
- Immediate vascular access is required.[11]

Contraindications

- Site of fracture, burn, infection, or bone diseases (e.g. bone tumor, osteoporosis, osteogenesis imperfecta).
- Recent orthopedic surgery or previous IO site.
- Lower limb in patients with severe abdominal trauma[10,11]

Procedure time

The time to perform IO was around 15-20 seconds for EZ-IO™,[10] 17-24 seconds for BIG™/ NIO™,[5,10] 20-24 seconds for manual needle,[5,10] and 50-67 seconds for FAST1™.[8,10]

Complications

Minor complications: dislodged IO rate was 16% for the proximal humerus, 10% for the distal femur, and 15% for the proximal tibia.[6] Needle dislocation was 0.8%, needle bending was 0.4% and parafusion was 0.4%.[3] Severe complications: fat emboli after IO insertion were not different from the non-IO group, and only CPR could cause emboli in animal studies.[12] Bone damage was observed in animal studies and found that metaphyseal bone was completely resolved at 3 weeks and complete epiphyseal closure at 6 months.[12]

Flow rate

Generally, the flow rate was 5 L/hr in the proximal humerus and 1L/hr in the proximal tibia. [6,10] However, cadaveric and critical human studies showed that the gravity flow rate was around 3 L/hr in sternal IO (SIO),[13] 2.4 L/hr in humeral IO (HIO),[13,14] and 1.8 L/hr in tibial IO (TIO).[13,14] Under 300 mm Hg pressure flow rate was around 3.6-9.6 L/hr in SIO,[13] 4.8-6 L/hr in HIO,[13,14] and 3-7.2 L/hr in TIO.[13,14]

Pharmacokinetic studies

The systematic review found that in non-cardiac arrest animal studies, IO had an equivalent bioavailability (area under the curve of plasma concentration (AUC)), maximum plasma concentration (C_{max}), and time to maximum plasma concentration (T_{max}) compared to IV administration for many drugs such as epinephrine, atropine, sodium bicarbonate, dextrose 50%, and calcium chloride.[12]

Mostly hypovolemic cardiac arrest animal studies found no statistically significant differences between IO groups (SIO,[15] HIO,[16,17] TIO[18]) and IV groups in C_{max} or T_{max}, but lower C_{max} in IO groups and longer T_{max} in IO groups,[15,16,18] such as lower C_{max} in the TIO group $56,292 \pm 11,504$ ng/mL compared to $74,258 \pm 11,504$ ng/mL in the IV group (p = 0.291), and longer T_{max} in the TIO group 120 ± 25 seconds compared to 94 ± 25 seconds in the IV group (p = 0.475).[18]

But one normovolemic cardiac arrest study found that C_{max} in the IV group was equal to both

HIO (p = 0.33) and TIO groups (p = 0.060), but C_{max} in the HIO group was higher than the TIO group (p = 0.007). The T_{max} in the IV group was equal to the HIO group (p = 0.328), but T_{max} in both IV and HIO groups were shorter than TIO group (p < 0.05).[17]

Location
- Sternum: 1 cm below the sternal notch (with FAST1™ only).
- Proximal humerus: The humerus should be internally rotated, the elbow flexed to 90 degrees, and the hand should be placed on the abdomen. Then the needle (length > 45 mm) is inserted 2 cm above the surgical neck at 45 degrees pointing to the contralateral hip.
- Distal femur: With the leg straightened and centered in the anterior plane, 1 cm proximal to the patella, and 1 to 2 cm medially.
- Proximal tibia: 1 cm to 2 cm inferomedial to the tibial tuberosity in the center of the tibia.
- Distal tibia: 2 cm proximal to the medial malleolus in the center of the tibia.[11]

A retrospective CT/MRI study found that the proper insertion depth was 26.0-56.5 mm in males and 27.5-52.5 mm in females for the proximal humerus, 20.5-42.0 mm in males and 32.5-45.5 mm in females for proximal tibia, and 16.5-34.5 mm in males and 14.5-30.5 mm in females for distal tibia. Females had a thicker soft tissue cover (+7.8 mm, 95% CI 3.7-10.1, p < 0.01) in the proximal tibia. Although, all 3 sites did not have gender-specific differences in the IO insertion depth.[19]

Technique
- When the needle passes through the cortical bone, loss of resistance is felt, the tip of the needle is in bone marrow cavity.
- Confirm the position of the IO needle by checking for the stability of the needle in the bone, and the ability to flush with saline, without extravasation.[11]
- For conscious patients, 20-40 mg (epinephrine-free, preservative-free) lidocaine is slowly injected through the IO catheter to relieve flush pain. And wait 2 minutes for the lidocaine effect before flushing.[11,20]

- Some studies recommended using an infusion pump or pressure bag for persistent, continuous flow[10,20] and stabilizer dressings with restricted ambulation to prevent IO dislodement.[20]

Duration
- US FDA recommended to use IO not more than 24 hrs, but could be extended to 48 hrs if IV access is not available.[11,20]
- One stable co-morbidities patients study found no serious adverse events up to 30 days-follow up, after 48 hrs IO insertion in both proximal humerus and proximal tibia. Although it had a limitation of using normal saline infusion only.[20]

Lab
- Systematic review showed that evidence on the agreement between IO and the arterial or venous sample was weak due to improper statistical analysis (recommended using the Bland-Altman method), and small sample size.[21]
- A small study of 17 CPR patients found that IO and IV samples were most comparable for sodium bicarbonate, base excess and pH. In addition, intraclass correlation coefficients were excellent for sodium.[22]

Clinical outcome
In normo-hypovolemic cardiac arrest animal studies found that no statistical difference in ROSC for SIO vs IV (p = 0.191),[15] HIO vs IV (p = 1),[16] or HIO vs TIO vs IV (p > 0.05)[17] and time to ROSC for SIO vs IV (p > 0.05),[15] or HIO vs IV (p = 0.22).[16]

In a retrospective study, overall ROSC is the same in all 3 IO sites by proximal humerus 36.3% (95% CI 32.6-40.6), distal femur 30.3% (95% CI 27.3-33.4), and proximal tibia 29.2% (95% CI 25.5-33.2).[6]

An APLS trial found that discharge survival was significantly higher in recipients of IV amiodarone (RR 1.26, 95% CI 1.06-1.50); absolute survival difference 5.5% (95% CI 1.5-9.5) and IV lidocaine (RR 1.21, 95% CI 1.02-1.45); absolute survival difference 4.7% (95% CI 0.7-8.8), but not in recipients of IO amiodarone (RR 0.94, 95% CI 0.66-1.32) or IO lidocaine (RR1.03, 95% CI 0.74-1.44). A limitation of this study was the route of administration

was not randomized, but drugs were randomized (amiodarone: lidocaine: placebo = 1:1:1). This trial suggested that both drug outcomes were better in the IV group.[23]

A retrospective study found that IO group was not associated with survival to discharge (OR 0.81, 95% CI 0.55-1.21, p = 0.31), but was associated with a lower likelihood of ROSC (OR 0.67, 95% CI 0.50-0.88, p = 0.004) and survival to hospital admission (OR 0.68, 95% CI 0.51-0.91, p = 0.009).[24] Multivariable adjusted OR between IO access and outcome were similar to the results from the overall cohort when the vascular access interval was included in the model for survival to discharge (OR 0.87, 95% CI 0.54-1.40, p = 0.56) and ROSC (OR 0.69, 95% CI 0.50-0.95, p = 0.02), although survival to hospital admission was no longer statistically significant (OR 0.72, 95% CI 0.51-1.01, p = 0.06).[24]

A secondary analysis of the PRIMED study found that intraosseous access was associated with poorer out-of-hospital cardiac arrest survival compared to IV (OR 0.24, 95% CI 0.12-0.46) and lower favorable neurological outcomes than IV (1.5% vs 7.6%). Sensitivity analyses revealed similar results by using the propensity score to adjust the probability of vascular access type.[25]

Meta-analysis suggested no significant association between the favorable neurological outcome and types of vascular access (OR 0.60, 95% CI 0.27-1.33, I^2 95%), but had a trend to favor IV in short-term survival (OR 0.71, 95% CI 0.59-0.85, I^2 86.45), and survival to hospital discharge (OR 0.66, 95% CI 0.42-1.04, I^2 88.75).[26]

The subgroup analyses found that time to intervention might be a significant outcome moderator. For example, the favorable neurological outcome, if the studies were not adjusted with time to intervention, the heterogeneity extensively decreased, and IO access was inversely associated with favorable neurological outcome (OR 0.22, 95% CI 0.17-0.30, I^2 0%).[26]

Another meta-analysis suggested that pooled results from four adult observational studies favored IV access with very low certainty of evidence in favorable neurological outcomes (OR 0.60, 95% CI 0.52-0.69, I^2 89), ROSC (OR 0.72, 95% CI 0.68-0.76, I^2 57) and survival to hospital discharge (OR 0.71, 95% CI 0.63-0.79, I^2 71).[27]

And time to drug administration led to resuscitation time bias in observational studies.[26,27]

Simulation training

In a crossover randomized simulation study,[1] 75 novice physicians were trained only one time to IO access with BIG™ Pediatric, EZ-IO™, NIO™ Pediatric, and Jamshidi needle. After 6 months without IO application, 68 physicians can perform IO correctly with a success rate of 100% for NIO™ Pediatric, 97% for EZ-IO™, 90% for BIG™ Pediatric, and only 43% for manual Jamshidi needle. Moreover, 3 mechanical devices had a lower procedure time than the Jamshidi needle (16-29 seconds vs 29.5-45 seconds, P < 0.001) and needle bending was found to be 57% for jamshidi needle but less than 10% with mechanical devices.[1] Finally, one simulation study suggested that training should be done more than 3 times a year but in uncommon high-risk scenarios every 6 weeks to ensure high performance throughout the year.[28]

Discussion

In the ideal, IO is equal to IV in pharmacokinetic parameters, therefore IO outcome should be equal to IV outcomes if there are the same scenarios, especially at similar duration of time to vascular access, which is supported by animal studies in normo-hypovolemic cardiac arrest studies.[12,15-18] However, in most retrospective[24] studies, clinical trials[23,25] and meta-analysis,[26,27] human studies found that hospital discharge, ROSC, and favorable neurological outcome in IV are higher than IO group, but these have some limitations. Especially vascular type access is not randomly assigned; and this can lead to selection bias, such as resuscitation time bias, found by meta-analysis of observational studies or non-randomized trial.[26,27] This bias can lead to the inverse outcome or dilutional effect of IO. Generally, longer vascular access leads to prolonged CPR, and poorer outcomes that are not followed by effective management such as epinephrine administration.[29] Other confounders are the site of IO and the quality of IO function that cause extensively different flow rates in these studies.[6,10,13,14] A well-designed pediatric septic shock RCT confirms that IO is superior to IV in ROSC (93.3% vs 60%, p = 0.002, power back calculation is 83) resulting from rapid vascular access in IO group (52.5 vs 90 seconds, p = 0.001)

and sensitivity analysis suggests that vascular access time had a trend to longer times in deceased group compared to the discharged group (patients in the death group had longer vascular access time than patients that were discharged from hospital) but it did not have statistical difference (75 vs 60 seconds, p = 0.881).[30] The value of IO is rapid vascular access, which leads to faster effective treatment (such as fluid or medications) resulting in better outcome.

In conclusion, intraosseous access provides rapid and reliable access to administer life-saving medications during cardiac arrest. However, IO has shown poorer neurological outcomes, ROSC and the survival outcomes compared to IV. Therefore, we suggest to insert IO after and/or simultaneously to IV insertion to improve clinical outcomes.

Financial support: no
Conflict of interest: no

References

1. Szarpak L, Ladny JR, Dabrowski M, et al. Comparison of 4 Pediatric Intraosseous Access Devices: A Randomized Simulation Study. *Pediatr Emerg Care.* 2020;36(10):e568-e572. doi:10.1097/PEC.0000000000001587.

2. Demir OF, Aydin K, Akay H, Erbil B, Karcioglu O, Gulalp B. Comparison of two intraosseous devices in adult patients in the emergency setting: a pilot study. *Eur J Emerg Med*. 2016;23(2):137-142. doi:10.1097/MEJ.0000000000000187.

3. Helm M, Haunstein B, Schlechtriemen T, Ruppert M, Lampl L, Gäßler M. EZ-IO™(®) intraosseous device implementation in German Helicopter Emergency Medical Service. *Resuscitation.* 2015;88:43-47. doi:10.1016/j.resuscitation.2014.12.015.

4. Clemency B, Tanaka K, May P, et al. Intravenous vs. intraosseous access and return of spontaneous circulation during out of hospital cardiac arrest. *Am J Emerg Med*. 2017;35(2):222-226. doi:10.1016/j.ajem.2016.10.052.

5. Lange P, Umar M, Walker JD, Riddle M, Mochmer P. Evaluation of the NIO™ and T.A.L.O.N Intraosseous Devices as Placed by U.S. Army Conventional Force Combat Medics-A Randomized Crossover Study [published correction appears in Mil Med. 2021 Nov 2;186(11-12):e1257]. *Mil Med*. 2022;187(7-8):e877-e881. doi:10.1093 milmed/usab323.

6. Rayas EG, Winckler C, Bolleter S, et al. Distal \femur versus humeral or tibial IO, access in adult out of hospital cardiac resuscitation. *Resuscitation*. 2022;170:11-16. doi:10.1016/j.resuscitation.2021.10.041.

7. Frascone RJ, Jensen JP, Kaye K, Salzman JG. Consecutive field trials using two different intraosseous devices. *Prehosp Emerg Care*. 2007;11(2):164-171. doi:10.1080/10903120701205851.

8. Byars DV, Tsuchitani SN, Erwin E, Anglemyer B, Eastman J. Evaluation of success rate and access time for an adult sternal intraosseous device deployed in the prehospital setting. *Prehosp Disaster Med*. 2011;26(2):127-129. doi:10.1017/S1049023X11000057\.

9. Tan BKK, Chin YX, Koh ZX, et al. Clinical evaluation of intravenous alone versus intravenous or intraosseous access for treatment of out-of-hospital cardiac arrest. *Resuscitation*. 2021;159:129-136. doi:10.1016/j.resuscitation.2020.11.019.

10. Astasio-Picado Á, Cobos-Moreno P, Gómez-Martín B, Zabala-Baños MDC, Aranda-Martín C. Clinical Management of Intraosseous Access in Adults in Critical Situations for Health Professionals. *Healthcare (Basel)*. 2022; 10(2):367. doi:10.3390/healthcare10020367.

11. Dornhofer P, Kellar JZ. Intraosseous Vascular Access. In: StatPearls. Treasure Island (FL): StatPearls Publishing; June 11, 2022.

12. Elliott A, Dubé PA, Cossette-Côté A, et al. Intraosseous administration of antidotes - a systematic review. *Clin Toxicol (Phila)*. 2017;55(10):1025-1054. doi:10.1080/15563650.2017.1337122.

13. Hammer N, Möbius R, Gries A, Hossfeld B, Bechmann I, Bernhard M. Comparison of the Fluid Resuscitation Rate with and without External Pressure Using Two Intraosseous Infusion Systems for Adult Emergencies, the CI-TRIN (Comparison of InTRaosseous infusion systems in emergency medicINe)-Study. *PLoS One*. 2015;10(12):e0143726. doi:10.1371/journal.pone.0143726.

14. Ngo AS, Oh JJ, Chen Y, Yong D, Ong ME. Intraosseous vascular access in adults using the EZ-IO™ in an emergency department. *Int J Emerg Med*. 2009;2(3):155-160. doi:10.1007/s12245-009-0116-9.

15. Smith S, Borgkvist B, Kist T, Annelin J, Johnson D, Long R. The effects of sternal intraosseous and intravenous administration of amiodarone in a hypovolemic swine cardiac arrest model. *Am J Disaster Med*. 2016;11(4):271-277. doi:10.5055/ajdm.2016.0249.

16. Holloway CM, Jurina CS, Orszag CJ, et al. Effects of humerus intraosseous versus intravenous amiodarone administration in a hypovolemic porcine model. *Am J Disaster Med*. 2016;11(4):261-269. doi:10.5055/ajdm.2016.0248.

17. Beaumont LD, Baragchizadeh A, Johnson C, Johnson D. Effects of tibial and humerus intraosseous administration of epinephrine in a cardiac arrest swine model. *Am J Disaster Med*. 2016;11(4):243-251. doi:10.5055/ajdm.2016.0246.

18. Hampton K, Wang E, Argame JI, Bateman T, Craig W, Johnson D. The effects of tibial intraosseous versus intravenous amiodarone administration in a hypovolemic cardiac arrest procine model. *Am J Disaster Med*. 2016;11(4):253-260. doi:10.5055/ajdm.2016.0247.

19. Miller C, Nardelli P, Hell T, Glodny B, Putzer G, Paal P. Sex differences in appropriate insertion depth for intraosseous access in adults: An exploratory radiologic single-center study [published online ahead of print, 2022 Aug 3]. *J Vasc Access*. 2022;11297298221115412. doi:10.1177/11297298221115412.

20. Philbeck TE, Puga TA, Montez DF, Davlantes C, DeNoia EP, Miller LJ. Intraosseous vascular access using the EZ-IO™ can be safely maintained in the adult proximal humerus and proximal tibia for up to 48 h: Report of a clinical study. *J Vasc Access*. 2022;23(3):339-347. doi:10.1177/1129729821992667.

21. Jousi M, Laukkanen-Nevala P, Nurmi J. Analysing blood from intraosseous access: a systematic review. *Eur J Emerg Med*. 2019;26(2):77-85. doi:10.1097/MEJ.0000000000000569.

22. Tallman CI, Darracq M, Young M. Analysis of intraosseous blood samples using an EPOC point of care analyzer during resuscitation. *Am J Emerg Med*. 2017;35(3):499-501. doi:10.1016/j.ajem.2016.12.005.

23. Daya MR, Leroux BG, Dorian P, et al. Survival After Intravenous Versus Intraosseous Amiodarone, Lidocaine, or Placebo in Out-of-Hospital Shock-Refractory Cardiac Arrest. *Circulation*. 2020;141(3):188-198. doi:10.1161/CIRCULATIONAHA.119.042240.

24. Feinstein BA, Stubbs BA, Rea T, Kudenchuk PJ. Intraosseous compared to intravenous drug resuscitation in out-of-hospital cardiac arrest. *Resuscitation*. 2017;117:91-96. doi:10.1016/j.resuscitation.2017.06.014.

25. Kawano T, Grunau B, Scheuermeyer FX, et al. Intraosseous Vascular Access Is Associated With Lower Survival and Neurologic Recovery Among Patients With Out-of-Hospital Cardiac Arrest. *Ann Emerg Med*. 2018;71(5):588-596. doi:10.1016/j.annemergmed.2017.11.015.

26. Hsieh YL, Wu MC, Wolfshohl J, et al. Intraosseous versus intravenous vascular access during cardiopulmonary resuscitation for out-of-hospital cardiac arrest: a systematic review and meta-analysis of observational studies. *Scand J Trauma Resusc Emerg Med*. 2021;29(1):44. doi:10.1186/s13049-021-00858-6.

27. Granfeldt A, Avis SR, Lind PC, et al. Intravenous vs. intraosseous administration of drugs during cardiac arrest: A systematic review. *Resuscitation*. 2020;149:150-157. doi:10.1016/j.resuscitation.2020.02.025.

28. Ghazali DA, Fournier E, Breque C, Ragot SP, Oriot D. Immersive simulation training at 6-week intervals for 1 year and multidisciplinary team performance scores: a randomized controlled trial of simulation training for life-threatening pediatric emergencies. *Emergencias*. 2019;31(6):391-398.

29. Yauger YJ, Johnson MD, Mark J, et al. Tibial Intraosseous Administration of Epinephrine Is Effective in Restoring Return of Spontaneous Circulation in a Pediatric Normovolemic But Not Hypovolemic Cardiac Arrest Model. *Pediatr Emerg Care*. 2022;38(4):e1166-e1172. doi:10.1097/PEC.0000000000002127.

30. El-Nawawy AA, Omar OM, Khalil M. Intraosseous Versus Intravenous Access in Pediatric Septic Shock Patients Admitted to Alexandria University Pediatric Intensive Care Unit. *J Trop Pediatr*. 2018;64(2):132-140. doi:10.1093/tropej/fmx061.

Review Article

Role of Digital Health in FGIDs, A Mini Review

Navapan Issariyakulkarn[*]

Abstract

Treating functional GI disorders (FGIDs) caused by abnormal gut-brain interactions requires an understanding of individual GI pathophysiology as well as the patient's behaviors. Many physicians frequently struggle to manage these patients due to a lack of knowledge regarding the patient's pathophysiology and behaviors. Many digital tools for collecting and recording patients' health information, which also include patient communication, are available to assist the physician in better understanding the patient. The purpose of this review is to assess how digital health can help FGIDs treatment and the interpretation of GI physiology testing.

Keywords: Functional GI disorders, FGIDs, digital health

Faculty of Medicine, Thammasat University, Pathum Thani 12120, Thailand
[*] **Corresponding author:** Navapan Issariyakulkarn, Faculty of Medicine, Thammasat University, Pathum Thani 12120, Thailand,
Email: drnavapan@yahoo.com

Introduction

Functional GI disorders (FGIDs), diseases of gut-brain interaction, require understanding the patient's GI pathophysiology and their adaptive behavior, for individual management. However, GI physiology tests require an expert to interpret the results case by case, there is more evidence that customized counseling leads to improve FGIDs treatment[1] and because there is no clear biomarker for tracking disease activity, treatment options are often based on the patient's history. Physicians suggest FGIDs patients to manually track their symptoms with dietary, behavioral, and other triggers in order to see whether there is a relationship, but compliance is poor, especially with paper trackers.[2]

The term "digital health" refers to the use of digital information, data, and communication technologies to collect, exchange, and analyze health data in order to improve patient health and health-care delivery.[3] The dominant concept is mobile health (mhealth), which is related to other concepts such as telemedicine, eHealth, and artificial intelligence (AI) in healthcare, according to a review of the definition in 2020.[4] Nowadays, digital health is becoming widely adopted in medical systems. In this article, we will review role of digital health in FGIDs divided by technology.
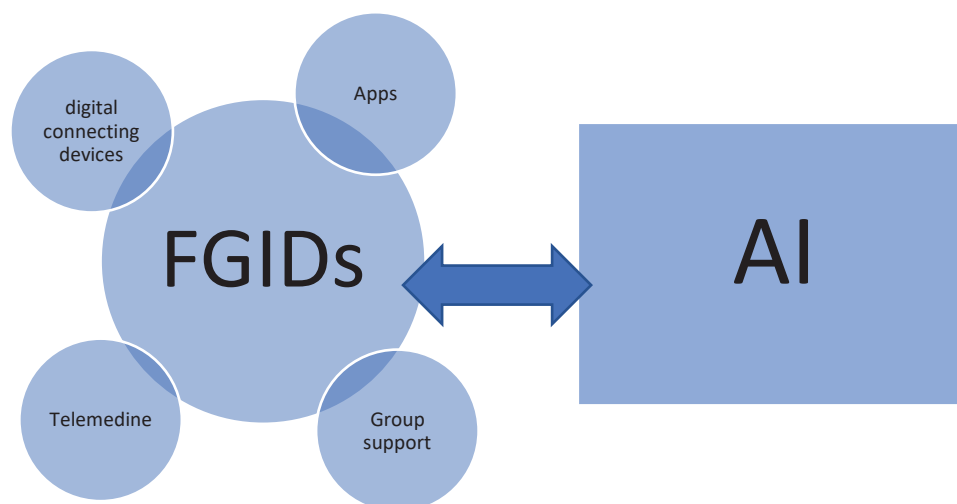
Figure 1 Types of digital health divided by technology.

1. AI and FGIDs

AI is becoming a popular field of study. According to PubMed, more than 3,800 papers totaling artificial intelligence research were published in a single year in 2022. In FGIDs, AI is mostly used to interpret GI physiology tests, find new parameters and analyze questionnaires and images in FGIDs patients. We focus on using AI for interpretation.

1.1 AI and GI physiology tests

In a study by Sandos R et al. from Sweden in 2006, it was shown that the interpretation of esophageal manometry (EM) with a water perfused system by AI showed an accuracy of 60-100%.[5] Nowadays, esophageal manometry has been developed into a high-resolution era. The results of AI interpreted esophageal manometry differ depending on algorithms and machine learning models. While AI interpretation of EM generally exhibits high sensitivity and specificity (over 80%), one study reported a 3% rate of misclassified swallows.[6-8]

Table 1 AI studies interpreting esophageal manometry according to Chicago classification (CC)

Author/year	Type of machine learning	Number of samples	Accuracy	Limitations
Wang (7)/2021	Supervised deep learning EMD- DL model	226 cases	Overall, 91.32% with 90.5% sensitivity and 95.9% specificity	Train AI by divided data into minor/normal/major motility disorders, whereas CC4.0 is no longer divided into minor and major motility disorders
Kou (8)/2022	Supervised with rule-based model, Xgboost, and artificial neural network (ANN) based on CNNs**	1741 cases	88% for 6-swallow-types model 93% for 3-category swallow-pressurization IRP value with mean absolute error of 4.5 (mmHg)	Overlap of EGJOO* with other swallow types causes confusion and misinterpretation may be due to an unbalance in training set categories and ambiguous diagnosis of EGJOO according to CC 4.0
Kou (6)/2021	Supervised with Long short-term memory (LSTM) of deep-learning model	1741 cases	88% accuracy but the number of misclassified swallows is high	This model is based on single swallow data Model is developed before CC 4.0

*EGJOO = Esophagogastric junction outflow obstruction   **CNN = convolutional neural network

Unsupervised machine learning was demonstrated in one study using simple linear discriminative analysis (LDA), but this model is only the first step toward automatic diagnosis.[9] Moreover, a long-term high-resolution esophageal manometry (HREM) recording for 24 hours, demonstrated in a study from Germany, using AI interpretation can reduce the time to interpret from 3 working days to 10-20 minutes.[10]

Other GI physiology tests, such as simultaneous videofluoroscopy and pharyngeal HRM, and high resolution electrogastrogram, using AI to classify between normal and abnormal patterns were showing an accuracy between 70-90%.[11,12] AI was used to find a new parameter for GERD diagnosis in ambulatory pH monitors, but the accuracy was not higher than the older methods.[13] In term of using AI in measuring pH impedance parameters, 80-90% accuracy of AI was shown in some parameters, including number of reflux episodes and PSPW index (post-reflux swallow-induced peristaltic wave). PSPW index is the novel pH impedance parameter which cannot be calculated by a software program and is a time-consuming manual measurement.[14]

Functional luminal imaging probe (FLIP) is a new technology combining with endoscopy, providing three-dimensional diameter, volume and pressure changes, which has recent studies using AI for distinguishing between subtypes of achalasia and fecal incontinence (FI) diagnosis. The results showed a high specificity and moderate sensitivity for FI[15] and a high accuracy for distinguishing between spastic (type 3) and non-spastic achalasia (type 1 and 2).[16]

1.2 AI for questionnaire analysis in FGIDs
GERD questionnaires were reported using AI to distinguish between GERD and non-GERD, including erosive esophagitis (EE) and non-EE, but the accuracy varied from 62-100%.[17] Furthermore, AI was shown to have an accuracy of about 55% in identifying symptomatic models between irritable bowel syndrome (IBS) with constipation and functional constipation when analyzing questionnaires in constipation patients.[18]

1.3 AI for image analysis in FGIDs
In image analysis, AI was used to analyze intestinal motility from video capsule endoscopy and showed 70% sensitivity.[19] In Thailand, the

study by Rattanachaisit P et al. from Chulalongkorn University showed AI diagnosed dyssynergic defecation with 60% accuracy from abdominal radiography.[20]

1.4 AI for other analysis methods in FGIDs

AI was used for diagnosing IBS with bowel sound analysis in one study. By utilizing an AI model, that uses a logistic regression based on IBS Acoustic Index models derived from 26 bowel sound features, the accuracy of diagnosing IBS was approximately 90%.[21] However, in a systematic review of computerized analysis of bowel sounds for the diagnosis of gastrointestinal conditions in 2018, it was not recommended to use bowel sounds without additional studies in clinical practice.[22]

1.5 AI for FGIDs treatment

An AI system (ENBIOSIS) was developed for a personalized nutritional strategy based on a patient's individual microbiota. A study of IBS patients using this system compared standard IBS-diet versus AI based diet and showed an improvement in IBS-SSS score in the AI based diet and a statistically significant increase in the Faecalibacterium genus in the personalized nutrition group.[23]

AI for interpretation of FGIDs tests, questionnaire analysis and images showed moderate accuracy especially in the GI physiology tests. To improve accuracy, it is important to develop more advanced machine learning models and have more training sets.

2. Applications (apps) and FGIDs

According to a systematic review and meta-analysis in 2021, personalized mobile interventions such as mobile apps can improve lifestyle behaviors in patients with chronic diseases.[24] Moreover, IBS patients showed a high compliance rate for symptom diaries recorded on a smartphone application.[25]

Dietary advice and lifestyle notifications are featured in more than half of the health apps available in smartphone stores. Only 15% of GERD-mobile applications are based on evidence-based studies, and the systematic review revealed a wide range of app quality heterogeneity.[26] According to the current published data, apps for IBS were found with the highest number of FGIDs, which included symptom tracking,[25,27] meals and GI symptoms,[28,29] and daily life stress and GI symptoms.[30] In addition, two randomized-controlled trials (RCT) of mobile apps and IBS were reported to improve quality of life and the efficacy of IBS-treatment.[29-31] One is the "Heali AI", a mobile nutrition app, using AI to scan barcodes for nutrition information and adapted to avoid FODMAPS diets for IBS patients.[29] Another is the "Zemedy" mobile app, which was developed to treat IBS patients through cognitive behavioral therapy (CBT).[31] Similarly, a web-based application of low FODMAPs showed good efficacy in managing IBS symptoms.[32] In functional gastroduodenal disorders, mobile app-based symptom reporting has been developed in pictograms and showed a good correlation with the symptom-based scoring systems.[33]

Table 2 Examples of mobile apps in FGIDs

Application	Disease	Description	Available
Zemedy	IBS	app to track stress, emotions, symptoms, and a tailored CBT 6- week training program	IOS, android https://www.zemedy.com/
Dieta	IBS	app can analyze and predict triggers, classify stool forms using AI captures, and offer personalized GI doctor and dietitian consultations.	IOS, android https://dietahealth.com/
augGI	Constipation	using AI to classify stool characterizations by patient-capture images and correlate them with a logged diet	https://www.auggi.ai/
bowelle	IBS	app for tracking food, symptoms, emotions, stress, bowel movements, and water intake and displaying them in graphs and connecting to Apple Health.	IOS https://bowelle.com/

Mobile applications show benefit in helping FGIDs patients, especially IBS patients and doctors for symptom management and psychological treatment. However, using the mobile application for symptom analysis should be cautioned due to the lack of studying mobile application accuracy. Moreover, the elderly and the mobile-unfriendly patients seem to have no benefit from applying.

3. Digital connected devices and FGIDs

Wearable devices have been developed for tracking physiologic changes with correlated health information such as step counts, vital signs, and sleep duration. A study with the data from Fitbit showed that a low number of activity metrics, in steps and sleep, related to the severity of constipation[34] and this was similar to a study of the "Lifecoder" pedometer from Japan which revealed a correlation between the high number of step counts and the improvement of symptoms in IBS patients.[35] The other innovative wearable devices are "AbStats", which is a biosensor placed on the abdominal wall for recording, classifying, and evaluating bowel function; and "G-Tech Patch", which is a wireless patch recording electrical signals from the GI tract.

4. Telemedicine

A systematic review of telemedicine and digestive diseases shows that telemedicine may be effective in managing disease activity and improving quality of life in digestive diseases.[36] However, home-based CBT and Skype hypnosis were reported to be less effective than standard CBT and face-to-face hypnosis in studies of IBS patients.[37,38] In Thailand, telemedicine is available, including web-based and mobile applications that charge per visit and per minute-consultation.

5. Group support

Patients with FGIDs frequently feel worried about their illness due to the absence of demonstrable pathology on standard testing. For example, IBS patients seem to feel frustrated, isolated, and dissatisfied with information received, available treatment, and the health system in general, so group education and group support allowing the patients to share experiences are recommended.[39] According to the most recent online search (Nov 2023), there are approximately ten FGIDs groups supported by Thai social media: the largest group in the Thai language is the GERD supported group, with 4600 members and the largest group in English is IBS support (official), with 103,000 members.

Conclusions

Many reports reveal that digital health can improve the efficacy of FGIDs treatment. Understanding the patient's pathophysiology and behaviors could help physicians select the appropriate treatment. Digital health may become an important modality in the new era of FGIDs treatment.

Acknowledgments

References

1. Pathipati MP, Shah ED, Kuo B, Staller KD. Digital health for functional gastrointestinal disorders. *Neurogastroenterol Motil*. 2023;35(1):e14296. doi:10.1111/nmo.14296.

2. Stone AA, Shiffman S, Schwartz JE, Broderick JE, Hufford MR. Patient compliance with paper and electronic diaries. *Control Clin Trials*. 2003;24(2):182-199. doi:10.1016/s0197-2456(02)00320-3.

3. Sharma A, Harrington RA, McClellan MB, et al. Using digital health technology to better generate evidence and deliver evidence-based care. *J Am Coll Cardiol*. 2018;71(23):2680-2690. doi:10.1016/j.jacc.2018.03.523.

4. Fatehi F, Samadbeik M, Kazemi A. What is Digital Health? Review of Definitions. *Stud Health Technol Inform*. 2020;275:67-71. doi:10.3233/SHTI200696.

5. Santos R, Haack HG, Maddalena D, Hansen RD, Kellow JE. Evaluation of artificial neural networks in the classification of primary oesophageal dysmotility. *Scand J Gastroenterol*. 2006;41(3):257-263. doi:10.1080/00365520500234030.

6. Kou W, Galal GO, Klug MW, et al. Deep learning-based artificial intelligence model for identifying swallow types in esophageal high-resolution manometry. *Neurogastroenterol Motil*. 2022;34(7):e14290. doi:10.1111/nmo.14290.

7. Wang Z, Hou M, Yan L, Dai Y, Yin Y, Liu X. Deep learning for tracing esophageal motility function over time. *Comput Methods Programs Biomed*. 2021;207(106212):106212. doi:10.1016/j.cmpb.2021.106212.

8. Kou W, Carlson DA, Baumann AJ, et al. A multi-stage machine learning model for diagnosis of esophageal manometry. *Artif Intell Med*. 2022;124(102233):102233. doi:10.1016/j.artmed.2021.102233.

9. Kou W, Carlson DA, Baumann AJ, et al. A deep-learning-based unsupervised model on esophageal manometry using variational autoencoder. *Artif Intell Med*. 2021;112(102006):102006. doi:10.1016/j.artmed.2020.102006.

10. Jell A, Kuttler C, Ostler D, Hüser N. How to cope with big data in functional analysis of the esophagus. *Visc Med*. 2020;36(6):439-442. doi:10.1159/000511931.

11. Jones CA, Hoffman MR, Lin L, Abdelhalim S, Jiang JJ, McCulloch TM. Identification of swallowing disorders in early and mid-stage Parkinson's disease using pattern recognition of pharyngeal high-resolution manometry data. *Neurogastroenterol Motil*. 2018;30(4):e13236. doi:10.1111/nmo.13236.

12. Agrusa AS, Gharibans AA, Allegra AA, Kunkel DC, Coleman TP. A deep convolutional neural network approach to classify normal and abnormal gastric slow wave initiation from the high resolution electrogastrogram. *IEEE Trans Biomed Eng*. 2020;67(3):854-867. doi:10.1109/TBME.2019.2922235.

13. Rogers B, Samanta S, Ghobadi K, et al. Artificial intelligence automates and augments baseline impedance measurements from pH-impedance studies in gastroesophageal reflux disease. *J Gastroenterol*. 2021;56(1):34-41. doi:10.1007/s00535-020-01743-2.

14. Wong MW, Rogers BD, Liu MX, Lei WY, Liu TT, Yi CH, Hung JS, Liang SW, Tseng CW, Wang JH, Wu PA, Chen CL. Application of Artificial Intelligence in Measuring Novel pH-Impedance Metrics for Optimal Diagnosis of GERD. *Diagnostics (Basel)*. 2023;13(5):960. doi: 10.3390/diagnostics13050960.

15. Zifan A, Sun C, Gourcerol G, Leroi AM, Mittal RK. Endoflip vs high-definition manometry in the assessment of fecal incontinence: A data-driven unsupervised comparison. *Neurogastroenterol Motil*. 2018;30(12):e13462. doi:10.1111/nmo.13462.

16. Carlson DA, Kou W, Rooney KP, et al. Achalasia subtypes can be identified with functional luminal imaging probe (FLIP) panometry using a supervised machine learning process. *Neurogastroenterol Motil*. 2021;33(3):e13932. doi:10.1111/nmo.13932.

17. Visaggi P, de Bortoli N, Barberio B, et al. Artificial Intelligence in the Diagnosis of Upper Gastrointestinal Diseases. *J Clin Gastroenterol*. 2022;56(1):23-35. doi:10.1097/MCG.0000000000001629.

18. Ruffle JK, Tinkler L, Emmett C, et al. Constipation Predominant Irritable Bowel Syndrome and Functional Constipation Are Not Discrete Disorders: A Machine Learning Approach. *Am J Gastroenterol*. 2021;116(1):142-51. doi:10.14309/ajg.0000000000000816.

19. Vilarino F, Spyridonos P, Deiorio F, Vitria J, Azpiroz F, Radeva P. Intestinal motility assessment with video capsule endoscopy: automatic annotation of phasic intestinal contractions. *IEEE Trans Med Imaging*. 2010;29(2):246-59. doi:10.1109/TMI.2009.2020753.

20. Rattanachaisit P, Poovongsaroj S, Patcharatrakul T, Gonlachanvit S, Vateekul P. Sa412 ABDOMINAL RADIOGRAPHY WITH ARTIFICIAL INTELLIGENCE FOR DIAGNOSIS OF DYSSYNERGIC DEFECATION (DD). *Gastroenterology*. 2021;160(6):S-498-S-499. doi:10.1016/s0016-5085(21)01894-1.

21. Du X, Allwood G, Webberley KM, Inderjeeth AJ, Osseiran A, Marshall BJ. Noninvasive Diagnosis of Irritable Bowel Syndrome via Bowel Sound Features: Proof of Concept. C*lin Transl Gastroenterol*. 2019;10(3):e00017. doi: 10.14309/ctg.0000000000000017.

22. Inderjeeth AJ, Webberley KM, Muir J, Marshall BJ. The potential of computerised analysis of bowel sounds for diagnosis of gastrointestinal conditions: a systematic review. *Syst Rev*. 2018;7(1):124. doi:10.1186/s13643-018-0789-3.

23. Vulpoi RA, Luca M, Ciobanu A, Olteanu A, Bărboi O, Iov DE, Nichita L, Ciortescu I, Cijevschi Prelipcean C, Ștefănescu G, Mihai C, Drug VL. The Potential Use of Artificial Intelligence in Irritable Bowel Syndrome Management. *Diagnostics (Basel)*. 2023;13(21):3336. doi:10.3390/diagnostics13213336.

24. Tong HL, Quiroz JC, Kocaballi AB, et al. Personalized mobile technologies for lifestyle behavior change: A systematic review, meta-analysis, and meta-regression. *Prev Med*. 2021;148(106532):106532. doi:10.1016/j.ypmed.2021.106532.

25. Weerts ZZRM, Heinen KGE, Masclee AAM, et al. Correction: Smart data collection for the assessment of treatment effects in irritable bowel syndrome: Observational study. *JMIR MHealth UHealth*. 2021;9(2):e27998. doi:10.2196/27998.

26. Venugopal LS, Musbahi A, Shanmugam V, Gopinath B. A systematic review of smartphone apps for gastro-oesophageal reflux disease: the need for regulation and medical professional involvement. *MHealth*. 2021;7:56. doi:10.21037/mhealth-20-126.

27. Beckers AB, Snijkers JTW, Weerts ZZRM, et al. Digital instruments for reporting of gastrointestinal symptoms in clinical trials: Comparison of end-of-day diaries versus the experience sampling method. *JMIR Form Res*. 2021;5(11):e31678. doi:10.2196/31678.

28. Zia J, Schroeder J, Munson S, et al. Feasibility and usability pilot study of a novel irritable bowel syndrome food and gastrointestinal symptom journal smartphone app. *Clin Transl Gastroenterol*. 2016;7(3):e147. doi:10.1038/ctg.2016.9.

29. Rafferty AJ, Hall R, Johnston CS. A novel mobile app (Heali) for disease treatment in participants with irritable bowel syndrome: Randomized controlled pilot trial. *J Med Internet Res*. 2021;23(3):e24134. doi:10.2196/24134.

30. Chan Y, So SHW, Mak ADP, Siah KTH, Chan W, Wu JCY. The temporal relationship of daily life stress, emotions, and bowel symptoms in irritable bowel syndrome-Diarrhea subtype: A smartphone-based experience sampling study. *Neurogastroenterol Motil*. 2019;31(3):e13514. doi:10.1111/nmo.13514.

31. Hunt M, Miguez S, Dukas B, Onwude O, White S. Efficacy of Zemedy, a mobile digital therapeutic for the self-management of irritable bowel syndrome: Crossover randomized controlled trial. *JMIR MHealth UHealth*. 2021;9(5):e26152. doi:10.2196/26152.

32. Ankersen DV, Weimers P, Bennedsen M, et al. Long-term effects of a web-based low-FODMAP diet versus probiotic treatment for irritable bowel syndrome, including shotgun analyses of Microbiota: Randomized, double-crossover clinical trial. *J Med Internet Res*. 2021;23(12):e30291. doi:10.2196/30291.

33. Sebaratnam G, Karulkar N, Calder S, et al. Standardized system and App for continuous patient symptom logging in gastroduodenal disorders: Design, implementation, and validation. *Neurogastroenterol Motil*. 2022;34(8):e14331. doi:10.1111/nmo.14331.

34. Shapiro A, Bradshaw B, Landes S, et al. A novel digital approach to describe real world outcomes among patients with constipation. *NPJ Digit Med*. 2021;4(1):27. doi:10.1038/s41746-021-00391-x.

35. Hamaguchi T, Tayama J, Suzuki M, et al. Correction: The effects of locomotor activity on gastrointestinal symptoms of irritable bowel syndrome among younger people: An observational study. *PLoS One*. 2020;15(12):e0244465. doi:10.1371/journal.pone.0244465.

36. Helsel BC, Williams JE, Lawson K, Liang J, Markowitz J. Telemedicine and Mobile Health Technology Are Effective in the Management of Digestive Diseases: A Systematic Review. *Dig Dis Sci*. 2018;63(6):1392-408.

37. Lackner JM, Jaccard J, Keefer L, et al. Improvement in gastrointestinal symptoms after cognitive behavior therapy for refractory irritable bowel syndrome. *Gastroenterology*. 2018;155(1):47-57. doi:10.1053/j.gastro.2018.03.063.

38. Hasan SS, Pearson JS, Morris J, Whorwell PJ. SKYPE HYPNOTHERAPY FOR IRRITABLE BOWEL SYNDROME: Effectiveness and comparison with face-to-face treatment. *Int J Clin Exp Hypn*. 2019;67(1):69-80. doi:10.1080/00207144.2019.1553766.

39. Halpert A. Irritable bowel syndrome: Patient-provider interaction and patient education. *J Clin Med*. 2018;7(1):3. doi:10.3390/jcm7010003.

Case report

Disseminated Nocardiosis with Intracranial Mycotic Aneurysm in A Patient with Autoimmune Hepatitis: A Case Report and Review of The Literature

Chaiwat Pongkaew[1], Anucha Apisarnthanarak[1],
Thana Khawcharoenporn[1], Nuntra Suwantarat[2], Sasinuch Rutjanawech[1],
Pansachee Damronglert[1], Suttichai Visuttichaikit [1]

Abstract

We are reporting a case of disseminated *Nocardia otitidiscaviarum* infection, manifesting as a ruptured intracranial aneurysm in an immunocompromised patient. The patient succumbed despite treatment with trimethoprim-sulfamethoxazole, amikacin, and levofloxacin along with surgical repairment. Nocardiosis should be one of the differential diagnoses for intracranial mycotic aneurysm among immunocompromised patients.

[1] Division of Infectious Diseases, Department of Internal Medicine, Thammasat University, Pathum Thani, Thailand.
[2] Chulabhorn International College of Medicine, Thammasat University, Pathum Thani, Thailand.
* **Corresponding author:** Suttichai Visuttichaikit, M.D. Division of Infectious Diseases, Department of Internal Medicine, Thammasat University, Pathum Thani, Thailand. Tel. +669 4484 7690, Fax. +66 2926 9793 E-mail: vsuttichai@gmail.com

Introduction

Nocardiosis is considered an opportunistic infection affecting immunocompromised patients. Intracranial mycotic aneurysm is a rare manifestation of central nervous system nocardiosis. To date, there are only 5 reported cases of intracranial mycotic aneurysms caused by nocardial infection. We are report a case of disseminated *Nocardia otitidiscaviarum* infection, a species that was rarely described as a significant pathogen in the medical literature, manifesting as a ruptured intracranial mycotic aneurysm in an immunocompromised patient.

Case report

A 51-year-old Thai man with autoimmune hepatitis and chronic hepatitis B virus infection presented to our hospital with altered consciousness for 7 hours. Prior to this presentation, he had been suffering from fever and productive cough for 12 days. His medications included tenofovir disoproxil fumarate 300 mg daily, prednisolone 30 mg daily, and azathioprine 50 mg daily, which had been prescribed for 7 weeks to treat chronic hepatitis B and autoimmune hepatitis before this presentation. Initial examination showed a temperature of 36.9°C, heart rate of 76 beats/minute, respiratory rate of 24 breaths/minute, and blood pressure of 186/112 mmHg. Chest auscultation revealed bronchial breath sound and coarse crepitation at the left upper lung area. Neurological examination revealed decreased level of consciousness with eyes opening, incomprehensible sounds, and response to pain. Motor power was at least grade 3 for all extremities. Papilledema was notable on ophthalmoscopy. Chest X-ray showed consolidations at both lungs predominant at left upper lung (Figure 1A). Emergency computed tomography (CT) scan of the brain showed acute hematoma in the bilateral frontal lobes with intra-ventricular hemorrhage and subacute infarction in the bilateral frontal lobes, genu of corpus callosum and left thalamus (Figure 1B). To search for the source of bleeding, CT angiogram of the brain was subsequently performed and revealed a 3.1 x 2.2 mm saccular aneurysm originating from the A2 segment of left anterior cerebral artery, suggesting a ruptured aneurysm (Figure 1C).

Bifrontal craniectomy was performed. The operative findings revealed subdural frank pus, more prominent in the left subdural space and a necrotic aneurysm with thrombus occlusion in the left anterior cerebral artery. Clipping the aneurysm with pus drainage was done. A pus Gram's stain showed branching filamentous, beaded gram-positive bacilli (Figure 1D) which were acid-fast on the modified Kinyoun stain. The sputum Gram's and modified Kinyoun stain showed the similar results. The treatment was started with intravenous (IV) trimethoprim-sulfamethoxazole (TMP-SMX) at the total daily dose of 15 mg/kg of TMP, 15 mg/kg/day of IV amikacin, and 750 mg/day of IV levofloxacin. *Nocardia otitidiscaviarum* was identified by matrix-assisted laser desorption/ionization time-of-flight mass spectrometry (MALDI-TOF MS) in an isolated colony from the pus bacterial culture. The antimicrobial susceptibility test by broth microdilution method revealed susceptibility to TMP-SMX (MIC 0.5 μg/mL), amikacin (MIC 2 μg/mL), ciprofloxacin (MIC 1 μg/mL), moxifloxacin (MIC 1 μg/mL), doxycycline (MIC 1 μg/mL), and linezolid (MIC 2 μg/mL). The isolate was resistant to amoxicillin-clavulanate (MIC 32 μg/mL), ceftriaxone (MIC 64 μg/mL), and imipenem (MIC 16 μg/mL). The final diagnosis of disseminated nocardiosis was made. Despite surgical and antimicrobial therapy, his level of consciousness did not improve. On day 5 of hospitalization, the patient developed status epilepticus and passed away 2 days later.
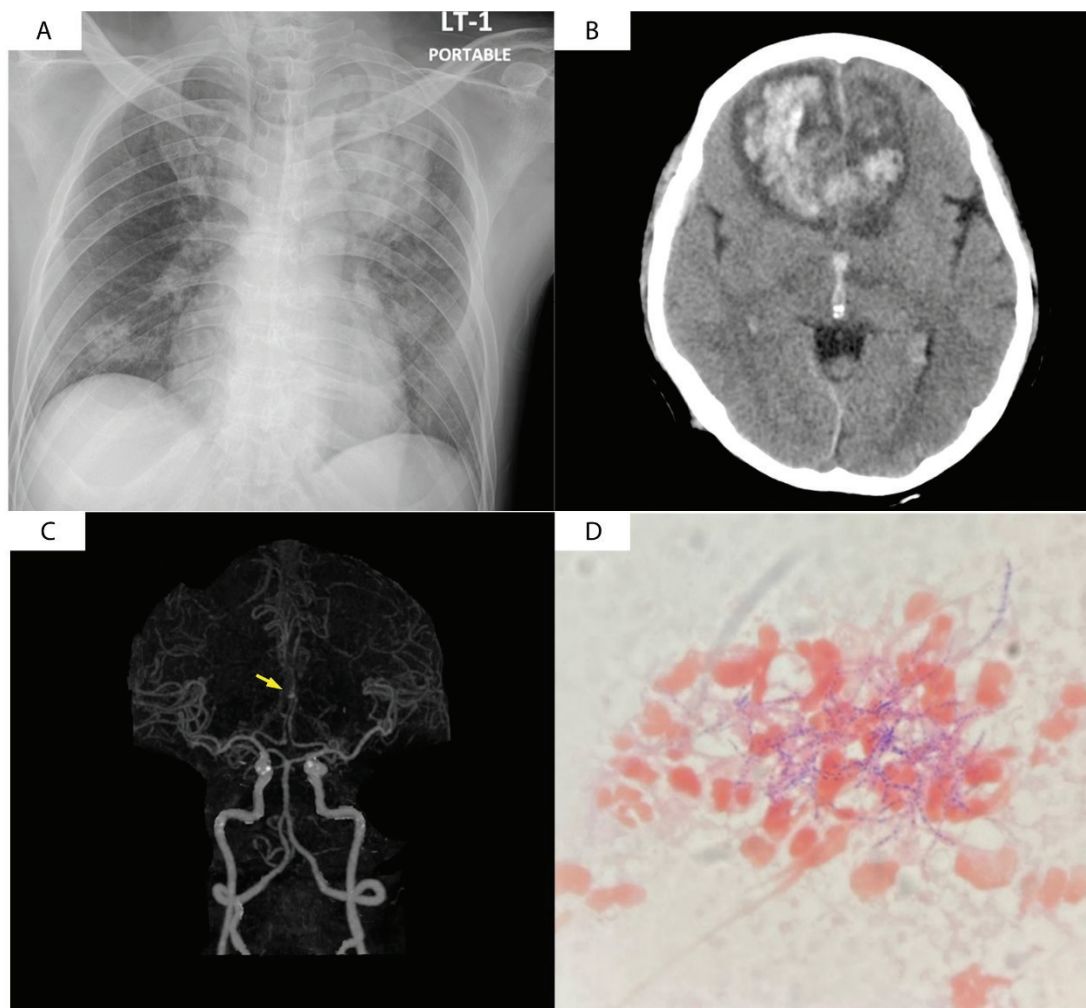
Figure 1 (A) Chest X-ray showed consolidations at both lungs predominantly in the left upper lung. (B) Computed tomography scan of the brain showed acute hematoma in the bilateral frontal lobes with intraventricular hemorrhage and subacute infarction in the bilateral frontal lobes, genu of corpus callosum and left thalamus. (C) Computed tomography angiogram of the brain reveled a 3.1 x 2.2 mm saccular aneurysm originated from A2 segment of left anterior cerebral artery (arrow). (D) A pus sample from the brain Gram stain showed branching filamentous, beaded gram-positive bacilli.

Discussion

Nocardia species are filamentous, Gram-positive, partially acid-fast, branched bacteria that are ubiquitous in the environment, particularly in the soil. *Nocardia* can be regarded as primary pathogens, without evidence of underlying illnesses or immunosuppressive therapy, although they are considered opportunistic pathogens.[1] The species *N. otitidiscaviarum* was first isolated from the mid-ear of a guinea pig and reported by Snijders in 1924. The first human infection due to *N. otitidiscaviarum* was reported in 1974 and was previously named *Nocardia caviae*. *N. otitidiscaviarum* is an infrequent cause of human nocardial infections. In some case series, it accounted for only 0.3-2.9% of all nocardial infections.[2] There have been 53 reported cases of *N. otitidiscaviarum* disease. Isolated pulmonary involvement was the most frequent presentation accounting for 35.8% of all cases, followed by isolated cutaneous infections accounting for 32.1%, while 18.9% had disseminated disease involving two or more organs. The central nervous system (CNS) was involved in 60% of those with disseminated disease. Isolated CNS infection accounted for 9.4% of cases.[5]

Certain risk factors predispose to nocardial infection. Individuals with weakened immune systems, such as patients with conditions requiring long-term or large doses of corticosteroid treatment, human immunodeficiency virus (HIV) infection, diabetes mellitus, chronic obstructive pulmonary disease, cirrhosis, malignancies, and stem cell or solid organ transplantation are at Increased risk of infection.[3] In our case, a prolonged course of corticosteroid was most likely a predisposing factor to nocardiosis.

Intracranial mycotic aneurysms represent 0.5-6.5% of all intracranial aneurysms in a systematic review. Patients with intracranial mycotic aneurysms often present with neurological signs and symptoms secondary to bleeding or rupture of the aneurysms such as acute onset of altered consciousness,[4,6] similar to our patient. Intracranial mycotic aneurysm from nocardial infection is a rare manifestation, while the most common manifestation of CNS involvement is brain abscess. There have been 5 reported cases of *Nocardia* spp. causing mycotic aneurysms in intracranial arteries.[5-9] Two of these 5 patients had a history of SLE treated with corticosteroid, one had a history of autoimmune hepatitis receiving corticosteroid, one had a history of multiple myeloma receiving corticosteroid and bortezomib, while another one had no evidence of immunosuppression. Three of them presented with disseminated disease and the others presented with isolated CNS infection. Two patients had an aneurysm at the anterior cerebral artery and *N. otitidiscaviarum* is the identified pathogen, similar to our patient. Most of them responded to surgical management combined with TMP-SMX-based antimicrobial therapy. The characteristics of these five cases are summarized in Table 1.

The diagnosis of nocardiosis is based on the identification of *Nocardia* spp. from the infected sites. Gram's and modified Kinyoun staining are commonly used for initial identification. Molecular methods for identifying *Nocardia* spp. including 16s ribosomal RNA sequencing and MALDI-TOF are fast, sensitive, and highly reliable. The species identification is important due to the species-specific differences in antimicrobial susceptibility patterns. Most *N. otitidiscaviarum* isolates are reported to be resistant to beta-lactams while usually being susceptible to amikacin, fluoroquinolones and TMP-SMX. Hence, TMP-SMX remains the standard agent for treatment.[10] For a definitive treatment of pulmonary and CNS nocardiosis, antimicrobial regimens should consist of agents with good penetration into the lung tissue and blood-brain barrier. These include TMP-SMX, ceftriaxone, meropenem, and fluoroquinolones. Overall mortality of *N. otitidiscaviarum* disease was 26.4%. Patients with disseminated disease had mortality rate of 30% while mortality of those with CNS disease reached 54.5%.[5] Even though our patient was started on the proper antimicrobial agents along with the surgical intervention, the outcome was still fatal.

In conclusion, intracranial mycotic aneurysm is an uncommon presentation of CNS involvement of nocardiosis and can have a severe outcome. Patients with intracranial mycotic aneurysms often present with neurological signs and symptoms secondary to bleeding or rupture of the aneurysms. Early diagnosis and species identification as well as antimicrobial susceptibility testing are needed for optimizing antimicrobial therapy. Physicians should have a high index of suspicion for this uncommon infection in patients presenting with such neurological manifestations while receiving long-term corticosteroids.

Table 1 The characteristics of previously reported cases of Nocardia causing aneurysms in intracranial arteries

Age	Sex	Comorbidity	Immunosuppressive drugs	Clinical presentation	Procedure	Site of aneurysm	Species	Antibiotic regimen	Outcome	Reference
60	Male	None	None	Headaches, fatigue, memory loss, and behavioral abnormalities for 3 weeks	Drainage of abscess with resection of the infected aneurysm	Internal carotid artery	*Nocardia abscessus*	Ceftriaxone and TMP-SMX for 6 weeks	Recovered	Farran et al.[6]
69	Male	Multiple myeloma	Bortezomib Lenalidomide Dexamethasone	Thoracic empyema and alteration of consciousness with right-sided motor weakness	Emergency clipping of the aneurysm	Left middle cerebral artery	*Nocardia farcinica*	TMP-SMX and Ceftriaxone followed by TMP-SMX and Moxifloxacin for a total of 12 months	Recovered	Chansirikarnjana et al.[7]
28	Female	SLE	Prednisolone	Headache, irritability, and nuchal rigidity	Surgical excision of aneurysm	Right middle cerebral artery	*Nocardia asteroides*	TMP-SMX for 3 weeks Cefotaxime and Amikacin for 2 weeks and Doxycycline 4 weeks	Recovered	Hadley et al.[8]
51	Male	Autoimmune hepatitis	Prednisolone	Subacute fever and dyspnea for 10 days	Aneurysm trapping	Anterior cerebral artery	*Nocardia otitidiscaviarum*	TMP-SMX and Amikacin and Moxifloxacin	Died	Duangprasert G et al.[9]
29	Female	SLE	Prednisolone	Necrotizing pneumonia with lung abscess, and alteration of consciousness	Life-saving decompressive craniectomy and EVD insertion	Right anterior cerebral artery	*Nocardia otitidiscaviarum*	TMP-SMX and high-dose Meropenem and Amikacin for 8 weeks followed by TMP-SMX and Moxifloxacin for 10 months	Recovered	Parengal et al.[5]
51	Male	Autoimmune hepatitis	Prednisolone	Alteration of consciousness	Bifrontal craniectomy with clipping aneurysm	Left anterior cerebral artery	*Nocardia otitidiscaviarum*	TMP-SMX and Levofloxacin and Amikacin	Died	Our case

References

1. Kageyama A, Yazawa K, Ishikawa J, Hotta K, Nishimura K, Mikami Y. Nocardial infections in Japan from 1992 to 2001, including the first report of infection by *Nocardia transvalensis*. *Eur J Epidemiol*. 2004;19:383-389.
2. Ishihara M, Takada D, Sugimoto K, et al. Primary brain abscess caused by *Nocardia otitidiscaviarum*. *Intern Med*. 2014;53(17): 2007-12.
3. Corti ME, Villafañe-Fioti MF. Nocardiosis: a review. *Int J Infect Dis*. 2003;7:243-50.
4. Alawieh A, Chaudry M, Turner RD, Turk A, Spiotta AM. Infectious intracranial aneurysms: a systematic review of epidemiology, management, and outcomes. *J NeuroIntervent Surg*. 2018;0:1-10.
5. Parengal J, Alebbi SM, Hamed MMM, Alqatami HM. Disseminated life threatening *Nocardia otitidiscaviarum* infection in a young female with newly diagnosed systemic lupus erythematosus, case report and review of literature. *IDCases*. 2021;26:e01265.
6. Farran Y, Antony S. *Nocardia abscessus*-related intracranial aneurysm of the internal carotid artery with associated brain abscess: a case report and review of the literature. *J Infect Public Health*. 2016;9(3):358-61.
7. Chansirikarnjana S, Apisarnthanarak A, Suwantarat N, et al. Nocardia intracranial mycotic aneurysm associated with proteasome inhibitor. *IDCases*. 2019;8:e00601.
8. Hadley MN, Robert MD, Spetzler F, Martin NA, Johnson PC. Middle cerebral artery aneurysm due to *Nocardia asteroides*: case report of aneurysm excision and extracranial-intracranial bypass. *Neurosurgery*. 1988;22(5):923-8.
9. Duangprasert G, Kebboonkird D, Ratanavinitkul W, Tantongtip D. A rare case of ruptured anterior cerebral artery infected aneurysm with angioinvasion secondary to disseminated Nocardia otitidiscaviarum: A case report and literature review. *Surgical Neurology International*. 2022;13:417.
10. Betrán A, Villuendas MC, Rezusta A, et al. Cavitary pneumonia caused by *Nocardia otitidiscaviarum*. *Braz J Microbiol*. 2010;41: 329-32.

INSTRUCTION FOR AUTHORS

AMJAM is an open-access journal publishes Original article, Review article, Brief Research, Case report, Special article (Invited by Editor), Editorial, and Letter to the Editor in all health sciences, medical specialties and alternative medicine. AMJAM publishes 4 times a year in April (Issue 1), August (Issue 2), December (Issue 3), and 1 Supplementary issue. All submitted articles will be evaluated using double-blinded review process by 2-4 reviewers.

Original Article should include a title page, a structured abstract of no more than 250 words, a text of no more than 3,000 words, no more than 7 tables and figures, and no more than 40 references.

Review Article should include a title page, a narrative abstract of no more than 150 words, a text of no more than 3,000 words, no more than 2 tables or figures, and no more than 30 references.

Case Report should include a title page, a narrative abstract of no more than 50 words, a text of no more than 1,200 words, no more than 2 tables or figures, and no more than 10 references.

Brief Research should include a title page, a narrative abstract of no more than 50 words, a text of no more than 1,200 words, no more than 2 tables or figures, and no more than 10 references.

Special Article (Invited by Editor) should include a title page, a text of no more than 3,000 words, no more than 2 tables or figures, and no more than 30 references. Abstract nor keywords are not required.

Editorial should include a title page, a text of no more than 1,000 words, no more than 1 tables or figures, and no more than 10 references. Abstract nor keywords are not required.

Letter to the Editor should not exceed 900 words, no more than 1 table or figure, and no more than 10 references. Abstract nor keywords are not required.

Commentaries are by invitation only. Please contact the journal office if you are interested in writing a Commentary.

MANUSCRIPT PREPARATION

Authors who are not fluent in English should have their manuscript checked by a native speaker of English and/or an editing service that provides such assistance. Please concept editorial office if author would like to receive suggestion on editing service. Manuscripts that do not follow the required format or are poorly prepared may be asked to be revised for resubmission. In the submitted cover letter author should state that "All authors have significantly contributed to the research."

All submitted manuscript must include institutional ethical approval certificate. Single space the entire manuscript, including title page, abstract, body, references, tables, and figure legends. Use left justification only, so that the right margin is ragged. Number pages consecutively, beginning with the title page. Use a standard font Times New Roman and set the font size to 12 points (for tables as well as text). All numbers published in AMJAM will be in Arabic numbers. Each component of the article should begin on a separate page, as follows: title page, abstract, body text, acknowledgements, references, appendices, tables and figure legends, and tables. All these components must be in a single file.

Title Page

The title page should include the following information: (1) the title of the manuscript; (2) the names of the author(s), including each author's highest academic degree or professional certification; (3) the departmental and institutional affiliation of each author, including city, state, and country; (4) the name, address, telephone number, fax number, and email address of the author responsible for correspondence, and (if different) the name and address to be used for reprint requests; (5) if relevant, a statement about any previous presentation of the data or findings in a preliminary report or abstract; (6) an abbreviated title of not more than 45 characters (including spaces), to be used as a running head in print and for searching results online; and (7) a word count for the body of the text (ie, excluding the abstract and the references). Acknowledgement of financial support and potential conflicts of interest must be included and should be placed in the Acknowledgements section (see below).

Abstract

Original Article should include a structured abstract of no more than 250 words. The following headings are suggested: Introduction/Objective, Design, Methods (or Interventions), Results, Conclusions, and Key words (3-5 words or phrases). If this list of headings is inappropriate, variations are permitted: for example, a study that involved no intervention would use the heading "Methods" rather than "Intervention"; or an analysis of an existing data set might use the heading "Methods" in place of both "Intervention". For brevity, parts of the abstract can be written in phrases rather than complete sentences (eg, "Design: Retrospective cohort study" or "Design: Before-after trial").

The contents of each section should conform to the guidelines below.

Body Text

The main sections and subdivisions of the body text should be indicated by side heads flushed with the left margin and two lines above the text. Keep Methods, Results, and Discussion distinct and separate. The Methods section should provide detail sufficient to allow others to reproduce your experiment. Methods may not be described or restated in figure legends or table notes, but must be all together in the Methods section. The Results section contains the previously unpublished data derived by this application of your methods, without commentary (beyond the minimum that might be necessary to ensure intelligibility to the reader). The Discussion section contains your interpretation of the reported data and comments on its meaning. There should be no separate section labeled "Conclusion." Avoid duplicating in the text data that have been provided in tables or figures (minimal duplication, for emphasis or clarity, is acceptable). Also avoid duplication within the text; for example, the Discussion section should not restate all the findings that have been presented in Results and/or in tables and figures.

Acknowledgments

Financial support. Information on financial support should be provided by authors. The Acknowledgments section should list all sources of financial support for the work, including any financial arrangement with a company whose product is related to the study. If there was no financial support, that too should be stated. Acknowledgments, including grant support, should be placed after the text.

Example:
- Financial support. The XXX Project is supported by the Thai Ministry of Health. Additional support for this study was provided by Becton-Dickinson.
- Financial support. None reported.

Conflict of interest. The Acknowledgments section must contain a statement of potential conflicts of interest. If the manuscript is accepted for publication, the disclosures will be published. The Acknowledgments section of the manuscript must list the name of each contributing author and any potential conflicts of interest for each author for the previous three years; if no potential conflict exists, that too should be stated.

Example:
- Potential conflicts of interest. K.L.H. reports having consulted for and having received grant support from Astellas and reports having received an honorarium from Cubist before starting employment with the New York Department of Public Health in 2009.
- Potential conflicts of interest. All authors report no conflicts of interest relevant to this article.

References
Use the Style Guide of the American Medical Association (AMA) as a reference. References should be cited consecutively in the text, with superscript numbers placed outside periods and commas and inside colons and semicolons. References cited only in tables or figure legends should be numbered as though all were cited at the point at which the table or figure was first mentioned.

A paper that is "in press" may be included in the reference list if it has been accepted for publication. Citations such as "in preparation," "submitted for publication," "unpublished data," and "persona communication" should be given in parentheses in the text only, including the names of all individuals to whom the information should be attributed, as well as each person's highest academic degree and the month and year of the information's origin. For personal communications, specify whether the communication was written or oral.

At the end of each manuscript, list the references in numerical order, single spaced, according to the order they are cited in the text. If there are 7 or more authors, list the first 3 authors' names, followed by "et al"; otherwise, list all authors. Abbreviations of journal names should conform to Index Medicus or MEDLINE. Unlisted journals should not be abbreviated. Authors are responsible for bibliographic accuracy. Journal titles should be cited as they existed at the time of publication. Format references according to the style given in the AMA Manual of Style, 10th Edition.

Journal article (example)
1. Pittet D, Simon A, Hugonnet S, Pessoa-Silva CL, Sauvan V, Perneger TV. Hand hygiene among physicians: performance, beliefs, and perceptions. *Ann Intern Med*. 2004;141:1-8.
2. Camins BC, Richmond AM, Dyer KL, et al. A crossover intervention trial evaluating the efficacy of a chlorhexidine-impregnated sponge in reducing catheter-related bloodstream infections among patients undergoing hemodialysis. *Infect Control Hosp Epidemiol*. 2010;31:1118-1123.

Journal article in press (example)
3. Figueroa P, Johanssen KL, Price FG, et al. Outbreak of Acinetobacter infection in a neonatal intensive care unit. *Pediatr Infect Dis J* (in press).

Paper presented at a professional meeting (example)
4. Chen LF, Freeman JT, Sexton DJ, Choi YI, Anderson DJ. NHSN definition of laboratory-detected BSI is overly sensitive for Enterococcus. In: Program and abstracts of the 19th Annual Scientific Meeting of the Society for Healthcare Epidemiology of America (SHEA); March 18–22, 2009; San Diego, CA. Abstract 359.

Book (example)
5. Heoprich PD. *Infectious Diseases. 2nd ed*. New York, NY: Harper & Row; 1977.

Chapter in a book (example)
6. Schaffner W. Psittacosis: ornithosis, parrot fever. In: Beeson PB, McDermott W, Wyngaarden JB, eds. *Cecil Textbook of Medicine. 15th ed*. Philadelphia, PA: W. B. Saunders; 1979:336-338.

Web page (example)
7.   Clinical laboratory fee schedule. Centers for Medicare and Medicaid Services website. https://www.
       cms.gov/ClinicalLabFeeSched/02_clinlab.asp#TopOfPage. Published 2010. Accessed April 2, 2010.

Tables and Figures
Tables and figures in articles are clear and well configured within article content (are not just copied-pasted from Excel)

Tables
Prepare tables with the MS Word table editor; text formatted to look like a table by use of tabs and hard returns is not acceptable and will be rejected. Include tables in the same file of the manuscript, not in separate files. Tables should be single spaced. Number tables in the order in which they are cited in the text, and provide a descriptive title for each table.

Every column in a table requires a head that describes the contents of the cells below. The units of measure for all data must be clearly stated in the heads, in the stub (leftmost) column, or in data cells, as appropriate. Do not use vertical lines, and do not use ditto marks for repeated information.

List and define any abbreviations in a note below the table, above the table footnotes (no footnote designator is required for this line), even if the abbreviations have been defined in the text. Use superscript letters for footnote designators.

The tables that are too large to be reproduced in print, if accepted for publication, will appear only in the online version of the article, and information about the online-only table (including a full or partial title) will be included in the print version of the article.

Example of Tables:

Table 1 Characteristics of study subjects

Characteristics	Congenital hypothyroidism		Non Congenital hypothyroidism		P-value
	N	%	N	%	
Gender					
Male	40	64.2	171	53.4	.108
Female	22	35.5	149	46.6	
Birth weight (g)					
< 2,500	13	21.0	56	17.8	560
≥ 2,500	49	79.0	258	82.2	
Gestational age (Week)					
< 36	6	15.8	32	11.0	.415*
≥ 36	32	84.2	260	89.0	
APGAR at 5 minutes					
Normal (> 6)	59	100	302	97.4	.365*
Abnormal (≤ 6)	0	0	8	2.6	
Maternal age (Year)					
< 20	1	1.9	46	45.7	.024
20 - 35	45	83.3	208	71.0	
> 35	8	14.8	39	13.3	
Maternal history of thyroid hormone disease					
Yes	12	19.7	2	0.6	< .001
No	49	80.3	309	99.4	
Sepsis					
Yes	6	10.2	42	13.5	.485
No	53	89.8	269	86.5	
Ototoxic					
Yes	11	18.64	103	33.0	.028
No	48	81.4	209	67.0	
TSH screening(mU/L) Mean (Standard deviation)	29.5 (46.6)		5.4 (3.8)		< .001*
TSH at diagnosis(mU/L) Mean (Standard deviation)	20.4 (27.1)				
FT4 at diagnosis(ng/dL) Mean (Standard deviation)	1.4 (0.8)				

Abbreviations: TSH, Thyroid-stimulating hormone; FT4, Free thyroxine; APGAR, Activity Pulse Grimace Appearance and Respiration

Table 3 Univariable risk regression of the hearing loss

Characteristics	Risk ratio	95% CI	P-value
Congenital hypothyroidism	2.00	1.09 - 3.67	.0286
Ototoxic	2.37	1.34 - 4.19	.003
Sepsis	3.11	1.74 - 5.58	.0007

Abbreviations: CI, confidence interval

Figure

- Size: Image with a minimum of 35 x 14 cm. (w x h) using a minimum resolution of 300 dpi. Larger image, please use the same ratio.
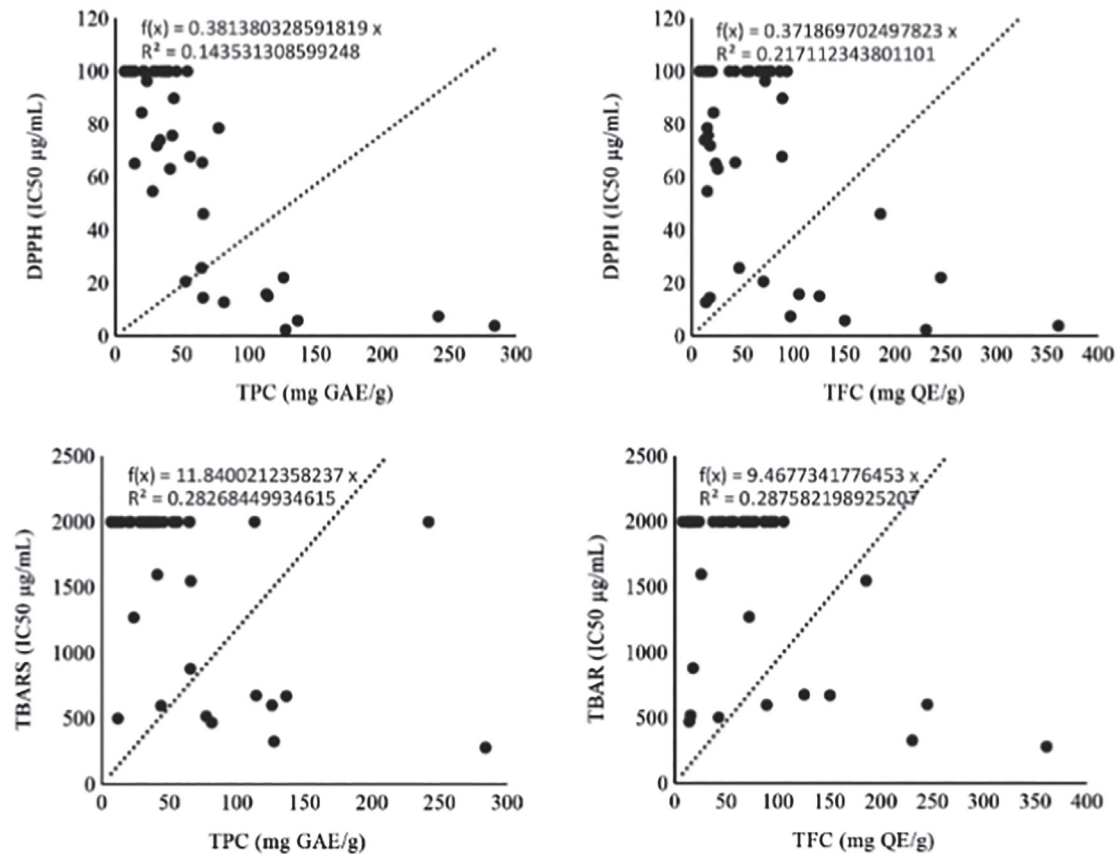- File types: PDF or MS Office files

Example of Figure:

Figure 1 The Pearson statistical correlation scatters plot of the linear relationship between (A) DPPH and TPC, (B) DPPH and TFC, (C) TBARS and TPC, and (D) TBARS and TFC.
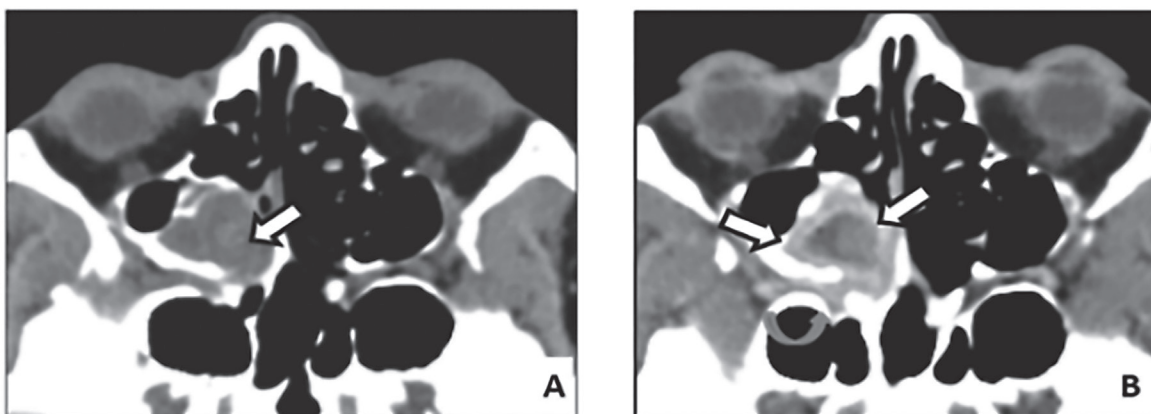

Figure 4 A and B: 58-year-old man with fungal ball at right ethmoid sinus was interpreted as inflammatory lesion. There is a hyperattenuating content (open arrow in A) with mucosal thickening at right posterior ethmoid sinus (open arrow in B) with fat haziness and increased enhancement at right PPF (curve arrow in B).